PP/MWCNT injection-moulded components: an analytical study of electrical properties and morphology

Doctoral Dissertation
Doctoral Program in Materials Science Engineering (30th Cycle)

PP/MWCNT injection-moulded components: an analytical study of electrical properties and morphology

By

Marta Zaccone

******

Supervisor:
Prof. Alberto Frache

Doctoral Examination Committee:
Dr. Simona Ceccia, Manufacture Française des Pneumatiques Michelin
Prof. Erlantz Lizundia, University of the Basque Country
Prof. Andrea Castrovinci, Professional University School of Italian Switzerland
Prof. Barbara Bonelli, Politecnico of Turin
Prof. Marco Sangermano, Politecnico of Turin

Politecnico di Torino
2017

Declaration

I hereby declare that, the contents and organization of this dissertation constitute my own original work and does not compromise in any way the rights of third parties, including those relating to the security of personal data.

Marta Zaccone

2017

* This dissertation is presented in partial fulfilment of the requirements for **Ph.D. degree** in the Graduate School of Politecnico di Torino (ScuDo).

Alla mia nonna

Acknowledgment

Questi tre anni di dottorato e la stesura di questa tesi sono stati lunghi ed impegnativi ed è giusto che io ringrazi tutti quanti hanno permesso di portare a termine questo lavoro. Prima di tutto devo ringraziare il mio relatore, il Prof. Alberto Frache, che mi ha seguito nel corso di tutto il progetto, l'azienda in cui lavoro e la mia responsabile la dott.ssa Maria Rosa Contardi, che mi hanno dato l'opportunità di seguire il mio percorso di dottorato. Devo anche ringraziare i laboratori della sede di Terni dell'Università di Perugia, che mi hanno concesso la possibilità di utilizzare le loro strumentazioni per parte della fase sperimentale ed in particolare la dott.ssa Ilaria Armentano per l'aiuto fornitomi per la parte analitica e l'Università di Torino, in particolare il dr. Federico Cesano e la Prof.ssa Domenica Scarano per il costante supporto nella realizzazione dei test elettrici e morfologici e nell'analisi dei dati ottenuti.

Più importanti di tutti però sono i ringraziamenti agli amici e ai colleghi che mi sono stati vicini in tutto questo periodo. Primo tra tutti Marco, che mi ha spinto, sostenuto, corretto, migliorato, supportato e sopportato costantemente e quotidianamente fino alla scrittura dell'ultima sillaba; Emma, Antonella e Giuseppe per il supporto indefinito nei test di laboratorio; Luana, Maria Teresa, Laura, Antonella ed Emma (di nuovo perché valgono doppio) per il sostegno "psicologico" fornitomi in tutti questi lunghi mesi: sono stati dei validissimi ascoltatori e spronatori. E infine, ma assolutamente non meno importanti, i miei genitori, mia sorella Chiara (anche per il supporto chimico e "bibliografico") e Alberto, che con infinita pazienza mi è stato vicino senza mai lamentarsi. A tutti voi dico grazie, con affetto e gratitudine per l'aiuto che mi avete dato.

These three years of PhD and the writing of this thesis were long and demanding. It is correct to thank all the people that made this work possible. First, I would like to thank my supervisor, Prof. Alberto Frache, who helped me during all the PhD period, the company where I work and my manager dr. Maria Rosa Contardi since they gave me the chance to attend the PhD. I'd like also to thank the laboratory of the University of Perugia, located in Terni, which lets me use their instruments for part of my experimental work. In particular, I'd like to thank dr. Ilaria Armentano, which helped me in the experimental part; the University of Turin, with dr. Federico Cesano and Professor Domenica Scarano for the constant support in both the electrical and morphological characterizations and the data analysis.

The most important thanks are for my friends and colleagues, who have been very close to me in this period. First of all Marco, who encouraged, sustained, corrected, improved, supported and stood me constantly and daily until the end of the thesis. Emma, Antonella and Giuseppe for the undefined help in the experimental tests; Luana, Maria Teresa, Laura, Antonella and Emma (again because they count double) for the "psychological" support they gave me during these long months: they were the most efficient listeners and supporters. Finally, but with the same importance, my parents, my sister Chiara (for the chemical and "bibliographic" support too) and Alberto, who stayed with me with infinite patience without ever complaining. I say thanks to all of you, with love and gratitude for the help you gave me.

Abstract

Since their early synthetization in the 30s, the interest in polymers potentialities has continuously expanded. Nowadays, the majority of everyday devices could not exist without plastics. The combination of their light-weight, versatility, easy processability and relatively low cost makes these materials essential in several industrial sectors. Their applications, in fact, range from consumer goods to specialist devices realization. Moreover, their powerful properties can be easily exploited, in combination with the numerous manufacturing techniques, with which they are transformed. Among all, melt mixing and injection moulding processes, which are the most known and used technologies to modify polymers, are effortlessly adopted to create new materials.

Nonetheless, it is reported in literature that both these techniques and their working conditions strongly affect the final properties of the final components, in particular for what concerns the injection moulding process. It is known, in fact, that a tough orientation of molecular chains and fillers occurs inside the molten material during this process. This phenomenon creates a marked anisotropic behaviour of the final properties of the components, with a consequent non-uniform distribution of properties. Studying this mechanism is important to understand how to modify and to optimize the processing conditions, in order to tailor the final properties of the prepared materials.

This thesis aims to investigate the electrical anisotropic behaviour of injection-moulded polymeric MWCNT-based nanocomposites, correlating the variations of process conditions and the morphological and electrical anisotropic properties of thermoplastic nanocomposites. With this purpose, multi-walled carbon nanotubes/polypropylene nanocomposites were prepared and manufactured using melt mixing and injection moulding processes. The processing parameters were changed and the variations in the electrical behaviour and in the morphological structure of the nanocomposites were observed. During the melt mixing phase, the temperature of the screw profile and the MWCNTs feeding zone along the screw were modified. During the injection moulding phase, three main parameters were modulated, namely injection rate, temperature of the mould and temperature of the melt. Moreover, an innovative injection moulding process, i.e. the Heat&Cool technique, was exploited in order to vary the temperature of the mould, quickly increasing and decreasing it.

The prepared specimens were characterized electrically through DC, AC and surface resistance measurements. A multi-direction electrical testing was used to evaluate the electrical percolation threshold in the three main spatial directions, i.e. longitudinal and transversal to the flux of the molten material inside the mould and in the through-thickness direction. The morphological structure of the sample was observed through both Optical and Scanning Electron Microscopy. The influence of the change of processing parameters on these properties was deeply studied.

As main results, different levels of inhomogeneity was observed. An inhomogeneous processing-induced morphological skin-core structure in the thickness was detected. The electrical behaviour appeared non-uniform and this aspect seems to be correlated directly to the internal morphological structure of the injection-moulded parts. Then, an alteration in the electrical behaviour is also observable in different positions of the same injection-moulded sample, namely nearer to or farther from the injection gate.

Finally, the change of the processing conditions appears to play a fundamental role in the formation of both the inhomogeneous morphological structure and the anisotropic electrical behaviour of the MWCNT-based nanocomposites. In fact, the increase of the temperature of the mould and of the injection rate act as the main responsible for the decrease of the electrical resistivity of the prepared nanocomposites.

Contents

List of Figures

List of Tables

List of Abbreviations

a_1:	Unit vector 1 of the carbon hexagonal lattice
a_2:	Unit vector 2 of the carbon hexagonal lattice
AC:	Alternating current
AFM:	Atomic force microscope
$AlCl_3$:	Aluminum chloride
AsF_5:	Arsenic pentafluoride
BF^-_4:	Tetrafluoroborate
Br_2Li:	Lithium bromide
CB:	Carbon black
CCVD:	Catalytic carbon vapor deposition
CF:	Carbon fibre
C_h:	Chiral angle
ClO^-_4:	perchlorate
CM:	Compression moulding
CNF:	Carbon nanofiber
CNT:	Carbon Nanotube
CVD:	Chemical vapor deposition
D:	Screw diameter
DC:	Direct current
DSC:	Differential scanning calorimetry

EDS: Electrostatic discharge

E&E: Electrics & Electronics

EG: Expanded graphite

EMI: Electromagnetic Interference

$FeCl_3$: Iron chloride

$FeCl^-_4$: Iron tetrachloride

FESEM: Field Emission Scanning Electron Microscope

GFA: co-rotating conveying intermeshing element

GFF: co-rotating conveying non-self-wiping element

GNP: Graphite nanoplatelets

GO: Graphene oxide

HCl: Hydrochloric acid

H&C: Heat&Cool technique

H_3PO_4: Phosphoric acid

H_2SO_4: Sulfuric acid

I_2: Iodium

ICPs: Intrinsically Conductive Polymers

IM: Injection moulding

IR: Infrared ray technique

K: Potassium

KB: Kneading block

$KMnO_4$: Potassium permanganate

KS:	Kneading disc
LED:	Light Emitting Diode
Li:	Lithium
MD:	Machine direction
MFI:	Melt Flow Index
MM:	Melt mixing
MWCNT:	Multi-wall Carbon Nanotube
n:	Negative doping
Na:	Sodium
OM:	Optical Microscopy
p:	Positive doping
Pac:	Polyacetylene
PANI:	Polyaniline
PC:	Polycarbonate
PE:	Polyethylene
PEDOT:	Poly-etilendiossitiofene
PP:	Polypropylene
PPP:	Poly-para-phenylene
PPS:	poly-para-phenylensulphur
Ppy:	Polypyrrole
RC:	Resistor-capacitor circuit
SEM:	Scanning Electron Microscope

SI:	solution intercalation
SP-C:	solution processing and curing
SWCNT:	Single-wall Carbon Nanotube
TD:	Transversal direction
TEM:	Transmission electron microscope
TGA:	Thermogravimetric analysis
TSE:	Twin-screw extruder

List of Symbols

ΔH_c	[J/g]	Crystallization enthalpy
ΔH_f	[J/g]	Measured sample enthalpy
ΔH_f^0	[J/g]	Thermodynamic heat of fusion
ΔH_m	[J/g]	Melting enthalpy
ε^*	[Fm^{-1}]	Complex dielectric constant
ε'	[Fm^{-1}]	Relative permittivity, real part of the dielectric constant
ε''	[Fm^{-1}]	Loss factor, imaginary part of the dielectric constant
ε_b	[%]	Strain at break
ε_y	[%]	Strain at yield
ϑ	[rad]	Phase angle
η^*	[Pa s]	Complex viscosity
μ	[$m^2V^{-1}s^{-1}$]	Mobility of the charge carrier
φ_C	[wt%]	Percolation threshold content
φ_F	[wt%]	Filler content
π	-	Bonding orbitals
π^*	-	Antibonding orbitals
ρ	[Ωcm]	Electrical resistivity
ρ_c	[Ωcm]	Core overall electrical resistivity
ρ_s	[Ωcm]	Skin overall electrical resistivity
ρ_y	[Ωcm]	*Y*-direction overall electrical resistivity

ρ_z	[Ωcm]	*Z*-direction overall electrical resistivity
Σ	[Scm^{-1}]	Electrical conductivity
σ_{AC}	[$\Omega^{-1}m^{-1}$]	AC electrical conductivity
σ_0	-	Scaling factor
σ_y	[MPa]	Stress at yield
τ	[s]	Relaxation time
ω	[$rads^{-1}$]	Angular frequency
A_s	[cm^2]	Sectional area of the resistor
C	[F]	Electrical capacitance
C_0	[F]	Vacuum electrical capacitance
E	[MPa]	Young's elastic modulus
$E_{gap}(\pi)$	[eV]	Energetic gap referred to π bands
$E_{gap}(\sigma)$	[eV]	Energetic gap referred to σ bands
F	[Hz]	Frequency
G'	[Pa]	Shear storage modulus
G''	[Pa]	Shear loss modulus
h_s	[mm]	Thickness of the skin layer
h_c	[mm]	Thickness of the core region
I	[A]	Electrical current
l	[mm]	Length of the resistor
n	[Cm^{-2}]	Charge density
q_i	[C]	Electrical charge

R	[Ω]	Resistance
R_c	[Ω]	Core overall electrical resistance
Rs	[Ω]	Skin overall electrical resistance
R_s	[Ω/sq]	Surface resistivity
R_z	[Ω]	*Z*-direction overall electrical resistance
R_y	[Ω]	Y-direction overall electrical resistance
t	[mm]	Thickness of the sample
t	-	Dimensionless exponent
$T_{50wt\%}$	[°C]	Temperature corresponding to a weight reduction of 50wt %
Tc	[°C]	Crystallization temperature
Tg	[°C]	Glass transition temperature
Tm	[°C]	Melt temperature
T_{max}	[°C]	Temperature corresponding to the maximum rate of weight loss
T_{onset}	[°C]	Temperature corresponding to a weight reduction of 5wt %
V	[V]	Voltage
w	[mm]	Width of the specimen
X_c	[%]	Degree of crystallinity
Y	[Ω^{-1}]	Admittance
|Z|	-	Absolute module of the electrical impedance
Z*	[Ω]	Complex electrical impedance
Z'	[Ω]	Real part of the electrical impedance
Z''	[Ω]	Imaginary part of the electrical impedance

Chapter 1

Introduction

Polymers represent a wide family of materials with peculiar and appealing features for the industrial world. Several strengths, like light-weight, colourability, easy processability, recyclability and relatively low cost, have made plastic essential materials for everyone everyday life. According to a reliable statistic of PlasticEurope, one of the leading European trade associations in this field, the plastic world production in 2015 was around 322 million tonnes. Moreover, in the same year, the 70% of plastic demand in Europe was concentrated in six countries. Italy occupied the second position in this classification, with a plastic demand of about 14% of the totality [1].

Plastic materials are largely used in a variety of applications, such as packaging, automotive, building and construction, agriculture, biomedical, electric and electronics. In some of these applications, polymers are used for their thermal and electrical insulating properties. Although this characteristic could be important in many fields, it becomes a limitation in other specific industrial sectors, in which both electrical and thermal conductivity are necessary.

Table 1: Electrical resistivity of thermoplastic, thermosetting polymers and elastomers.

Polymer	Electrical Resistivity [Ωm]
Polyamide 6 (PA6)	6×10^{11}
Polyamide 66 (PA66)	1.5×10^{13}
Polycarbonate (PC)	4×10^{13}
Polyethylene (PE)	10^{13}
Polypropylene (PP)	1.2×10^{14}
Polyethylenterephtalate (PET)	10^{17}
Polymethyl Methacrylate (PMMA)	10^{12}
Polystyrene (PS)	$10^{15} - 10^{17}$
Neoprene	10^{9}
Silicon Rubber	10^{12}
Phenolic Resin	10^{10}
Epoxy Resin	$10^{10} - 10^{14}$

From the electrical point of view, two are the traditional main requirements, which conductive plastics are asked to fulfil: electrostatic dissipation in EDS (i.e., electrostatic discharge) applications [2, 3, 4 and 5] and electromagnetic shielding n EMI shielding devices [6, 7, 8 and 9].

The accumulation of electrostatic charges on the surfaces of electrical and electronic devices can be due to sparks and electric arcs, arising during a grounding discharge. It may constitute a problem in terms of people safety and integrity of the devices themselves. On the other hand, it is important to underline how critical electromagnetic interference and its shielding could be.

Most of the electronic goods, such as televisions and stereo-systems, typically have analog and digital circuits, very close to each other. These circuits may suffer the influence of interferences from external sources, and therefore they require some kind of electromagnetic shielding.

Another challenging area of research concerns the use of electrically conductive polymers in multifunctional integrated devices, particularly in the automotive sector. Reducing the use of copper and other metals in dashboard sensors and replacing them with conductive compounds are becoming needs for the biggest carmakers. This leads to considerable advantages in terms of both weight reduction and cost of separating the metal component from the polymeric ones in the post-consuming phase. National research projects [10, 11] have faced this demanding task. As an example, as output of the project itself, an innovative process for creating electrically conductive or piezo resistive traces by using a laser beam has been studied [12].

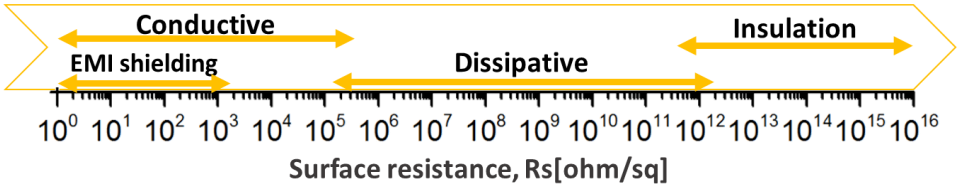

Figure 1: Different surface electrical resistivity in order to cover several applications in E&E industrial sector.

1.1. Scope and structure of this thesis

The aim of this project is to investigate the correlation between the electrical and the morphological anisotropic behaviour of injection-moulded PP/MWCNT nanocomposites. The thesis is structured into five chapters, in which the electrical properties in the three main directions, the morphological structure of the injection-moulded components and the influence of the processing techniques and conditions on these features are presented.

In **Chapter 1** a global state of the art on the main topics discussed in this work is reported. This chapter is structured in four main thematic sections, in order to illustrate all the aspects related to this research. First, the theory of the electrical conductivity of polymers and a focus on the available technical solutions to improve

the electrical conductivity of typically insulating materials like polymers are reported. Then, a description of the electrical percolation theory for nanocomposites filled with electrical conductive fillers is delineated. After, the main polymers manufacturing techniques (i.e. melt mixing and injection moulding processes) are explained. In this section, a specific paragraph is dedicated to the description of an innovative injection moulding technique Heat&Cool. Finally, a discussion of the state of the art related to the effect of the modification of the processing conditions on the electrical properties of the nanocomposites is reported.

Chapter 2 briefly describes the experimental section. A complete description of the nanocomposites preparation is reported. The melt mixing and injection moulding processes are described, particularly taking into account the variations of the processing conditions from the standard ones. Moreover, a detailed explanation of the characterization methods both morphological and electrical are reported. Standard and non-conventional DC and AC conductivity techniques are exploited in order to study the 3D electrical conductivity over the specimens. Optical and scanning electron microscopy are used to investigate the morphological structure of the prepared nanocomposites and to correlate it to their electrical behaviour.

In **Chapter 3** the electrical behaviour of the MWCNT-based nanocomposites, prepared with a conventional injection moulding process, and the presence of an anisotropic process-induced skin/core structure are studied by both electrical and morphological analysis. A theoretical mathematical model is proposed in order to explain the formation of this structure and to correlate morphology to electrical properties. Complete thermal, mechanical and rheological characterization of the nanocomposites were performed. Part of the related results are extracted from the published paper "Relationship between morphology and electrical properties in PP/MWCNT composites: Processing-induced anisotropic percolation threshold" *Materials Chemistry and Physics* 180 (2016) 284-290.

Chapter 4 is focused on in-depth studying the effect of the modification of the processing conditions on the electrical properties and the morphology of the injection-moulded parts. The influence not only of the changes of melt mixing conditions but also of the modification of the injection moulding parameters (i.e. injection rate, mould temperature and melt temperature) were investigated. An innovative injection moulding technique was used in order to manufacture the MWCNT-based nanocomposites. The Heat&Cool dynamic injection-moulding process, which leads to heat and cool the mould surfaces rapidly, was adopted in order to tailoring the electrical properties and the morphological structure of the

final components. Moreover, the electrical and morphological behaviour of different areas of the injection-moulded samples (in particular, nearer and farther the injection gate) was studied. The AC electrical behaviour was also measured for the MWCNT-based formulations. A complete morphological characterization was performed.

Finally, in **Chapter 5** general conclusions are reported.

1.2. Electrical conductivity of polymers

Electrical conductivity is a physical property, which represents the ability of a material to carry an electrical current. The transport of electricity through matter always requires the presence of charged particles. Conductors usually consist of a regular lattice of atoms, in which free electrons can move and transport electricity through the material. Typically, metals, graphite, and a few other chemical compounds belong to this group. On the other hand, polymers do not belong to this group and their electrical behaviour is not simply regulated by the conventional solid-state physics, characteristics of covalent crystals. Therefore, compared with well-ordered materials, polymers are disordered and often weakly bonded. These aspects affect the properties of plastic materials and from the electrical point of view, polymers are insulators with a reduced capacity of charge conduction.

According to Ohm's law, for metallic materials, (1.1) the voltage is proportional to the flowing current as reported below:

$$V = R \cdot I \tag{1.1}$$

where, V is the voltage (V, in Volt), R is the resistance of the system (ohm, Ω) and I is the flowing current (ampere, A). The electrical resistance is so defined as the ratio of the voltage and the electric current. It is linked to the geometrical factors of the device, in which a current flows and a voltage is applied. It can be described in terms of the resistivity ρ, as reported in (1.2):

$$R = \rho\left(\frac{l}{A_s}\right) \tag{1.2}$$

where l is the length and A_s is the section area of the material. Moreover, if A_s is considered as the product of width and thickness, another electrical parameter can be calculated. The surface resistivity R_s, which can be defined as the electrical

resistance existing between two parallel electrodes in contact through the surface of the material, can be derived from 1.2 as follows:

$$R = \rho\left(\frac{l}{A_s}\right) = \rho\left(\frac{l}{w \cdot t}\right) = \frac{\boldsymbol{\rho}}{\boldsymbol{t}}\frac{l}{w} = \boldsymbol{R_s}\frac{l}{t} \quad (1.3)$$

where, *w* is the width and *t* is the thickness of the tested specimens, respectively. Resistivity is an intrinsic property of each material and it considers the nature of the electrical resistance of the material [13].

Correspondingly, the inverse of resistivity is the electrical conductivity, which is related to the ability of a material to conduct an electric charge [14].

$$\sigma = \frac{1}{\rho} \quad (1.3)$$

In turn, the conductivity is linked to two fundamental parameters, the density *n* and the mobility μ of the charge carrier,

$$\sigma = \sum_i q_i n_i \mu_i \quad (1.4)$$

where q_i is the charge of the i^{th} species. These parameters, in polymers, suffer of several external factors, such as the environment (i.e. temperature, atmosphere, and moisture), the applied potential and the manufacturing process conditions.

The bulk structure determines several properties of the polymer. As already well known, polymers have both regular crystalline and disordered amorphous regions. From the properties point of view, thinking of polymers as a continuous amorphous matrix, in which crystalline regions are present, is more convenient. Electrically speaking, these ordered zones modify the conductivity of the polymer, lowering it. It depends on the conduction mechanisms. If an ionic conduction occurs, the mobility of the ions through the crystalline zones will be low. On the other hand, if an electronic conduction occurs, it will be faster but the interface between the crystalline and amorphous regions will act as a trapping region. Therefore, the correct energy graph for a polymer is reported in Figure 2. The uniform crystalline region, with a regular distribution of atoms, is surrounded by amorphous zones. In the amorphous region, energy states are neither uniform nor well distributed. Boundaries consist of the interface areas between crystalline and amorphous regions [15].

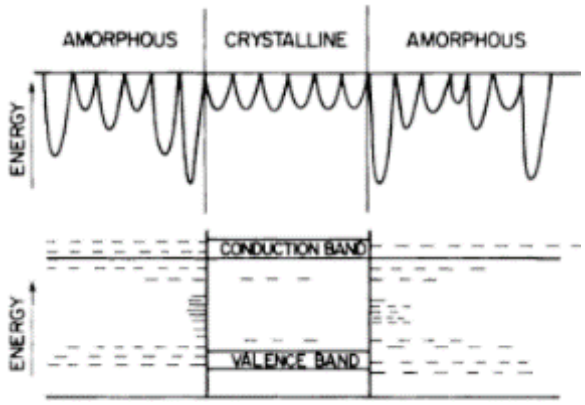

Figure 2: Energy state diagram for polymer with crystalline and amorphous zones [15].

Dielectric spectroscopy

The dielectric and electric properties of polymers can be measured as a function of frequency (time) by dielectric spectroscopy. This technique is based on the interaction of an external electric field with the electric dipole moment and charges of the polymer. A polarization occurs and the atomic and molecular charges are displaced from their equilibrium. Several polarization mechanisms can occur. Electronic polarization induces a dipole moment, moving electrons from their equilibrium positions. Atomic polarization creates a disequilibrium between two ions of opposite charge and again, a dipole moment is induced. In polymers, polarization is mainly due to charge migration and orientation of permanent dipoles. In the first case, conductivity is generated by migration of both extrinsic (like impurities) and intrinsic (like migrating protons) charges. In the second kind of polarization, permanent dipoles are oriented in the applied electric field direction and an orientation occurs. This polarization includes time-dependent motions of molecular segments, which are measurable by dielectric spectroscopy. The loss of orientation of dipoles after removing the electric field is called dipole relaxation.

Dielectric measurements are based on the evaluation of the impedance Z, which in alternating current (AC) measurement, corresponds to the ratio between the applied voltage V and the resulting current I. Since in this kind of system the amplitude and the phase angle of both output and input quantities may change, the impedance is expressed as a complex number. Its component results in the relation below:

$$Z = Z' - iZ'' \tag{1.5}$$

where, Z' and Z'' are the real and imaginary parts of the impedance, respectively. Its reciprocal value is the admittance, Y.

Dielectric spectroscopy allows performing several model studies on equivalent circuits, formed by different compositions of resistors and capacitors. In these circuits, a resistance (R) represents the dissipative part of the dielectric, whereas a capacitance (C) is the storage component and corresponds to the ability of storing the electric field. Various combinations of polarization mechanisms can be described with different combination of series and parallel of resistors and capacitors circuits. An RC parallel circuit, as shown in Figure 3, is the simplest possible combination and can be used to model charge migration polarization in a given frequency range [16].

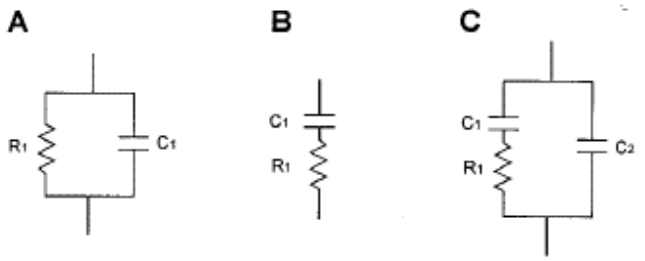

Figure 3: Equivalent circuits for the material properties modelling [16].

The impedance is the sum of the contributions of resistance and capacitance:

$$\vec{Z} = \frac{1}{\frac{1}{R}+i\omega C} \tag{1.6}$$

where, $\omega = 2\pi f$ is the angular frequency. The real and imaginary components of Z are:

$$Z' = \frac{R}{1+(\omega CR)^2} \tag{1.7}$$

and

$$Z'' = -i\frac{\omega CR^2}{1+(\omega CR)^2} \tag{1.8}$$

When resistance and capacitance are in series (as in Figure 3B), the classic Debye equations for a single dipole with a single relaxation time occurs. Nevertheless, the contribution of atomic and electronic polarization to the stored

energy is always present and it can be represented by a further capacitance in parallel with the RC series. The obtained admittance of that circuit, given in Figure 3C is:

$$\vec{Y} = i\omega C_2 + \frac{i\omega C_1(1-i\omega\tau)}{1+(\omega\tau)^2} \quad (1.9)$$

where, $\tau = RC_1$ and corresponds to the relaxation time of the system. The admittance is often reported in terms of the complex dielectric constant:

$$\varepsilon^* = \varepsilon'_\infty + \frac{(\varepsilon'_0-\varepsilon'_\infty)}{1+i\omega\tau} \quad (1.10)$$

By separating equation (1.10) into its real and imaginary components, the Debye equations (1.11) and (1.12) can be obtained:

$$\varepsilon'(\omega) = \varepsilon'_\infty + \frac{(\varepsilon'_0-\varepsilon'_\infty)}{1+(\omega\tau)^2} \quad (1.11)$$

$$\varepsilon''(\omega) = -i\frac{(\varepsilon'_0-\varepsilon'_\infty)\omega\tau}{1+(\omega\tau)^2} \quad (1.12)$$

The complex dielectric properties, the relative permittivity, ε' and the loss factor, ε'' are functions of frequency. The plot, in the complex plane, of ε' versus ε'' is a semicircle, known as the Cole-Cole plot [16, 17]. In the same way, the plot of imaginary versus real part of the impedance is called Nyquist plot. An RC parallel equivalent circuit produces a semicircle and the equivalent resistance is the result of the intersection between the semicircle and the Z' axis. Another possible graph, the Bode plot, consists in the absolute value of impedance ($|Z| = \sqrt{[(Z')^2 + (Z'')^2]}$), as a function of the logarithm of frequency. At higher frequencies, a purely capacitive dielectric response is obtained and impedance is directly proportional to frequency. The third possible representation is based on imaginary impedance as a function of frequency. Three zones are shown: a low frequency region where electrode polarization dominates, a middle frequency zone where migrating charges polarization has a major role, and a high frequency zone where dipole relaxation governs. The three described graphical representations are reported in the Figure 4 below.

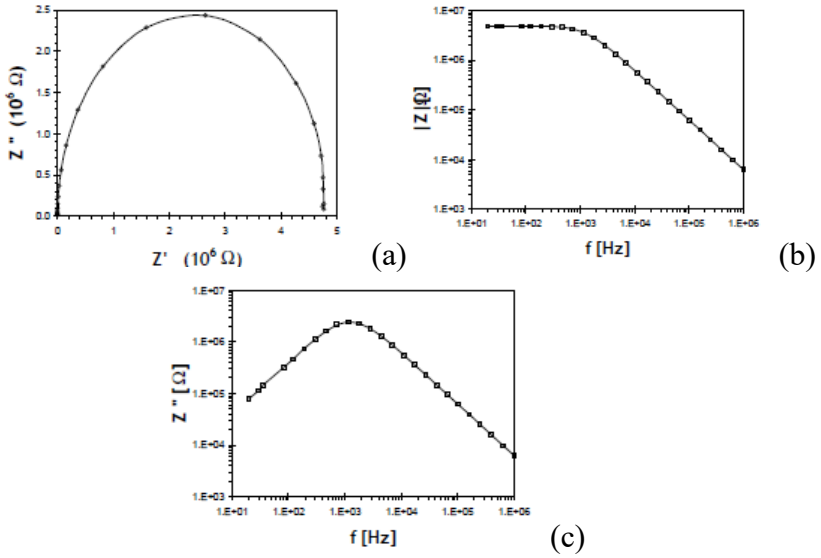

Figure 4: (a) The Nyquist plot; (b) The Bode plot; (c) Z'' vs. frequency [16].

It is worth summarizing the global electrical conductivity of a material, which is formed by the sum of both DC and AC electrical resistivity. The first contribution is due to the movement of electrons in phase with the applied electric field and it is usually independent of frequency. On the contrary, the AC contribution is directly dependent of the angular frequency. In an insulating material, the dipole reorientation is the dominant mechanism of electrical conductivity and this phenomenon, related to AC resistivity, continuously increases with frequency. Conversely, in a conductive material, the transport of charges in phase with the applied electric field and independent of frequency, is predominant and, for this reason, the AC contribution can be considered negligible with respect to the DC.

In a conductive filler/polymer nanocomposite, the electrical conductive behaviour is different and it strongly depends on the ratio between filler and matrix, and the aspect ratio, alignment and dispersion of fillers. When the filler content is low, the insulating polymer matrix controls the electrical resistance, and the AC frequency-dependent conductivity dominates. As the filler content increases, a transition from an insulating to a conductive behaviour near the percolation threshold occurs. In this region, electrical charge transport mechanisms, like conduction, hopping, and tunnelling contribute to reduce the overall electrical resistance. Conduction requires a physical contact between neighbouring fillers in order to have a transfer of charge from one to another. On the other hand, hopping and tunnelling mechanisms occur without any physical contact.

In nanocomposites, also a critical frequency (f_c) characterizes the electrical transition from insulating to conductive behaviour: below f_c the DC current becomes dominant, while beyond such frequency, the AC current coming from dipole reorientation prevails. Consequently, the global electrical conductivity can be considered frequency-independent in the lower frequency range. A continuous increase of the filler content provides a higher number of filler connections and therefore a flow of electrical charge. In this way, the overall conductivity becomes frequency independent in the entire frequency range [18].

1.3. Intrinsically Conductive Polymers

In the last decades, many studies have been dedicated to find alternatives to the limiting aspect of the insulating nature of polymers. A possible solution is represented by the polymerization of Intrinsically Conductive Polymers (hereinafter named ICPs) [19, 20 and 21]. Studies on these particular materials started in 1977, when Heeger, McDiarmid and Shirakawa found out that polyacetylene (PAc) could become electrically conductive itself, after an adequate pre-treatment [22]. The phenomenon of their electrical conductivity can be explained with the conduction bands theory, developed for inorganic conductive materials. In traditional polymers, the electronic structure of the macromolecular backbone is completely constituted by σ bands. A high energetic gap between bonding and antibonding levels, $E_{gap}(\sigma)$, makes polymers insulating materials. For polyethylene, for example, this energetic gap is around 8 eV. A continuous network of adjacent double bonds, instead, constitutes conjugated polymers as ICPs. Carbon atoms with hybridization sp^2 build σ bonds while a p_z orbital allows a π overlapping with another p_z orbital of an adjacent carbon atom.

This generates an electronic delocalization along all the polymeric chain and, increasing the number of conjugated double bonds, two bands, a valence and a conduction one, respectively are produced. It is a fundamental condition for the polymer conductivity. The valence band is full of electrons and it is constituted by π bonding orbitals, while the conduction band is completely empty and it is constituted by π* antibonding orbitals. The amplitude of the energetic gap $E_{gap}(\pi)$, originated between these two bands, tends asymptotically to a limit value, inferior to $E_{gap}(\sigma)$, and determines the intrinsically electrical properties of the polymer (see Figure 5). Typical values of $E_{gap}(\pi)$ for conductive polymers are around 1- 4 eV [23].

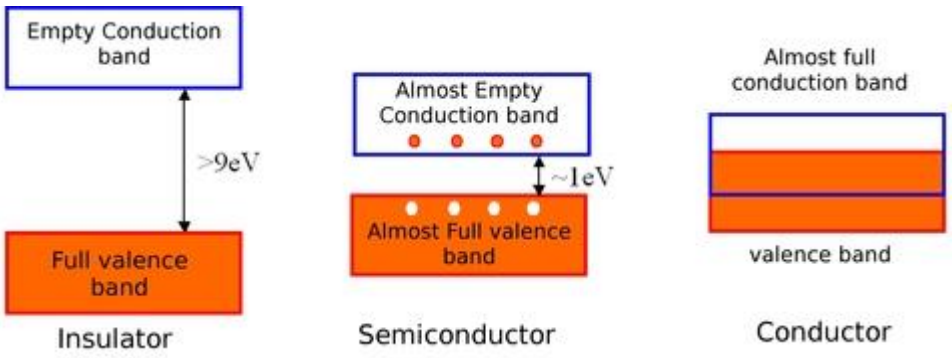

Figure 5: Typical E_{gap} for insulators, semi-conductors and conductors materials.

In order to obtain high values of conductivity, the polymer needs a doping treatment with appropriate chemical species: it consists in an electrical charge transport. There a two different possibilities of doping. The first one occurs when electron acceptor substances, such as Lewis acids like $FeCl_3$, I_2, $AlCl_3$, are added to the polymer. In this case, a *p* (positive) doping is done: the polymer tends to leave electrons, creating positive charges along the macromolecule. Consequently, there is the formation of new energetic levels, which place themselves between the valence and the conduction bands. These levels are actually responsible for conductivity in conjugated polymers.

The second possibility of doping arises when electron donors, such as alkaline metals or liquid ammonia, are added to the polymer. An *n* (negative) doping occurs. The obtained electrical conductivity of ICPs gives them both semiconductor and conductor properties, if they are in the neutral state or in the doped state respectively. On the contrary, when an insulating polymer is present, the possible electronic transitions are only of σ type and the correspondent energy gap $E_{gap}(\sigma)$ results so high that no electrical conductivity is possible in the material [24, 25].

ICPs have a great advantage: they combine high electrical conductivity, typical of metals, and light-weight typical aspect of polymers. Besides PAc, other ICPs are poly-para-phenylene (PPP), poly-para-phenylensulphur (PPS), polyaniline (PANI), polypyrrole (PPy), poly-etilendiossitiofene (PEDOT) [24]. The electrical conductivity of these polymers can range from $< 10^{-10}$ S/cm, typical value for insulators, to $\approx 10^{-5}$ S/cm, corresponding to a semiconductor conductivity, to greater than 10^{4} S/cm, peculiar value for conductors, nearly similar to metals [26, 27]. Typically, ICPs are used in industrial applications in metal replacement. When these polymers are in their electro-conductive doped state they can be used in several sectors, such as corrosion resistant coatings [28, 29], batteries [30],

electrochemical cells [25], sensors [31]. Conversely, when ICPs are in their semi-conductive neutral state, their properties can be modulated and modified. In this way, new possible fields of applications open up. As examples, they can be used as LEDs [32] and photovoltaic cells [33].

Although these promising properties, ICPs are expensive polymers and their high cost is mainly due to long and complicated processes of polymerization and doping. In order to obtain the desired conductivity values, a specific planning of the chemical structure has to be designed [34]. For these reasons, right now, ICPs are not suitable materials for a large-scale industrialization and for typical plastic processing techniques.

Table 2: Conductivities of ICPs with selected dopants [30].

Polymer	**Doping materials**	**Conductivity [Scm^{-1}]**
Polyacetylene	I_2, Br_2Li, Na, AsF_5	10^4
Polypyrrole	BF^-_4, ClO^-_4, tosylate	500 – 7.5 x 10^3
Polythiophene	BF^-_4, ClO^-_4, tosylate, $FeCl^-_4$	10^3
Polyphenylene	AsF_5, Li, K	103
Polyfuran	BF^-_4, ClO^-_4	100
Polyaniline	HCl	200

1.4. Electrically conductive fillers

Mixing polymers with a conductive filler could be a valid alternative to ICPs, not only from the economical point of view, but also and probably most important from the processability point of view. In this way, a new composite material is produced with different and improved properties compared to the neat polymer. Carbon-based and metallic fillers are mostly used with this purpose. In particular, carbon-based fillers include carbon black, carbon fibres, carbon nanotubes (single and multi-walled), graphite (also in its expanded form), graphene and all the graphene

related materials (as examples, graphene oxide or reduced graphene oxide). On the other hand, several metallic fillers, in fibres, particles or powder form, are employed in order to enhance electrical properties of polymers.

1.4.1. Metallic fillers

The interest for metal-based composites is mainly due to the possibility of obtaining a conductive behaviour, both electrical and thermal, close to that of the metallic fillers, maintaining typical physical properties of plastics, like their processing advantages and mechanical properties [35, 36]. Using metallic additives in polymers opens a variety of possible applications, such as anti-fouling, corrosion-resistant paints, and maintenance and repair products. In particular, metallic compounds are widely used in EMI shielding devices.

These composites exhibit enhanced conductivity properties, which can be strongly affected by many factors, such as fillers concentration, size and shape of the particles, volume fraction and spatial arrangement in the matrix, interactions between fillers and matrix and manufacturing process [37]. Boudenne et al. [38], in fact, demonstrated that metallic particle sizes deeply influenced the electrical conductivity behaviour and the percolation threshold of PP/copper-based composites. The smaller the used fillers are the lower the obtained percolation threshold is. The probability to form a conductive path with the smaller particles is higher, indeed, than with the larger ones.

Diverse metallic particles can be used, namely nickel, copper, silver, aluminium and iron. These additives, in form of powders, show a defined morphology and a higher intrinsic conductivity than traditional carbon-based fillers, like carbon black [39]. Nevertheless, a density increase is also reached when significant metal loadings are employed. This aspect limits their use in those applications in which light-weight is required. Metallic fillers were used both in thermoplastic polymers and in thermosetting resins, obtaining satisfying conductive results [38, 40, 41 and 42]. Finally, it is worth mentioning steel fibres, typically used in EMI shielding applications: they guarantee high electrical conductivity with content of about 15wt %.

1.4.2. Carbon-based fillers

Among the carbon-based fillers, carbon black (hereinafter CB) is the most used and the most known additive to make polymers conductive. CB is virtually pure basic carbon in the form of colloidal particles. They are produced by incomplete combustion or thermal decomposition of gaseous or liquid hydrocarbons under

controlled conditions. Its physical appearance is that of a black, finely divided pellet or powder. They are aggregates of microcrystals of graphite and their characteristic size is around 10 and 500 nm. Observing CB particles under an electron microscope, they have a spherical structure. Three main characteristics of these particles - their size, structure and surface chemistry - constitute the basic properties of CB. These three aspects, in fact, have a large effect on practical properties of CB, such as its blackness and ease of dispersion, when it is added to polymers.

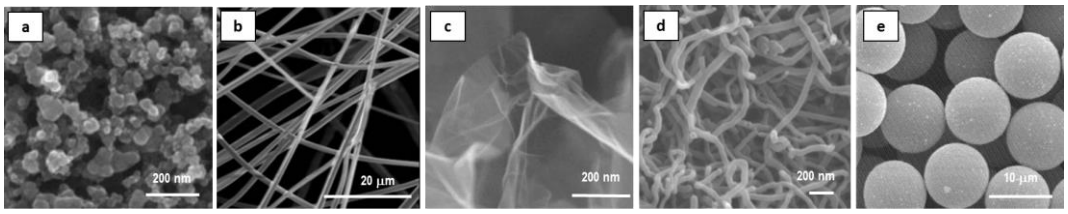

Figure 6: Electron microscope image of several conductive particles: (a) carbon black, (b) carbon fibres, (c) graphene, (d) carbon nanotubes, (e) steel.

The diameter of the particles is a fundamental property: in general, the smaller the particle size is, the higher the blackness of CB is. Despite this, dispersion becomes difficult due to an increase in coagulation forces. The size of the structure itself also affects CB blackness and ease of dispersion. Generally, the increase of structure size improves the dispersion of the additive in a polymer matrix, but lowers blackness. CB with a larger structure shows excellent conductive properties. Finally, from the chemical point of view, various functional groups exist on the surface of CB. When a large amount of hydroxyl groups, due to the oxidation treatment, are present, CB has a greatly enhanced affinity with the polymer in which it is embedded and it shows better dispersion capacity [43].

As reported in literature, CB contributes to electrical conductivity rather than to thermal conductivity [44, 45 and 46]. CB has a relatively low cost and a high conductive efficiency if compared with other carbon-based fillers. Nevertheless, as said before, it is important to underline that the term carbon black represents a family of fillers and each component differs from the other for its purity, size of its particles and its intrinsic peculiarities [47]. All these parameters influence the properties and the cost of the final products. Current worldwide production is about 8.1 million metric tons per year. Approximately 90% of CB is used in rubber applications (a typical use is in tires), 9% as a pigment in printing inks or coatings, and the remaining 1% as an essential ingredient in hundreds of various applications in plastic products (in relation with its conductive properties) [48, 49].

Especially for this last sector, many experimental and commercial grades have been studied and fine-tuned in order to obtain the highest electrical conductive value at the lowest quantity of additive in the formulation [50, 51, 52 and 53]. Concerning this point, it is necessary to note that CB reaches competitive conductivity only with high amount in compound, if compared with other conductive fillers. This is a consistent drawback, not only from the economical point of view, but also from the properties of the final component point of view: elevated quantities affect the mechanical properties, increasing the brittleness of the material [54].

Differently from carbon black, carbon fibres (CFs), typically vapor grown carbon fibres, guarantee at the same time good electrical and mechanical performance. CFs are one-dimensional fillers and, due to their circular shape parallel to the axis of the fibre, an anisotropic behaviour both for mechanical and conductive (thermal and electrical) properties is present [37]. The anisotropy could be intensified during the processing phase (i.e. extrusion or injection moulding). For this reason, a precise and preliminary design of the final product is necessary, in order to reach the desired performance.

Graphite and all its chemical and physical variations, up to graphene, represent another family of possible carbon-based fillers. Compared to above cited additives, graphite does not provide high electrical conductivity. It is more often used in applications, in which thermal conductivity is required. Graphite is characterized by a lamellar structure in which all layers are stacked on top of each other. Based on the exfoliation level, a multi-layer traditional graphite can be obtained as far as a single layer of graphene. Generally, the higher the exfoliation grade is, the less the needed filler content is. However, this assumption is actually true as long as the exfoliation process does not affect the quality and the surface dimensions of the additive.

It is necessary dedicating some words to graphene since a growing interest is arisen around this challenging material in the last decade. It was found from the bulk graphite the first time in 2004 [55]. Graphene is composed by one atom-thick two-dimensional layers of carbon atoms (sp^2 bonded), arranged in a repeating hexagonal lattice [56]. This filler has been attracted great interest due to its outstanding unique electric, mechanical (1.0 TPa for Young's modulus and 130 GPa for tensile strength) and thermal (5300 W m^{-1} K^{-1}) properties [57, 58 and 59]. Several methods have been exploited to obtain graphene (such as micromechanical exfoliation of graphite [55], chemical vapor deposition on metal substrates [60], thermal or chemical reduction of graphene oxide [61] or exfoliation of graphite

intercalation compounds [62]), but its intrinsic features, strictly depending on its purity, are strongly affected by the synthesis method [63]. Commercially, it is very difficult to purchase high-purity grades of graphene and often expanded graphite (EG), graphite nanoplatelets (or nanoplates, GNP) or graphene oxide (GO) are sold as pure single layer graphene. This is a big problem from not only the properties point of view, but also economically speaking. As it is well known, a significant difference in price distinguishes graphene from all other carbon-based fillers. It guarantees higher performance but it has a higher cost compared to carbon black or graphite. Moreover, a great confusion is generated because of all these different kinds of materials and different referred terms. For this reason, recently, a complete classification of all graphite-related materials has been done, in order to give a more precise definition and clarity. Consequently, as an example, it is worth to differentiate between GNPs, which are two-dimensional materials with thickness or lateral size less than 100 nm and GO, which represents a specific grade of graphene with extensive oxidation [64]. In order to obtain a lower percolation threshold and possibly a lower cost, a different solution can be adopted. More than one carbon-based fillers, preferably with different aspect ratios, can be used to create hybrid conductive blends [65 – 70]. Several studies [65, 69] demonstrated theoretically that the conductive path can be created with a combination of different carbon-based fillers and that the portion of fillers with higher aspect ratio mostly influences the percolation threshold in the hybrid system. Percolation thresholds of these systems are usually next to the average value of the systems in which only one kind of filler is used. Economically, this is a great advantage, because a large amount of high-aspect-ratio and expensive fillers can be substituted with low-aspect-ratio and cheaper fillers. Additionally, mixtures between conductive fillers and non-conductive fillers have been investigated. Grunlan et al. [67] observed an increase in electrical conductivity when a small amount of clay was added to the polymer blend in presence of CB. Furthermore, the use of large quantities of calcium carbonate in conductive compounds, based on MWCNTs, seems to reduce the electrical resistivity of the final compound [65].

1.4.2.1. Carbon nanotubes

A separated paragraph has to be dedicated to carbon nanotubes (hereinafter CNTs), which were used as the carbon-based conductive fillers in this thesis work. Since 1991 when Sumio Iijima discovered CNTs [71] as secondary products of fullerene production, the attention around these materials has grown exponentially. In the last decades, scientific interest around this subject was mostly dictated by the potentialities of CNTs from mechanical, thermal, electric and electronic points of view. Indeed, they are considered stronger than steel and harder than diamond, with electrical and thermal conductivities higher than traditional metals. These extraordinary characteristics led to thousands of publications and patents on potential CNTs application sectors, also in daily life, such as transport, health and environment. Nevertheless, they struggled to become widespread commercial products. Originally, the bottleneck was represented by a limited and non-constant quality production, with the related consequence of an uncompetitive cost of CNTs compared with other traditional carbon-based fillers [72, 73]. In the last years, instead, CNTs acquired a complete maturity on an industrial scale: simultaneously their price decreased and their quality increased. A special interest is represented not only by their overwhelming electrical properties, but also by the possibility of obtaining polymer nanocomposites, exploiting typical plastic manufacturing techniques. In this way, CNT-based nanocomposites with superior electrical properties can be prepared.

Two main types of CNTs are produced. Single-walled carbon nanotubes (SWCNTs) consist of a single layer of graphene wrapped seamlessly in a cylinder-shape tube. They usually have diameters from a minimum of 0.7 nm to a maximum of 10 nm (averagely less than 2 nm) and a length up to centimetres. [74, 75, 76]. On the other hand, multi-walled carbon nanotubes (MWCNTs) include an array of such tubes, which are concentrically disposed. They can typically have diameters from 2 nm to 100 nm and lengths of tens of microns [76, 77].

Different tubular structures are possible, namely armchair, zigzag or chiral shapes (Figure 7 and 8). They depend on how the graphene layer of the nanotube is rolled up. As illustrated in Figure 7, two are the main parameters, which determine a structure over another one: the chiral vector ($C_h = na_1 + ma_2$) and the chiral angle, between C_h and a_1, unit vector of the carbon hexagonal lattice. When n and m are equal and the chiral angle corresponds to 30°, an armchair SWCNT is obtained. Then, if m or n are zero and the chiral angle is zero, the nanotube has a zig-zag structure. Finally, if the chiral angle has a value between 0° and 30°, a chiral nanotube is achieved [78].

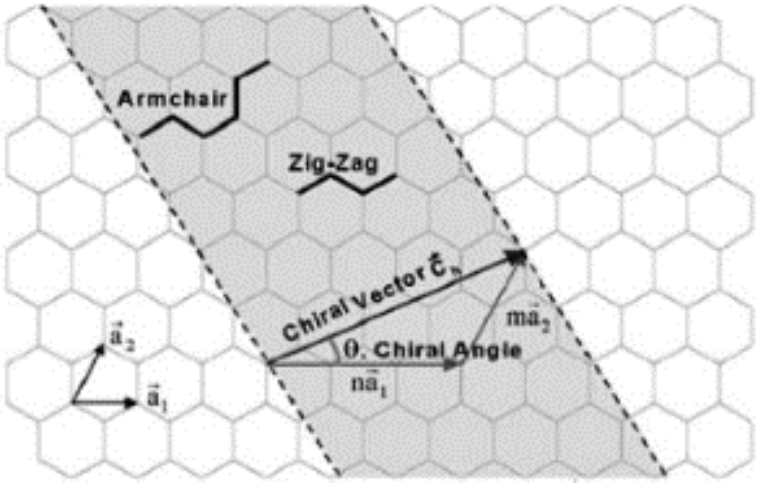

Figure 7: Schematic rolling up of a graphite sheet in order to form a CNT [78].

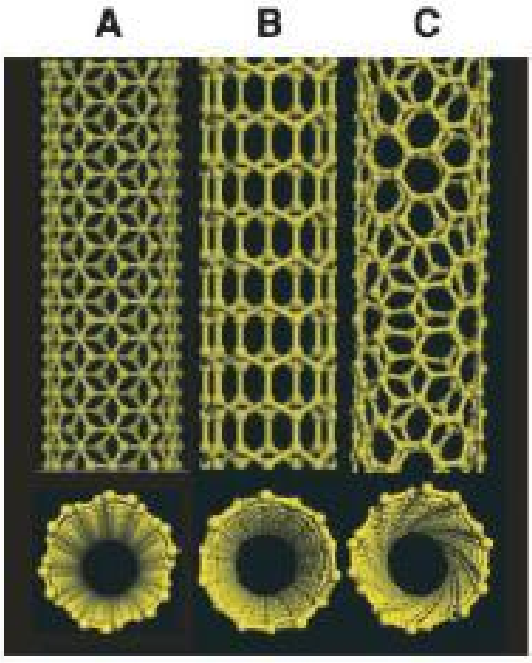

Figure 8: Different structural configuration for SWCNTs: A. armchair, B. zigzag, C. chiral [77].

Their very high aspect ratio (ratio between length and diameter, in general 10^3 – 10^5) lets to consider them virtually as mono-dimensional nanostructures and for this reason, they have peculiar and unique properties.

From the electrical point of view, CNTs may behave as metallic or semiconducting materials, depending on the rolling up of the graphitic sheet. Because of the nearly one-dimensional structure, electronic transport in metallic CNTs occurs without scattering along nanotube lengths. This aspect enables them to carry current capacity 1000 times higher than copper wires and without heating [79, 80 and 81]. Thermally, their properties are specifically due to the easy propagation of phonons along the nanotube. A phonon is a quantum acoustic energy, result of CNTs lattice vibrations [82, 83]. The thermal conductivity, measured at room temperature, for a MWCNT is around 3000 W/mK and it is greater than that of natural diamond [77, 78 and 84].

Also from the mechanical point of view, CNTs are promising materials. Wong et al. [85] performed the very first direct tensile measurement on MWCNTs. Using an atomic force microscope (AFM) they obtained an average Young's modulus value of 1.28 TPa and a first bending strength measurement of about 14 GPa. Nevertheless, Yu et al. performed the last measurement. They obtained a stress–strain curve, using an electron microscope. The measured values are 0.27–0.95 TPa for the modulus and strengths are in the range of 11–63 GPa [86]. On the other hand, a complete measurement on SWCNTs resulted more problematic, due to difficulties in their handling. However, Salvetat et al. observed a tensile modulus of 1 TPa for small diameter SWCNT bundles [87]. Again Yu et al. managed to measure tensile moduli in the range of 0.32–1.47 TPa and strengths between 10 and 52 GPa. [81, 88].

The first technique, used for the production of MWCNTs, was the arc growth [89]. In any case, commercially the most attractive method is the chemical vapor deposition (CVD), typically on catalytic particles [72, 90]. This kind of process provides high CNTs yield and a low cost production. Several more processes can be exploited in order to induce the carbon vaporization: some examples, as reported in Figure 9, are electric arc discharge, laser ablation or solar energy [91]. Using chemical methods represents a valid alternative to the above-mentioned physical techniques. A possibility can be the synthesis of carbon materials through a catalytic decomposition or electrolysis of hydrocarbons. Another option is using a heat treatment of a polymer or a low temperature pyrolysis [92]. Some other methods for CNTs production are plasma torch method [93], underwater AC electric arc method [89] and production in a microgravity environment [94].

Obtaining SWCNTs to a large industrial scale is presently difficult and they are very expensive and still produced on a small scale. Synthesis methods for SWCNTs result in high quantities of impurities, which are usually eliminated through an acid treatment, with a consequent further increasing in SWCNTs cost. Moreover, this process though introduces other impurities and a decrease in the nanotube length. It is clear that the production process method strongly affects the CNT properties, even if they can be tuned by a modification of the diameter. Commercial access to MWCNTs is typically less problematic [77, 78].

In the last decades, the use of CNTs created a new class of nanocomposites. Commercially, in particular MWCNTs were first used as electrically conductive fillers in polymer nanocomposites. Due to their high aspect ratio and with respect to the used polymer matrix, worthy conductivity values (0.01 to 0.1 S/cm) were obtained with quantities in compounds as low as 5wt %. Much lower levels are necessary for EDS automotive applications, such as fuel lines and filters. Moreover, CNT-based nanocomposites have been used as electrostatic assisted painting for mirror housings and as EMI shielding devices for the microelectronics industry.

It is important to note that relevant electrical conductivities can be achieved, maintaining other performance, such as mechanical and rheological properties, especially needed for thin moulding applications. In fact, the incorporation of CNTs in polymer nanocomposites leads to a contemporaneous increase in elastic modulus and mechanical strength [78, 95]. Gojny et al. demonstrated that around 1wt % of MWCNTs in a thermosetting resin like epoxy can enhance stiffness and fracture toughness by 6 and 23%, respectively [96]. Other studies proved the role of CNTs as reinforcing fillers not only in polymers [97], but also in metallic and ceramic materials [98, 99]. Properties improvement is due to several factors, such as CNTs diameter, their aspect ratio (L/D), the alignment in the matrix, their dispersion and the interfacial interaction between matrix and CNTs themselves. From the mechanical point of view, the critical point is precisely the dispersion of the nanotubes in the polymer matrix. If a homogeneous dispersion is reached, a mechanical enhancement is achieved, because nanotube - matrix adhesion actively provides stress transfer [77, 78].

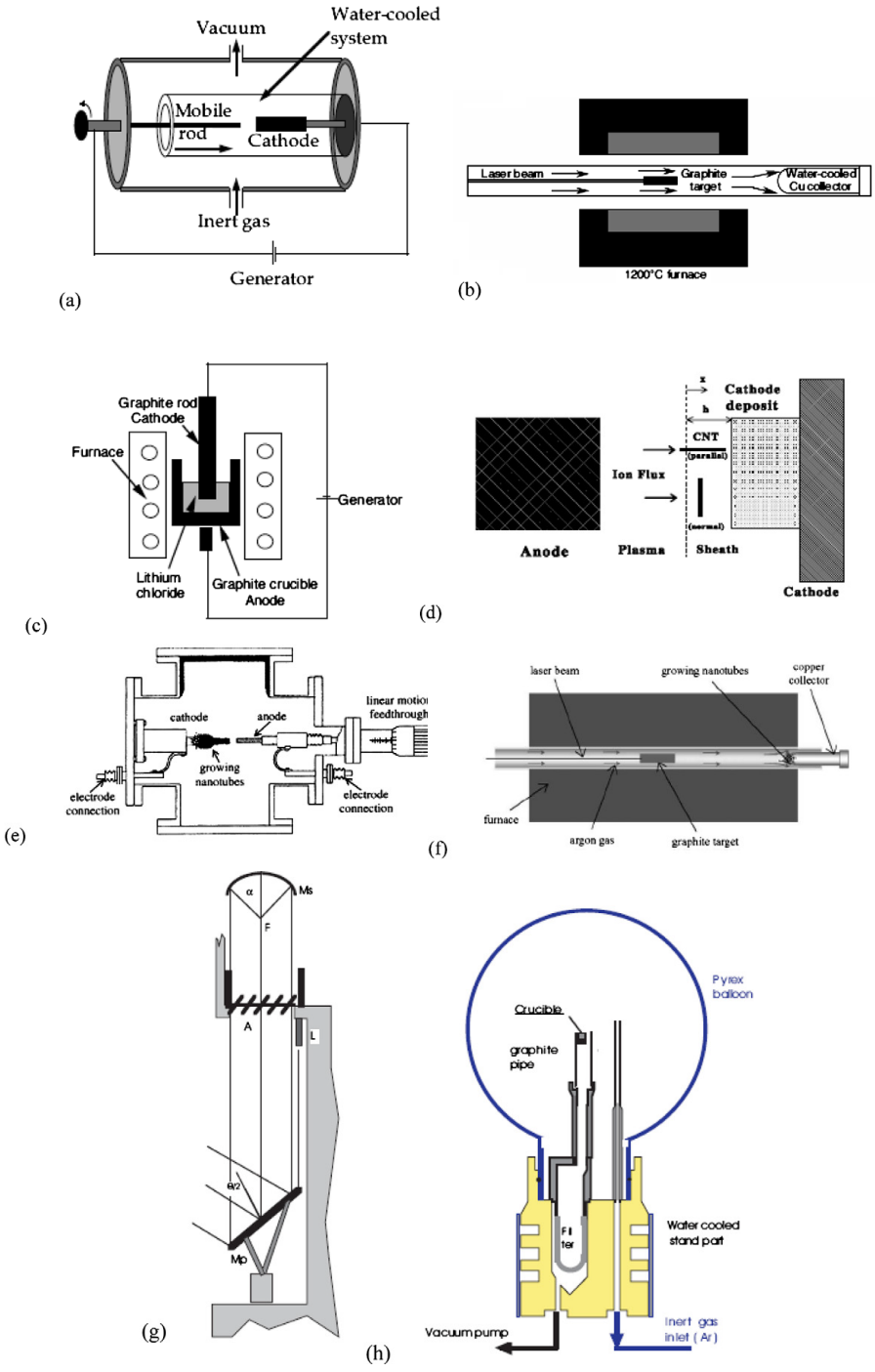

Figure 9: Producing processes for CNTs. (a) Electric-arc method, (b) oven laser-vaporization device, (c) electrolysis system, (d) arc discharge and CNTs formation and transport, (e) arc-discharge technique, (f) laser ablation, (g) solar furnace apparatus, (h) solar chamber [78].

Table 3: Electrical conductivity and resistivity of different conductive fillers [2, 7].

Conductive fillers	Electrical conductivity [Scm^{-1}]	Electrical resistivity [Ω cm]
Silver	6.8×10^5	-
Copper	6.4×10^5	-
Aluminium	4.0×10^5	-
Steel	6.3×10^4	-
Carbon fibres	-	1.7×10^{-3}
Carbon nanofibers	-	10^{-4}
Graphite	5×10^2	-
MWCNTs	10^3- 10^5	$10^{-3} – 10^{-4}$
SWCNTs	$10^2 – 10^6$	$10^{-3} – 10^{-4}$

1.4.3. Percolation theory

As previously mentioned, a perfect filler dispersion is required for maximum mechanical reinforcement. In order to improve mechanical properties maintaining an equilibrium between the other properties, agglomerates bigger than 1 mm have to be avoided, because they actually act as defects. Conversely, the formation of a conductive network by a secondary agglomeration is necessary to obtain high electrical conductivity values. In fact, the explanation of electrical, rheological, and mechanical properties in composites is often due to the creation of matrix-particles interconnections, with the consequent transfer of electrical current or mechanical stress from one another [100, 101 and 102]. It is simple to understand that the electrical conductivity of a composite critically depends on the filler volume fraction in the compound. As reported in Figure 10, at low filler contents, the conductivity is closer to that of the pure insulating polymer and the distance between particles is large (greater than 10 nm). The global conductivity here is due to transport processes within the matrix.

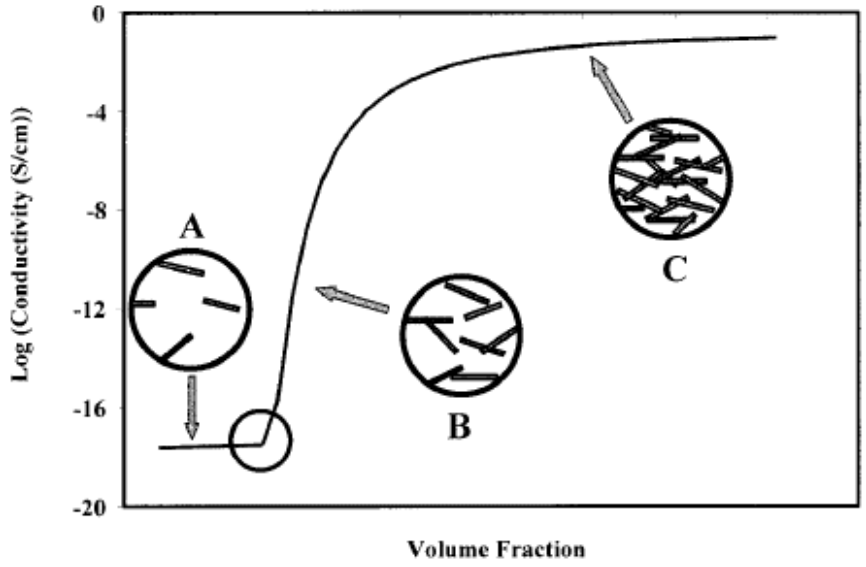

Figure 10: Influence of filler volume fraction on the electrical conductivity [103].

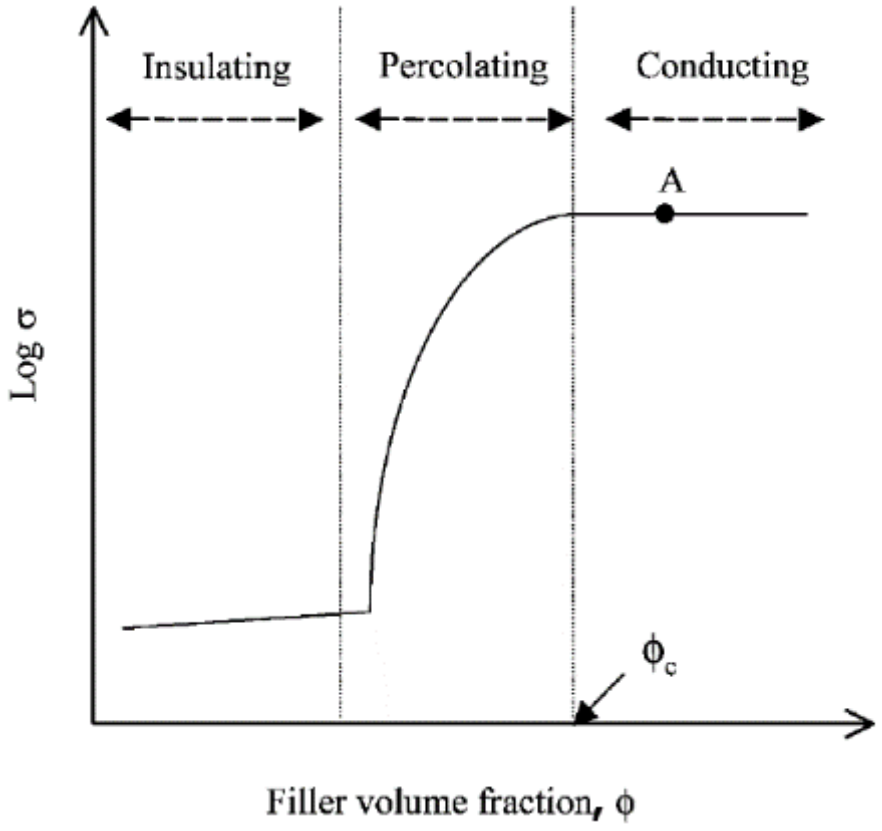

Figure 11: Percolation behaviour of electrical conductivity [104].

As observed in Figure 11, increasing the amount of filler in the matrix, the distance between fillers reduces (below 10 nm) and an initial conducting path is created. At this filler range, called percolation threshold, electrical conductivity suffers small changing in filler quantities and drastically increases in several orders of magnitude. A larger amount of conducting paths is present and, in this way, a 3D conductive network is formed. In this region, electrical conductivity is the result of several factors, namely the polymer, the filler and the interaction between them. Finally, in the plateau region, as reported in the graph above, the filler content is enough to create a continuous conductive path and all the particles are in contact to each other. Fillers mainly define conductivity [103, 105 and 106]. The percolation threshold is defined as the lowest concentration of filler, above which the particles form a continuous conductive network. This phenomenon is described by the percolation theory, which gives a phenomenological description of the electrical conductivity and corresponds to the following power-law relationship [14, 107, 108, 109 and 110]:

$$\sigma = \sigma_0(\varphi_F - \varphi_C)^t \tag{1.13}$$

where σ is the electrical conductivity, φ_F is the filler content, φ_C is the percolation threshold, σ_0 is a scaling factor related to the conductivity of the filler, and *t* is a dimensionless exponent, linked to the dimensions of the conductive network. Several models may calculate the percolation threshold and the critical exponent *t*. Generally, when *t* is around 1 - 1.3, a 2D network is formed. On the other hand, if *t* is near 1.6 - 2 a 3D conducting network is present [108, 111, 112].

In order to better understand the percolation phenomenon, in particular in polymer-CNT nanocomposites, it is worth to underline the effect of this structure on the electrical properties. Alig et al. [100, 113] have proposed a model structure in which CNT-polymer, polymer-polymer and CNT-polymer-CNT interactions coexist, as shown in Figure 12.

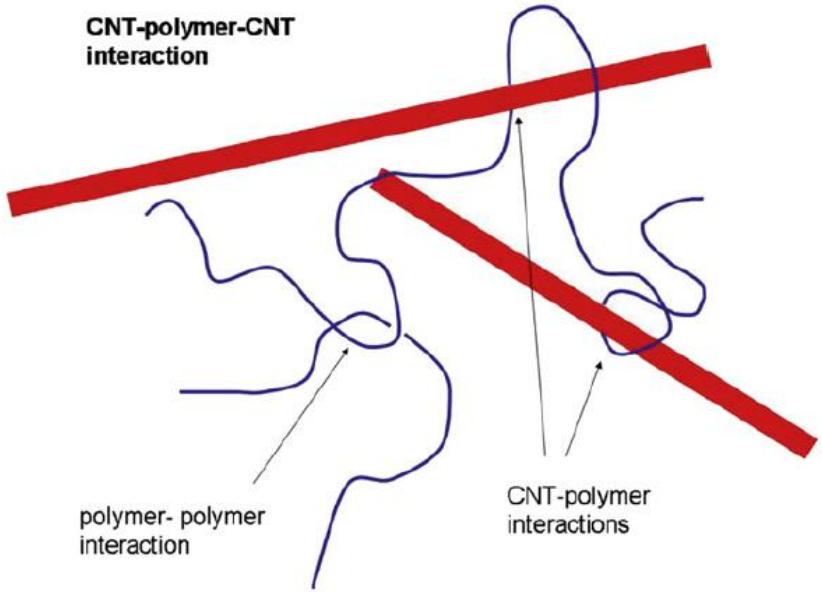

Figure 12: Schematic illustration of CNT-polymer, polymer-polymer and CNT-polymer-CNT interactions [100].

CNTs usually do not have a direct contact and, for this reason, CNT-polymer-CNT interactions and the connectedness cause the transfer of the electrical current [114], the mechanical stress or the phonons. In the case of a conductive network, the charge transfer is assumed to be dominated by the tunnelling effect between neighboured CNTs [100]. Presently, the electrons flow through an insulating barrier via quantum mechanical tunnelling between neighbouring conductive regions is considered the primary conductive mechanism. This behaviour is described with a fluctuation-induced tunnelling model [111, 115]. Nevertheless, the charge transport within the polymer has to be taken into account. The same is valid also for the majority of CNT-based polymers [100].

Influence of the filler shape

The percolation threshold and the electrical conductivity of the composite are affected by several factors. In particular, the conductivity and the volume concentration of the used fillers have to be taken into account. Nevertheless, the filler characteristics, such as size, shape, surface area, morphology, distribution and orientation inside the polymer matrix have a fundamental role in the electrical percolation of the composite [107]. Specifically, the shape of the filler may strongly influence the percolation behaviour and the conductivity. Jing et al. [116] reported that for spherical particles like CB, smaller particles reduce the percolation threshold. Other studies demonstrated that using fillers with a high aspect ratio

greater than 1, like carbon fibres, CNTs or expanded graphite platelets, drastically lower the percolation threshold [103, 117, 118, 119 and 120]. A possible explanation for this phenomenon may be the presence of fillers contact, which allows electron conduction and tunnelling between particles [107]. As an example, the experimental results of Bigg et al. [121] are reported. The influence of two different carbon fibres aspect ratios is studied. The relationship between aspect ratio and percolation threshold is shown in Figure 13. Only 1vol. % is required with carbon fibres with an aspect ratio of 1000. On the contrary, fibres with a value of 10 as aspect ratio need a concentration of about 10vol. % to reach the same resistivity of 100 Ωcm [105].

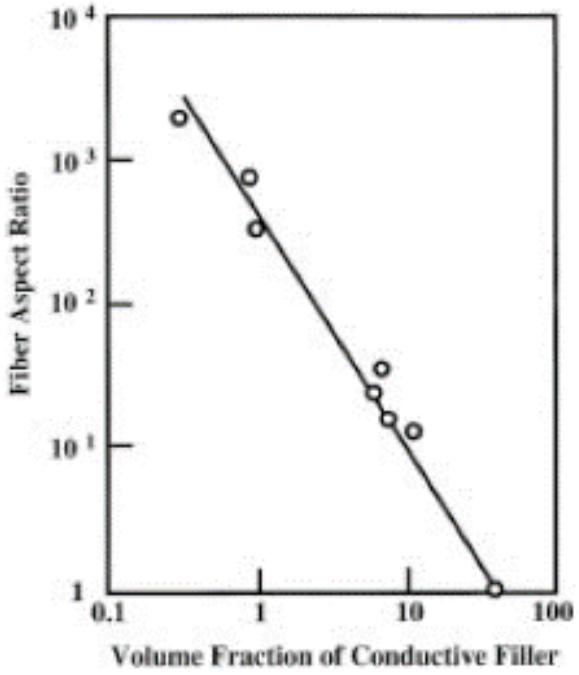

Figure 13: Relationship between the aspect ratio of carbon fibres and their percolation threshold value, in order to produce a composite with a resistivity below 100 Ωcm [105].

Table 4: Percolation thresholds of some PP-based compounds with carbon-based fillers. Different manufacturing processes are used. MM: melt mixing; TSE: twin-screw extruder; SI: solution intercalation; IM: injection moulding; CM: compression moulding.

Polymer Matrix	Conductive filler	Percolation Threshold, φ_c [wt%]	Processing details	Ref.
PP	CB	25	MM/IM	[122]
PP	EG	3	SI/CM	[123]
PP	CF	5	TSE/IM	[124]
PP	CNF	3	MM/IM	[125]
PP	MWCNT	3	TSE/IM	[126]
PP	MWCNT	1.5	MM/CM	[127]
PP	SWCNT	0.1	MM	[128]

Influence of the polymer matrix

Not only the filler, but also the polymer matrix and its properties can modify the electrical behaviour (conductivity and percolation) of the final composite [129]. Mechanical and thermal properties, related to the chemical nature of polymers themselves (i.e. thermoplastic, thermosetting or elastomer) have a significant impact on the electrical properties. Thermoplastic polymers are usually processed above melting temperature and used below this temperature. The thermal shrinkage, which occurs during solidification, induces internal stresses and reduces the distance between particles. This leads to high electrical conductivity values [105]. The crystallinity of the polymer matrix may also affect the electrical conductivity of the final composites. High crystallinity values induce the formation of the continuous conductive network outside the crystallites, where the fillers are forced. In less crystalline or amorphous polymer a more homogeneous dispersion of the fillers occurs. This results in higher percolation threshold [106]. Moreover, crystal morphology, size and concentration of spherulites also influence the electrical conductivity and percolation threshold [107, 130].

Table 5: Percolation thresholds with MWCNTs and different polymer matrices. Several manufacturing processes are used: MM: melt mixing; TSE: twin-screw extruder; μIM: micro-injection moulding; IM: injection moulding; CM: compression moulding; SP-C: solution processing and curing.

Polymer Matrix	Conductive filler	Percolation Threshold, φ_c [wt%]	Processing details	Ref.
PC/ABS	MWCNT	0.5/3	TSE/IM	[131]
PC	MWCNT	3	TSE/IM	[132]
PA12	MWCNT	1.2	TSE/IM	[133]
PA6	MWCNT	6	μIM	[134]
PP	MWCNT	1.4 – 1.8	TSE/IM	[135]
PP	MWCNT	1.3	MM	[136]
PE	MWCNT	5	TSE	[137]
PLA	MWCNT	<5	TSE/IM	[138]
Epoxy	MWCNT	0.02 – 0.04	SP-C	[139]

1.5. Polymer processing

From the technological point of view, polymers are versatile materials and they offer large possibilities of manufacturing. Both thermoplastic and thermosetting polymers can be transformed in several ways, according to their initial state (liquid, powder or solid granules) and the complexity of the desired shape, exploiting different techniques. The processing stages of heating, shaping and cooling can be continuous, like in the melt mixing process or discontinuous, like in injection moulding, but they can be usually automated, becoming suitable for mass production. A wide range of processing methods are available to modify polymers such as thermoforming, roto-moulding, extrusion or injection blow moulding, film extrusion and so on, but probably melt mixing and injection moulding are the most known and largely used in manufacturing plastic industry [140].

1.5.1. Melt mixing

Speaking about manufacturing processes, the modification of the polymer itself and of its own properties represents a key point. Adding fillers or additives in the raw polymer matrix creates a new material and the melt mixing process is used to realize this new formulation (or compound). This technique derives from the extrusion, a continuous process in which semi-finished products are prepared (i.e. sheets, pipes, blown film, yarns). The used machine is the extruder and it is the same for both the technologies. The screw represents the difference: in the extrusion process, a single screw extruder is used. On the contrary, in the melt mixing process generally a twin-screw extruder is employed, in order to guarantee a good mixing among the components of the formulation. Several technological alternatives can be exploited to fulfil this requirement: the twin screws, in fact, can rotate in opposite directions (counter-rotating) or in the same direction (co-rotating). In the counter-rotating twin-screw extruder, the material is forced into the gap between the two screws. In the co-rotating solution, the molten material passes from one screw to another at the intermeshing point, undergoing to an intensive mixing, as reported in the Figure 14 below. For this reason, it is considered the best solution to obtain the proper dispersion and homogeneity in the final compound.

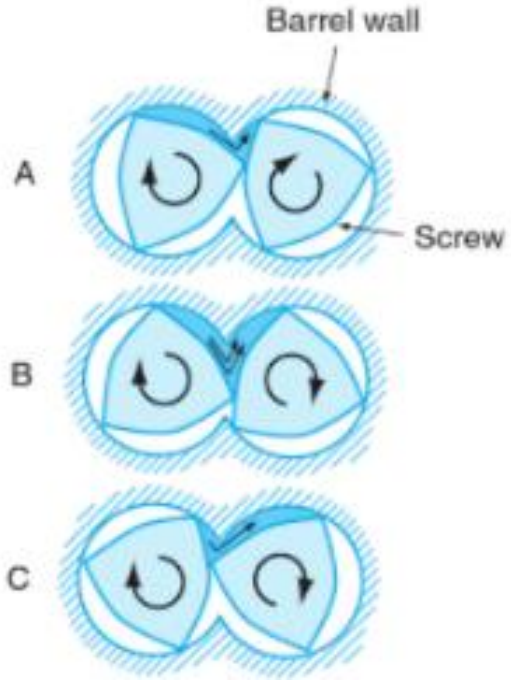

Figure 14: Molten material transport in a co-rotating twin-screw extruder.

In a twin-screw extruder, whose scheme is reported in the Figure 15 below, the polymer, in granules form, is fed through a hopper into the barrel. Here it is melted, homogenised and forced through a shaped die. It develops as a continuous tie, which is cooled in a water bath. At the end of the cooling phase, it is chopped into short granules. The chopped granules are typically 3 - 4 mm long [140].

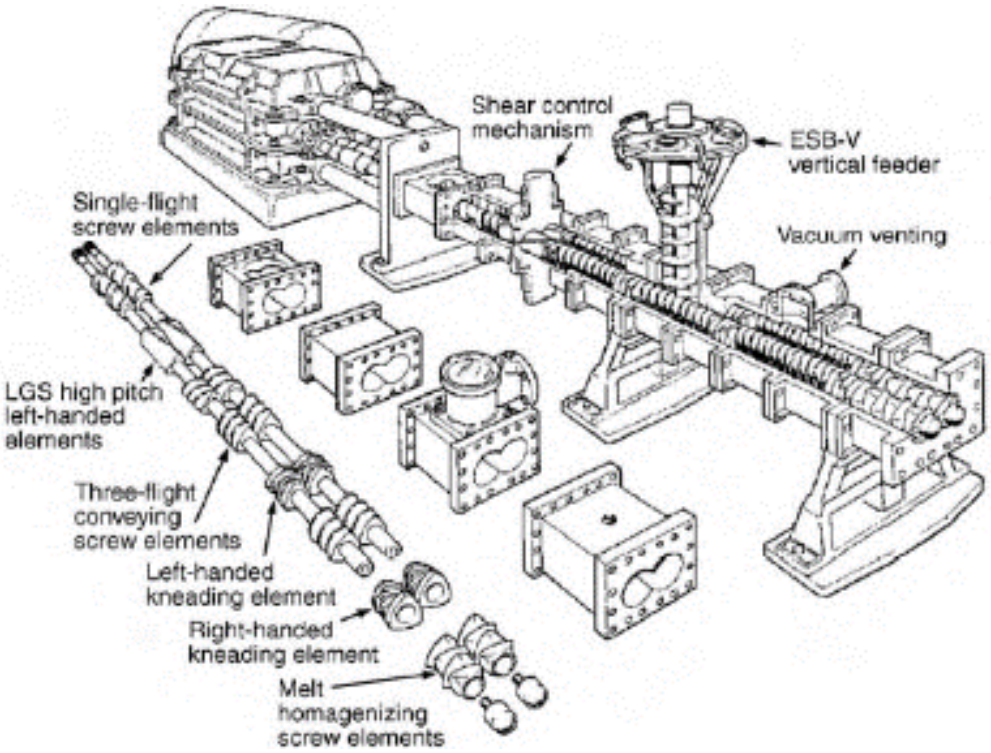

Figure 15: Scheme of the twin-screw extruder modular structure. Barrel section [141].

Typically, melt mixing extruders have modular screws (Figure 16). This means that a central rod is present and several modules are added. Each module is based on elements with different tasks. Kneading blocks provide the shear strength necessary to destroy filler agglomerates and to mix them with the polymer. They can have different thickness and reciprocal oriented angles. On the other hand, conveying elements allow the molten polymer to move along the screw during the process.

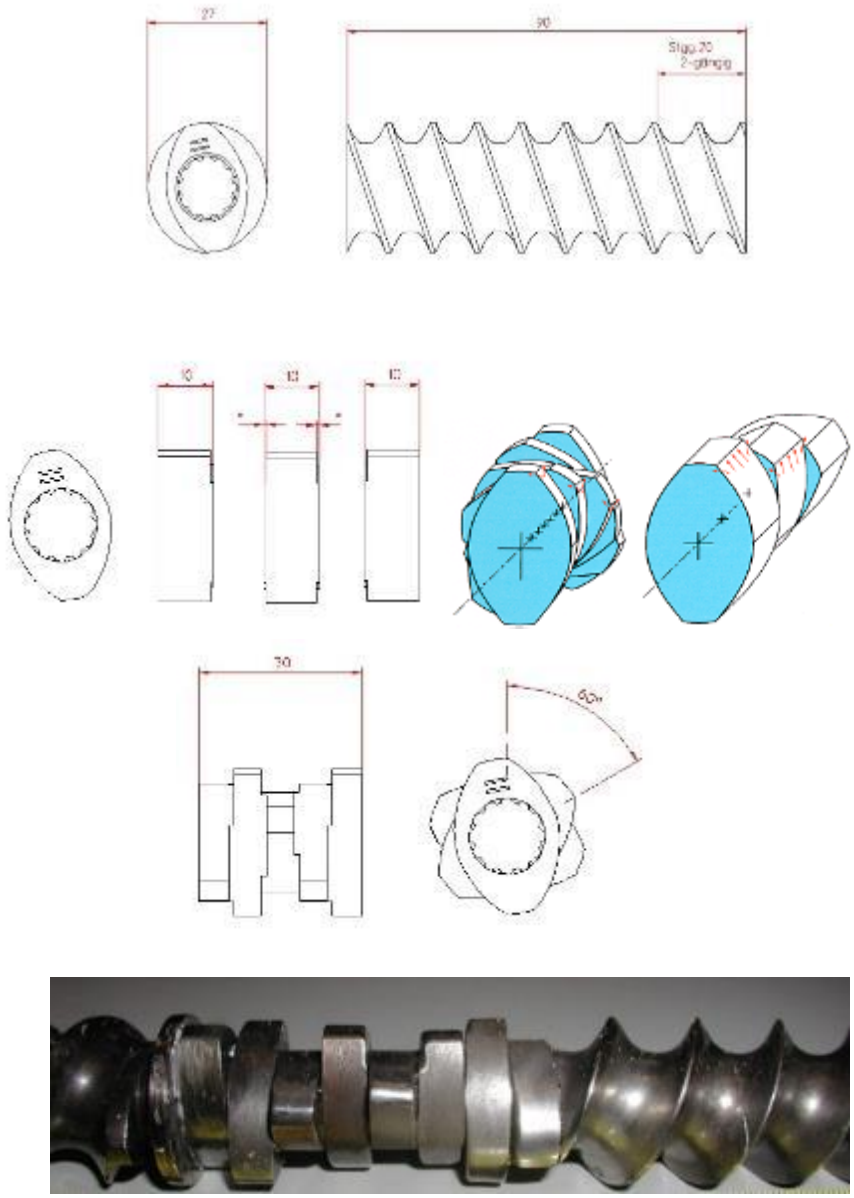

Figure 16: Different types of screw elements. Conveying elements at the top and kneading block in the middle. A portion of a real screw at the bottom.

The correct design of the structure of the screw, in term of number and position of modules, is fundamental to have an optimal distribution and dispersion of the fillers/additives in the polymer matrix. These two mixing mechanisms are key points of the melt mixing process. As can be clearly observed in the scheme reported in Figure 17, the distributive mixing (or laminar or extensive mixing) stretches interfacial area between components without a cohesive behaviour and then, distributes them throughout the volume. Conversely, the dispersive mixing

(or intensive mixing) tends to reduce the dimension of the elements with a cohesive behaviour. This characteristic is due to van der Waals forces within the agglomerates and to surface tension of the elements of the compound. A well-mixed dispersively and distributively compound is as desired as difficult to obtain. Intermediate situations, such as a single complete dispersive or a total distributive mixing, are more probable than the previous described condition.

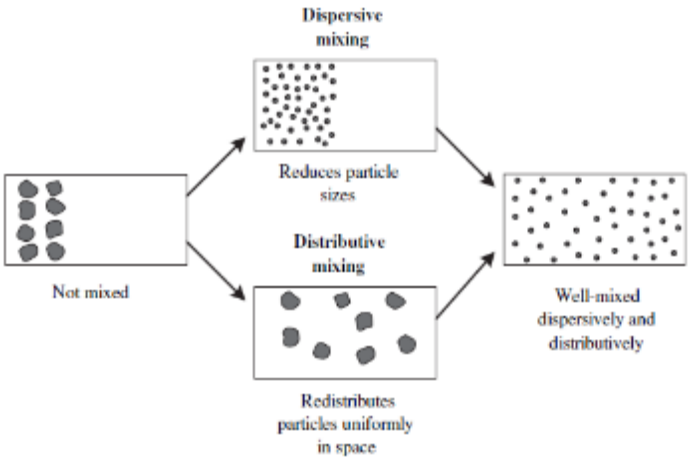

Figure 17: Dispersive and distributive mixing of solid agglomerates [141].

Volumetric or gravimetric dosing units are commonly used in order to feed additives and fillers (Figure 18 below). They ensure a precise and constant flow during the process. Multi-dosing systems are usually used when more than one additive is added in the formulation.

Figure 18: Single and multiple gravimetric dosing units.

These dosing units can be placed in different zones along the length of the screw. The entry of fillers next to the main hopper or nearer the extrusion die strongly affected their size and their interconnection with the polymer matrix. The longer is their path in the extruder, the longer is their residence time. Consequently, the longer is the residence time, the higher is the mixing potentiality but also the higher is the size reduction of the fillers. Therefore, it is clear that this aspect intensely influences the properties of the final formulation.

The choice of the right dosing unit is also fundamental to have the correct flow rate. A too high flow rate can induce an accumulation of materials in the main hopper or in the lateral dosing units. In order to avoid this problem, an increase of the screw speed is necessary. On the contrary, the combined increase of flow rate and screw speed leads to an overstated growth of the torque and of the absorbed energy of the engine of the extruder. Moreover, elevate shear strength is applied to the molten material in this particular condition. A possible solution is the increment of the temperature profile, remaining under the degradation temperature of the materials.

1.5.2. Injection moulding

One of the most common processing methods for plastics is injection moulding. Originally, the injection-moulding machine was based on the pressure die casting technique for metals. The first machine, designed for celluloid, was patented in the USA in 1872. Very few developments in injection moulding processes followed this first attempt and only in the 1920s, in Germany, a renewed interest was taken in this process.

In the late 1930s, when a wide range of thermoplastics became available, the introduction of a hydraulically actionized machine occurred. Then, in the 1950s, a new generation of equipment was developed: in fact, in 1952 W.H. Willert invented a reciprocating screw plasticizing injection unit [142].

In principle, injection moulding is a simple process. Several phases complete the cycle process and they are divided, as follows:

1. a thermoplastic polymer, in the form of granules or powder, passes from a feed hopper into the barrel, where it is heated so that it becomes soft. In the heated barrel, where the reciprocating screw is, both shear heating and heat conduction of the barrel gradually melt the polymer. At the same time, the hydraulic clamping unit pushes the two mould halves together and exerts

sufficient force to keep the mould securely closed while the material is injected.

2. the polymer is transported by the rotating screw from the back of the barrel to the front. The reciprocating screw has three different zones, each with a specific function, as illustrated in Figure 19 below. The section of the screw nearest the hopper is the feed section, in which no compression takes place. It conveys the not-melted plastic from the hopper throat into the barrel, where it begins to melt. They are molten by friction and heat, obtained through the external electric heater bands. The friction is caused by the pellets sliding against themselves and against the inner wall of the barrel and the screw surface. The majority of the melting occurs in the transition (or compression) section, where compression of the polymer takes place and a mixing action occurs in order to obtain a better material and temperature uniformity. The minor diameter of the screw is increased and this provides gas removal and melt densification. Then, the metering zone, where the minor diameter has reached its maximum, provides the final shear heating and mixing of the melt and no further compression takes place. Screw rotation and melting continue until an enough amount of molten polymer is available in front of the screw, to fill the mould.

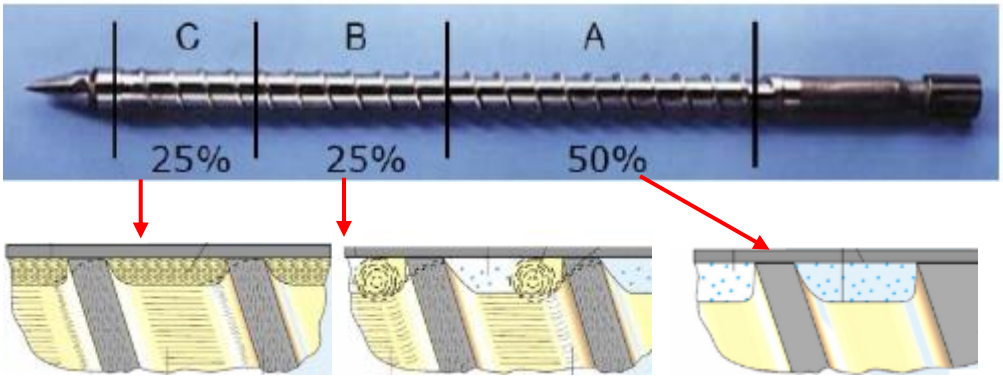

Figure 19: Different sections of the injection moulding screw. A. feed zone, B. transition zone, C. metering zone. Correspondingly, schematic behaviour of the polymer granules before and of the molten material after along the screw length.

3. the screw rotation stops and the molten material is injected, through a nozzle under high pressure, into a relatively cold mould, which is clamped tightly closed. When the volume of the molten material ahead of the screw tip is sufficient to fill completely the mould, the cavity and the runner system (the channels leading to the mould cavity), the polymer enters the cavity. This

amount of material is the shot size. A check valve at the tip of the screw avoids the melt to flow back along the screw, since it is pushed forward. The injection rate, which is determined by the advancing velocity of the screw, and pressure are monitored until the end of the process.

4. Pressure is kept on the material. The molten polymer inside the mould, indeed, begins to cool as soon as it makes contact with the interior surfaces of the mould. As the plastic cools, it solidifies into the shape of the designed component. During the cooling and solidification phase, the screw begins to rotate and melt new material for the next shot. However, during cooling a shrinkage of the part occurs. The packing of material in the injection stage allows additional material (the cushion) to flow into the mould and to reduce the amount of visible shrinkage. The mould cannot be open until the required cooling time has elapsed. In this phase, a backpressure is employed and it corresponds to the amount of hydraulic pressure applied to the back of the screw as it rotates.
5. the clamp opens the mould and the component is removed and ejected. When the mould is opened, an automatic mechanism is used to push the part out of the mould [143, 144].

The explained injection moulding cycle is schematically described in the Figure 20 below.

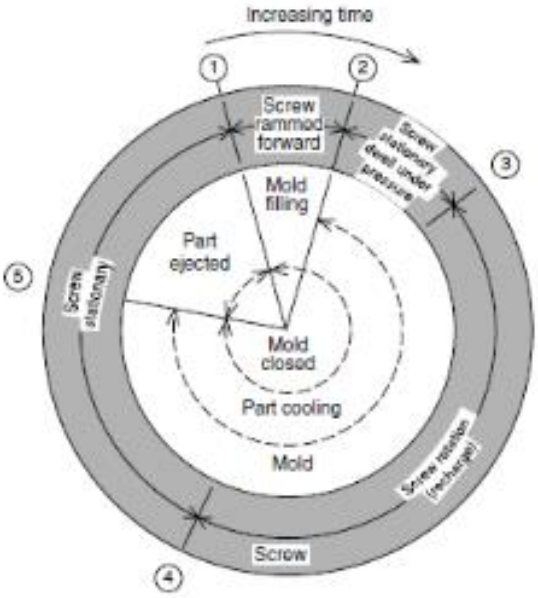

Figure 20: Injection moulding cycle [141].

Therefore, an injection-moulding machine essentially is based on four parts (Figure 21):

a. Injection unit, responsible for both heating and injecting the material into the mould. Its main components are the hopper, the heated barrel, the reciprocating screw and the nozzle.
b. Clamp unit: generally, injection-moulding machines are characterized by the tonnage of the clamp force they can provide.
c. Injection mould
d. Control system

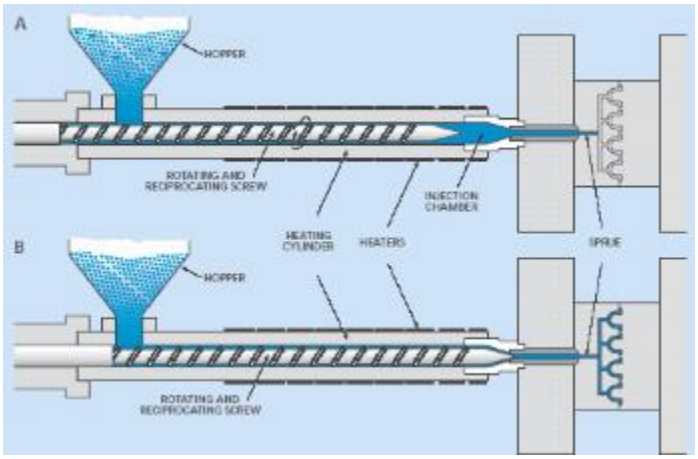

Figure 21: Schematic cross-section of a typical screw injection-moulding machine, showing the screw in the retracted (A) and forward (B) position.

Injection mould

Moulds, typically made of steel or aluminium, are constituted of several parts and they consist of two halves (Figure 22 a) and b)): the core and the cavity. When the mould is closed, the space between the core and the cavity forms the part cavity, which is filled with the molten polymer during the manufacturing process. First, the molten plastic enters the mould through the sprue. As already said, the runners conduct the molten polymer from the sprue to the cavities through a gate. Commonly, more than one gate is used and a specific runner feeds each of them. The configuration of runners and gates influences the filling of the mould. This can modify the process parameters, such as required injection pressure and orientation of material flow, which affect the mechanical properties. Sometimes hot runners are used in order to maintain in a molten state the flux of material before entering the cavity.

Cooling channels represent another type of channel, present in the mould. These channels, gained in each half of the mould, allow water or a similar heat-exchange fluid to flow through the mould walls, adjacent to the cavity, and to cool the molten material. In this way, the solidification phase is fastened. The mould temperature is usually controlled above room temperature and it depends on the type of processed polymer. Because the cooling step is usually the longest phase in the injection moulding cycle, a cold temperature of the mould is generally recommended. Because of the wide range of mould and part designs, it is very difficult to specify mould temperatures. A typical range of mould surface temperatures for polyolefins is 20-50°C.

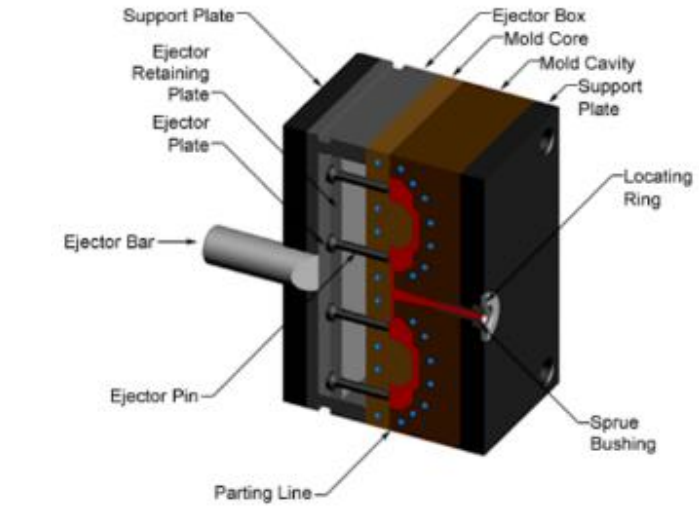

(a)

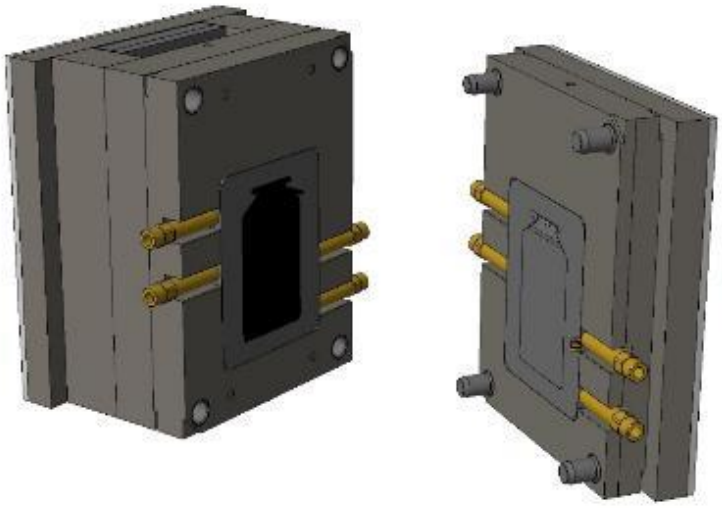

(b)

Figure 22: Schematic cross-section of a close (a) and open mould (b).

The best cooling level is achieved when the water is in a turbulent flow. In general, an increase in coolant flow rate removes more heat than a decrease in coolant temperature. As the polymer flows into the mould, the material in contact with the mould surface solidifies very quickly, forming a skin layer and an inner flow channel, through which the material continues to flow.

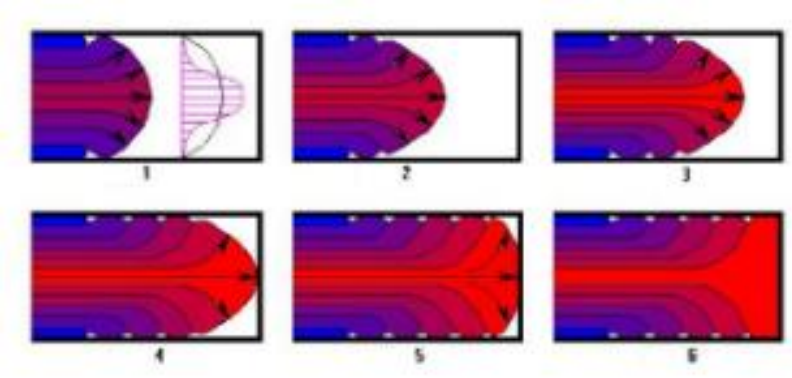

Figure 23: Fountain flow of the molten polymer entering the cavity of the mould.

The filling way at moderate flow rates is a forward flow, as shown schematically in the Figure 23 above. During the early stages of filling, the flow is radial and the melt front circular. The flow behaviour changes as the melt front passes the gate. The front shape can be either flat for isothermal filling or curved into cold moulds. In the front region, the melt at the centre fountains out to the mould wall to form the skin layer. Thus, the inner central core decelerates from the maximum velocity to the mean one, at which the front advances. The front acquires, in this moment, a velocity component in the thickness direction, besides the already present component in the flow direction. For this reason, a fountain effect or fountain flow occurs. Rose et al. created this specific term [145]. This phenomenon can impart considerable orientation to the resulting injection moulded part, determining the quality, morphology and properties of the final component. While an orientation is required in extrusion to improve the mechanical properties, in injection moulding, this aspect has to be avoided, because the consequent frozen stresses can cause distortions and anisotropic behaviour in the final components [146].

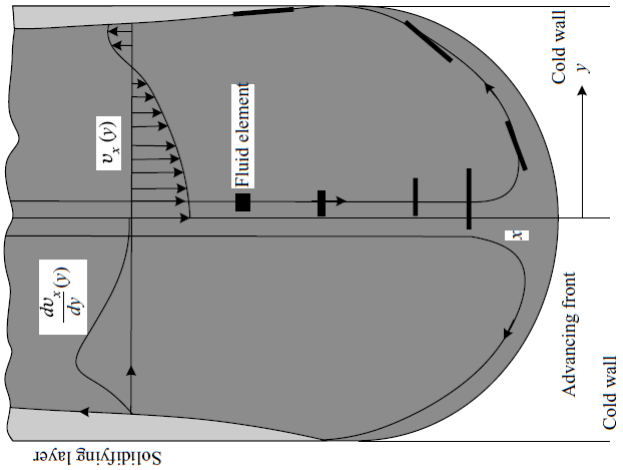

Figure 24: Representation of the flow of the molten material between two cold walls. Black rectangles represent the stretching and orientation of the fluid particles in the central zone. The velocity profile is in the x direction (the coordinate system is positioned on the front) [141].

Two skin layers, oriented parallel to the flow direction, and a core region, oriented perpendicular to the flow and in-plane directions are formed, as observable in Figure 24 above [18, 132]. Shear deformations are responsible for the skin layers, whereas the core layer is mainly due to the extensional flow. Therefore, fibres and fillers in the skin regions tend to have a marked orientation, parallel to the flow direction. Their behaviour is different in the core region, where no preferential orientation occurs [147, 148]. From the electrical point of view, the skin layers generally have a higher resistivity than the core region. This is the result of a reduced percolation due to the shear. The structure of the skin is affected by process parameters, such as melt temperature, injection speed and mould temperature [149, 150] (Figure 25).

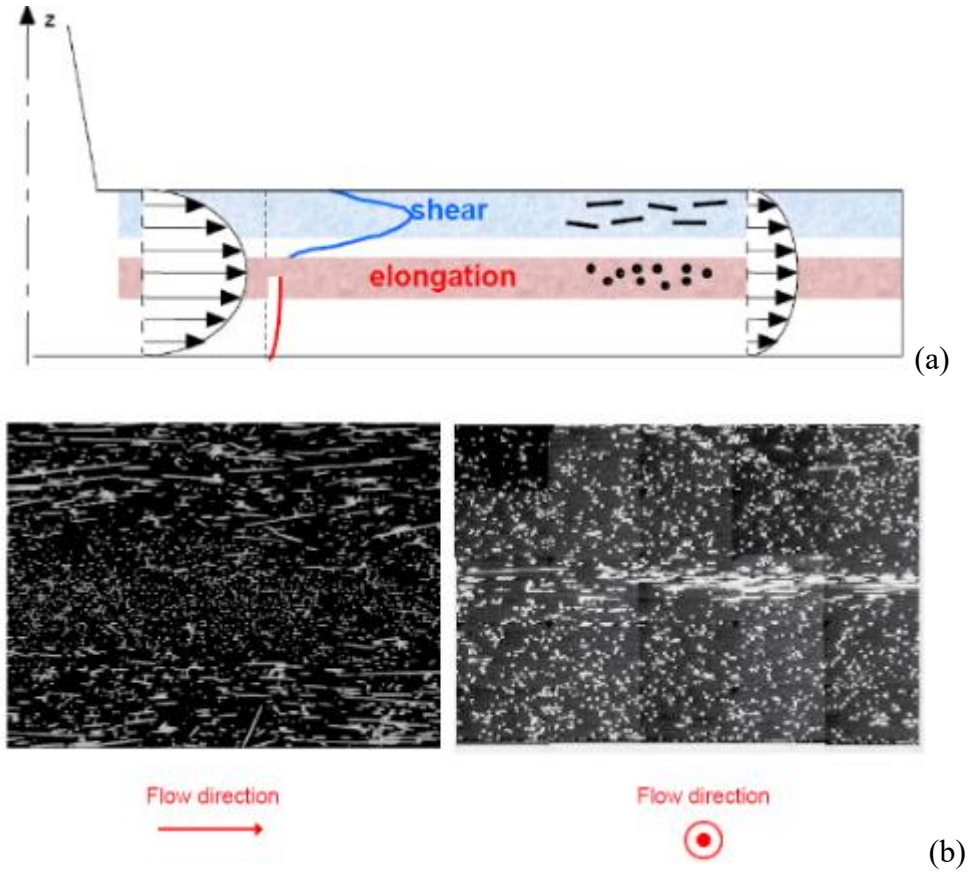

Figure 25: (a) Fillers orientation inside the mould cavity. In the skin layers, near to the mould walls, shear flow is dominant and a marked orientation of fillers occurs. In the core region, the front flow is mainly controlled by elongation and no fillers orientation is present. (b) Micrographs of an injection moulded composites parallel (on the left) and perpendicular (on the right) to the flow direction [147].

Shrinkage

As said before, thermoplastic solidification suffers a volumetric shrinkage. In crystalline polymers, the shrinkage is associated with crystallization. When the polymer solidifies, the chains in the crystalline regions pack tightly together resulting in a reduction in volume. Conversely, in amorphous materials, the shrinkage is generally lower and it is associated to the glass transition temperature (Tg). In both cases, the amount of shrinkage depends on various processing parameters, including the mould temperature and the cooling rate. Moreover, shrinkage is a time-dependent phenomenon. In fact, it can continue after removing the component from the mould.

The viscosity of the polymer is an important property to consider if an optimization of the injection moulding process is desired. Different process parameters, such as temperature and shear rate, affect the viscosity of the plastic material during the process. Increasing both the melt temperature and the injection rate reduces the viscosity, making easier the filling of the mould. In addition, an increase of the injection rate may also yield a more uniform part temperature, which can reduce differential shrinkage (i.e. warpage). Therefore, three main variables strongly influence the molten material behaviour and its final properties at the end of the process. They are:

1. Injection pressure
2. Injection rate
3. Melt temperature

The injection moulding process has several advantages in comparison with other processing technologies: it can be easily automated and it allows achieving high level of productivity. Thin-walled and geometrically complicated parts can be obtained. It is a versatile process and a wide range of products can be realized through injection moulding. On the other hand, process parameters strongly affect the properties of the polymer during and after the manufacturing process. This leads to a variability in the component characteristics. Moreover, injection moulding is an expensive process, because of the high cost of equipment and moulds.

1.5.3. Heat&Cool

The Heat&Cool technology (hereinafter H&C) is a particular technical system, linked to the injection moulding process. This technique is a dynamic variation, in a single injection cycle of the mould temperature, consisting in a controlled heating (above the glass transition temperature, Tg for amorphous polymer and the melting temperature, Tm for semi-crystalline polymers) and a rapid cooling.

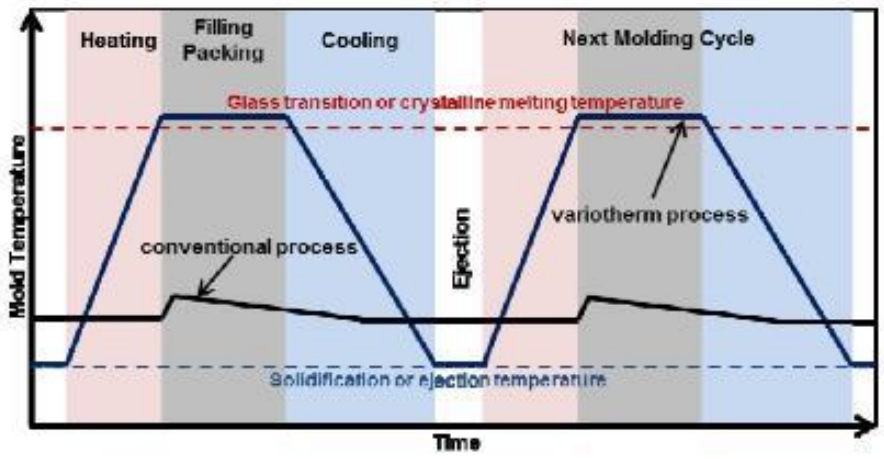

Figure 26: Heat&Cool injection moulding cycle in comparison with a conventional injection moulding cycle.

The H&C process eliminates the technological constraint, represented by the constant temperature of the mould in the conventional injection moulding process, necessary to extract the solidified part. In fact, the heating of the mould above Tg and Tm (for amorphous and semi-crystalline polymers respectively) reduces the skin layer, inevitably created, during the injection phase, at the interface between the hot molten material and the cool metallic surface of the mould.

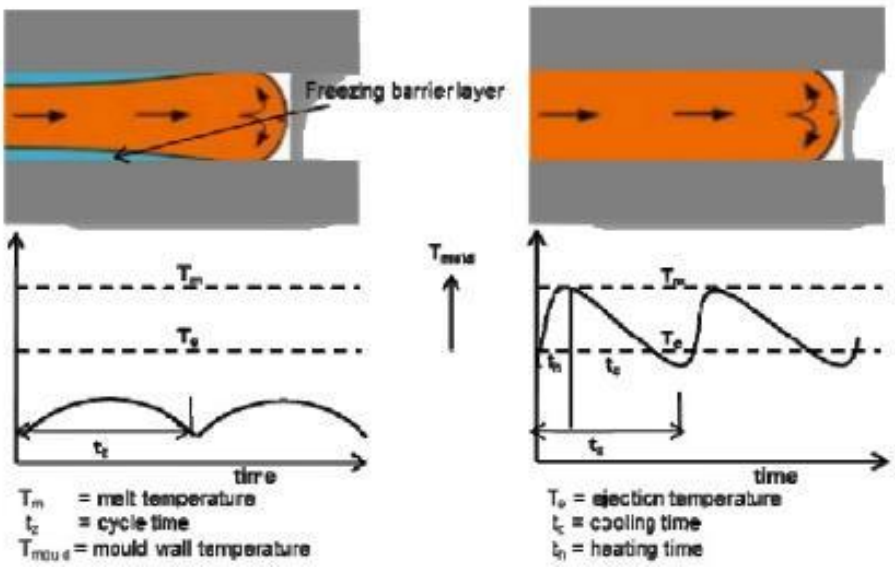

Figure 27: On the left, formation of frozen skin layers during a conventional injection moulding process (T mould is constant). On the right, completely molten polymer in all the component thickness during an H&C injection moulding process (dynamic variation of T mould).

The configuration and the design of dynamic conditioning circuits strongly affect the quality of heating and cooling phases. The temperature inside the mould cavity has to be as uniform as possible during the injection cycle. A correct design of the dimension and an equilibrate distribution of the runner have to be taken into account. With the right configuration of the conditioning circuits (i.e. number, sectional area and position of the runners) a hundred grade thermal excursion is achievable in few seconds (with pressurized steam water).

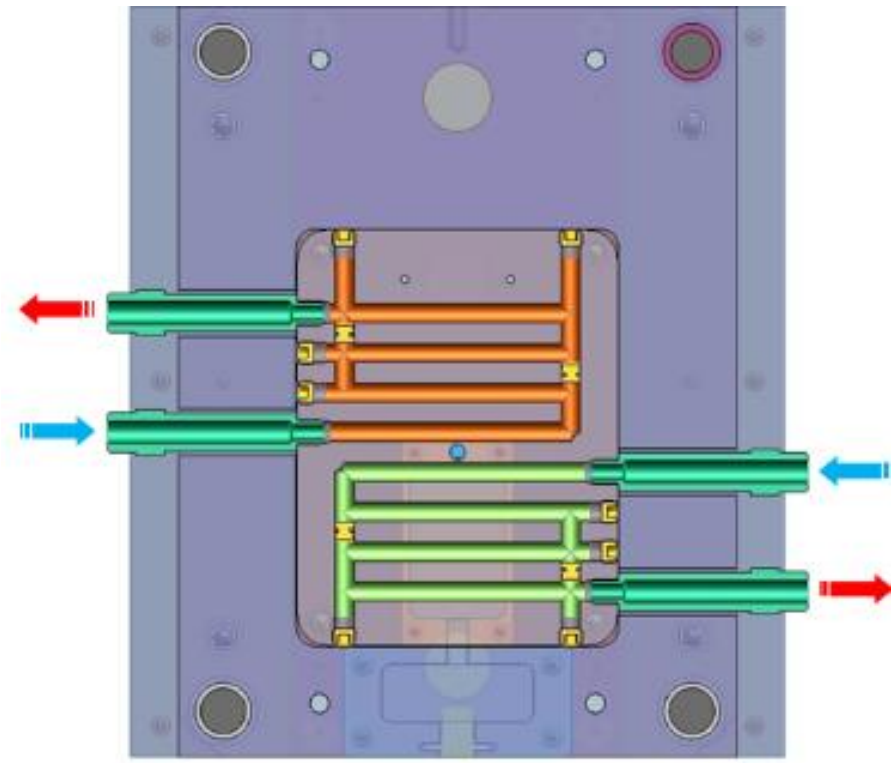

Figure 28: Example of H&C configuration for the thermal management of a mould.

The positioning, number and configuration of the runners in an H&C mould is very different in comparison with a mould used in a conventional injection-moulding process, as it can be seen in the Figure 29 below. They are placed, in fact, nearer the cavity surface in order to have a better heat exchange.

Figure 29: Designed mould for the H&C injection moulding process on the left and designed mould for the conventional injection moulding process on the right. As highlighted in the blue circles, not only the distance between the runners and the cavity, but also their number is significantly higher in the H&C configuration.

As previously reported, two different independent processes regulate temperature variations at the mould surfaces: heating is more often controlled by the regulation of temperature inside the mould, whereas a fluid circulation governs the cooling cycle.

Commercially, four different physical processes are available to control the heating cycle:

1. Forced convection, which can use several fluids like oil, pressurized water or hot air
2. Conduction, which exploits ceramic heaters or electrical cartridge heaters
3. Radiation with external heaters (IR lamps, electrical or gas radiators)
4. Internal or external magnetic induction

These types of heating processes offer different efficiencies and heating rate. The internal induction allows using the highest temperatures and the fastest heating rates, while steam pressurized water represents the best balance between efficiency and heating rate. With this technique, which can reach 170°C-180°C, essentially all the commercially most used technopolymers can be manufactured (i.e. polyamides, polycarbonate, ABS, copolymers PC/ABS, polymers with different fillers, such glass fibres or CNTs). A comparison of different specifications for the cited techniques is reported in the table below:

Table 6: Comparison of parameters for different heating techniques in H&C process.

Technical specification	IR Heater	Ceramics Heater	Ext. Induction	Int. Induction	Steam pressurized water	Electrical cartridges
Max. Temp [°C]	No limitation	No limitation	No limitation	No limitation	120 to 150	350
Heating speed [°C/s]	15	20	25	25	10	6
Size parts	1	0,1	3	1-2	1-2	1

As initially said, H&C is a dynamic injection moulding process and the cycle times are fundamental, because they can be often longer than in a conventional injection moulding process. For this reason, the right choice of the heating technique and the correct design of the whole H&C system have a significant role in the reduction of the cycle time. Sometimes, in fact, the heating phase can be completely hidden in the mould-handling phase. A decreasing velocity characterizes the previously reported heating techniques: internal or external magnetic induction > ceramic conduction heating > fluid convection heating (water, oil, steam or air) > conduction with electrical cartridge heaters > IR radiation. Moreover, modifying the average temperature of the mould surfaces, different cycle times and consumed energy can be reached, as reported in the Table 7.

On the other hand, generally, the cooling process is successfully based on thermal exchange with forced convection of water. H&C offers several advantages, especially from the aesthetical point of view. Typical superficial defects (i.e. evident junction lines, flow lines, sink marks), present in the conventional injection moulding process, can be reduced or avoided, with this innovative technique. The aesthetic of the moulded parts is enhanced. Moreover, a considerable reduction in the skin layer is achievable and an easier mould filling, also for thin-wall component, is possible. The heating cycle, in fact, leads to increase the thickness of the fluid molten material, reducing the sizes of the frozen skins, in contact with the surfaces of the mould.

Table 7: Comparison of heating time and consumed energy for the main heating techniques in H&C process.

Av. T (°C)	Saturated steam		Super-heated water		Hot oil		Induction	
	Heating time (s)	Consumed energy (kWh)	Heating time (s)	Consumed energy (kWh)	Heating time (s)	Consumed energy (kWh)	Heating time (s)	Consumed energy (kWh)
140	36	1.38	32	1.21	79	5.11	33	0.67
160	24	1.05	22	0.97	47	3.59	19	0.7
180	19	0.97	18	0.87	33	2.95	13	0.77
200	16	0.91	15	0.82	25	2.58	6	0.84

1.5.4. Effect of the processing conditions on the electrical behaviour

The distribution of fillers in a polymer composite mainly depends on the manufacturing techniques. In extrusion and injection moulding techniques, an anisotropic orientation of the particles in the flow direction is quite always present. This alignment is unavoidable and it has to be minimized optimizing the process conditions. The dispersion of fibres and their inter-spacing, in fact, is strongly influenced by processing conditions, and the polymer itself. Moreover, in the case of conductive fillers with a high aspect ratio, like MWCNTs, the anisotropy leads to a weakening of the conductive network formation and to a shift of the percolation threshold [150]. Consequently, not only the electrical conductivity but also the percolation threshold cannot be isotropic in such components. Moreover, the aspect ratio of the fillers is altered and the final properties of the moulded part are modified [105, 107].

Considering the realization of CNT-based nanocomposites, Alig et al. [100] demonstrated the importance of a non-uniform distribution and dispersion of CNTs and the necessity of the creation of an agglomerated structure in the polymer matrix in order to reach higher electrical conductivities of the formulations [151 - 157].

The manufacturing processes and the change in their parameters influence the formation of this clustered network. Starting from the melt mixing process, in fact, the initial agglomerates of fillers have to be well dispersed in the polymer. When the second processing phase (i.e. injection or compression moulding) occurs, secondary agglomerates or clusters have to be present in order to create an inhomogeneous filler network, which determines the final electrical properties of the component. During the cooling phase, when the temperature decreased under the Tg until room temperature, this final structure is frozen.

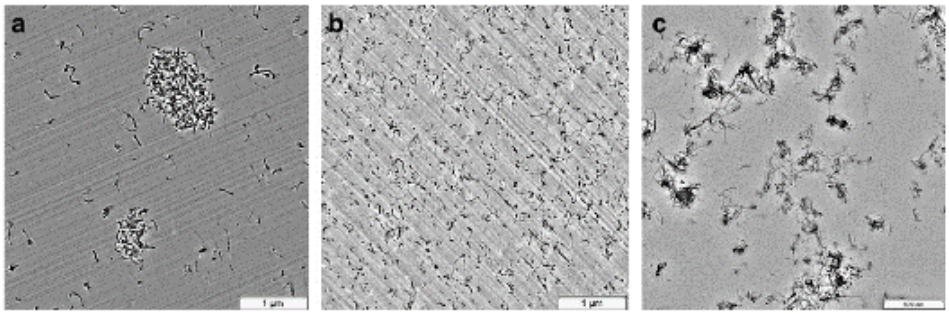

Figure 30: TEM micrographs of MWCNTs arrangements in PC matrix: (a) initial agglomerates, (b) well-dispersed MWCNTs, (c) secondary agglomerates [98].

Moreover, in their work they reported the influence of process conditions on electrical behaviours of both amorphous (PC) and semi-crystalline (PP) CNT-based formulations. In the amorphous matrix, the formation of the conductive secondary agglomeration and the increase in conductivity occurs when the process temperature exceeds the glass transition temperature of the polymer. The structure is then blocked during cooling below Tg. In the semi-crystalline polymer, the fixing of the conductive network takes place when the PP crystallizes and the process temperature drops under the crystallization temperature, Tc. Interestingly, the shrinkage has a significant role in the increase or the decrease of the electrical conductivity of the final component. As reported in the previously cited article [99], in PC matrix the conductivity increased during cooling also because of the higher shrinkage, typical of amorphous polymers. The distance between CNTs is, indeed, reduced. In the PP matrix, instead, CNTs are blocked in the crystalline structure, with few possibilities of movement, and a reduction of the matrix conductivity occurs.

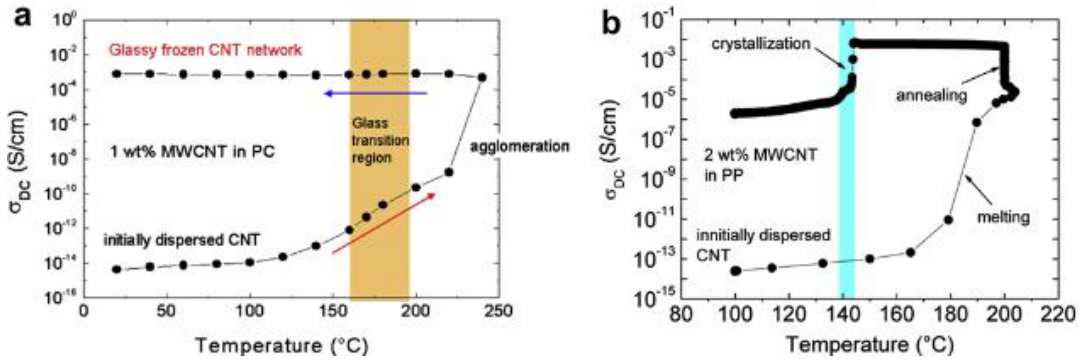

Figure 31: (a) Electrical conductivity of amorphous MWCNT-based nanocomposite (1%wt in PC). The conductivity changes after cooling below the Tg of the compound. (b) Electrical conductivity of a semi-crystalline MWCNT-based nanocomposite (2%wt in PP). The change in conductivity occurs after isothermal annealing and crystallization [100].

It is important to underline that the mechanism of charge transport in a conductive network and of mechanical reinforcement are different. The optimum mechanical reinforcement is obtained with a completely random distribution of CNTs, while acceptable electrical conductivity values are reached with the formation of a secondary agglomeration and an inhomogeneous distribution of CNTs in the polymer.

Another point to highlight is the effect of melt mixing process on CNTs size and on percolation threshold. In fact, during this process, CNTs can be shortened [158, 159] and a modification in the percolation threshold may occur. Too elevate melt mixing energy and too long residence time, fundamental factors to reach a good dispersion, may lead to nanotubes shortening [100, 160].

Therefore, it is evident that the chosen process influences the formation of the conductive network. Comparing injection and compression moulding techniques, differences in conductive network can be easily found out. Figure 32 (a and c) shows the very fine (less than 1 mm) and strongly oriented conductive bands, obtained with injection moulding. They differ from the thicker (up to 10 mm) and not oriented lines, which are produced by compression moulding (in Fig. 32 b) [161].

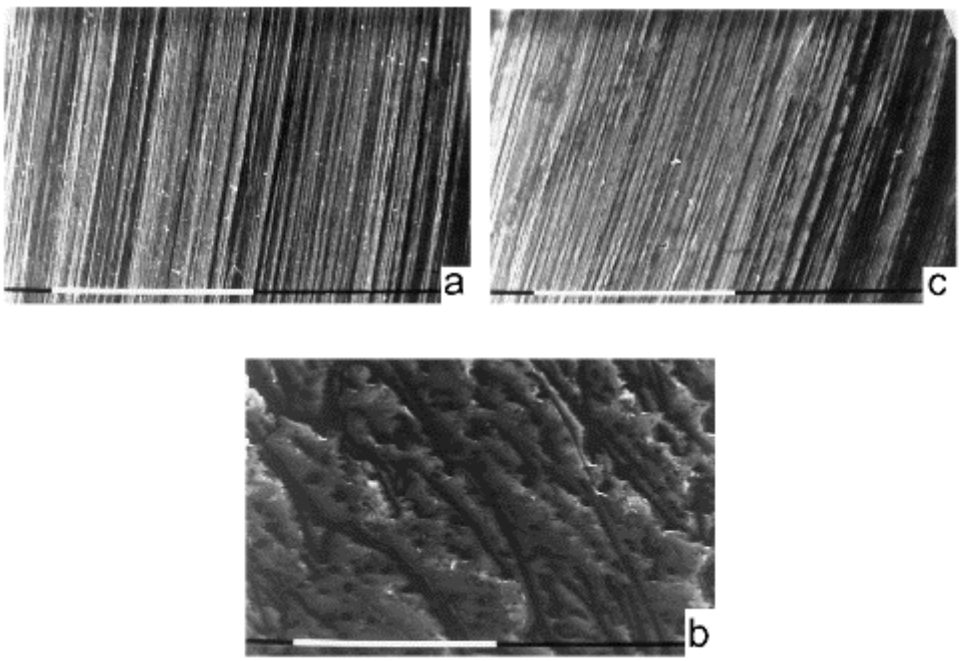

Figure 32: Effect of different processing on the percolation network of conductive fillers based compounds. (a) and (c) injection moulded components, PE and PP based respectively; (b) compression moulded component, PP based [161].

In order to achieve a good balance between electrical properties and conductive network formation, an optimization of processing parameters is desirable. Injection moulding is a complex process and many processing conditions can be controlled. Many studies reported that, in particular, the melt temperature, the injection rate, the holding pressure and the mould temperature are four parameters, which seem to have the highest influence on the orientation of fillers [100, 131, 149, 150 and 162].

A review paper [149] collected different literature results on the effect of modification of process parameters on the electrical conductivity of injection-moulded parts. According to this research, the increase in the melt temperature has a powerful positive effect on the electrical surface and bulk resistivity, which strongly decrease. Moreover, this effect is equal for both amorphous and semi-crystalline polymers. On the other hand, an increase of the injection speed seems to have a negative effect on the electrical properties [163]. Alig et al. [100] also confirm these results. In their paper, they demonstrated the negative effect on the electrical conductivity of both increasing the injection rate and decreasing the melt temperature. They explained this behaviour with the destruction of the conductive network due to increasing shear stresses and viscosity of the polymer.

Only a viscosity reduction, in fact, seems to help MWCNTs agglomeration, favouring van der Waals bonds [133, 162]. Moreover, both researcher groups stated that low electrical resistivity are obtainable with the combination of high melt temperature and low injection rate.

Holding pressure and mould temperature were found to have only slight influence on the increase of electrical conductivity [100, 131, 149, 150 and 164]. On the contrary, Nanocyl internal experimental studies [135] attributed a relevant role to the effect of the mould temperature on the electrical properties. They provided two different reasons to explain the increase of electrical conductivity: firstly, higher mould temperature can have an annealing effect on the injection-moulded parts, favouring the chain reorientation and relaxation. Secondly, an increase in polymer crystallites size is provided and the possibility for MWCNTs to create a conductive network is favoured. Other researchers [132, 165, 166] have found a relevant role of the increment of the T mould on the electrical behaviour of the nanocomposites with different polymer matrices.

Chapter 2

Experimental

2.1. Materials

The first part of the experimental section of this thesis derives from a collaboration with the University of Turin and Perugia during which was decided to develop innovative and smart solutions for the automotive sector. For this reason, a commercial polypropylene injection-moulding grade, already used for the manufacturing of interior components of cars, was selected in order to prepare the electrically conductive formulations. From an industrial point of view, this choice could have guaranteed to develop nanocomposites suitable for this market segment.

Therefore, the random copolymer polypropylene (PP Moplen RP 348 R) was selected as polymer matrix. It was produced by Lyondell Basell and purchased by COM.ITAL (Italian distributor). As previously said, this grade, nucleated and antistatic additivated, is typically used in the automotive sector. It is an injection-moulding grade, with a Melt Flow Index (MFI) of 25 g/10 min (measured at 230°C and 2.16 kg). Its density is 0.9 g/cm^3.

Multi-walled carbon nanotubes, Nanocyl NC7000, were used as conductive fillers and they were purchased by Nanocyl (Belgium). As reported by the manufacturer, they are averagely 10 nm in diameter and 1.5 μm in length. These MWCNTs are produced via catalytic carbon vapor deposition (CCVD) process. They have a surface area of 250-300 m^2/g. The percentage of pure carbon in their composition is 90%.

2.2. Sample preparation

2.2.1. Melt mixing and processing conditions

Different contents of carbon nanotubes were added to PP. MWCNTs were homogeneously mixed with the polymer matrix in a co-rotating twin-screw extruder, Leistritz 27E. Screws have a diameter, D, of 27 mm and a length of 40D. This extruder represents a pilot line, which can simulate the industrial melt mixing process of a thermoplastic polymer. The screw profile and the processing temperature profile are reported in the Figure 33 below.

Along the screw, elements with different melt mixing functions are visible. In particular, the screw profile is built up by kneading blocks (located in four separated areas) and conveying blocks in the other parts of the screw. Each element is designed with a specific alfa-numerical code, which is referred to the kneading/conveying ability of each part. All the codes of the screw profile are reported in the keys box in the figure below. The letters of the codes are referred to German words and, in detail:

- the **GFA** acronym stands for **G**leichlauf – **F**örderelement **A**uskämmend, i.e. co-rotating conveying intermeshing element
- the **GFF** acronym stands for **G**leichlauf – **F**örderelement **F**reigeschnitten, i.e. co-rotating conveying non-self-wiping element (which leads high free volume), located under the main hopper.
- the **KB** acronym stands for **K**net**B**lock, i.e. kneading block
- the **KS** acronym stands for **K**net**S**cheibe, i.e. kneading disc

For what concerns the conveying elements, the first number (which is usually 2) is referred to the combination of two elements in each of the two screws, which constitute the co-rotating extruder. The second number is linked to the step of the thread of each element. The third number represents the length of the conveying part (in mm). On the other hand, in the kneading blocks/discs, the first number is referred to the number of blocks/discs, present in that particular kneading element. The second number is referred to the combination of two elements in each of the two screws. The third number represents the length (in mm) of the global element or of the single disc in the case of narrow or single kneading elements, respectively. Then, the number in degrees denotes the angular shift of one block/disc to another in the same element. Finally, the letter present at the end of the kneading element acronym helps the operator to build in the correct way the kneading elements during the assembly of the screw profile.

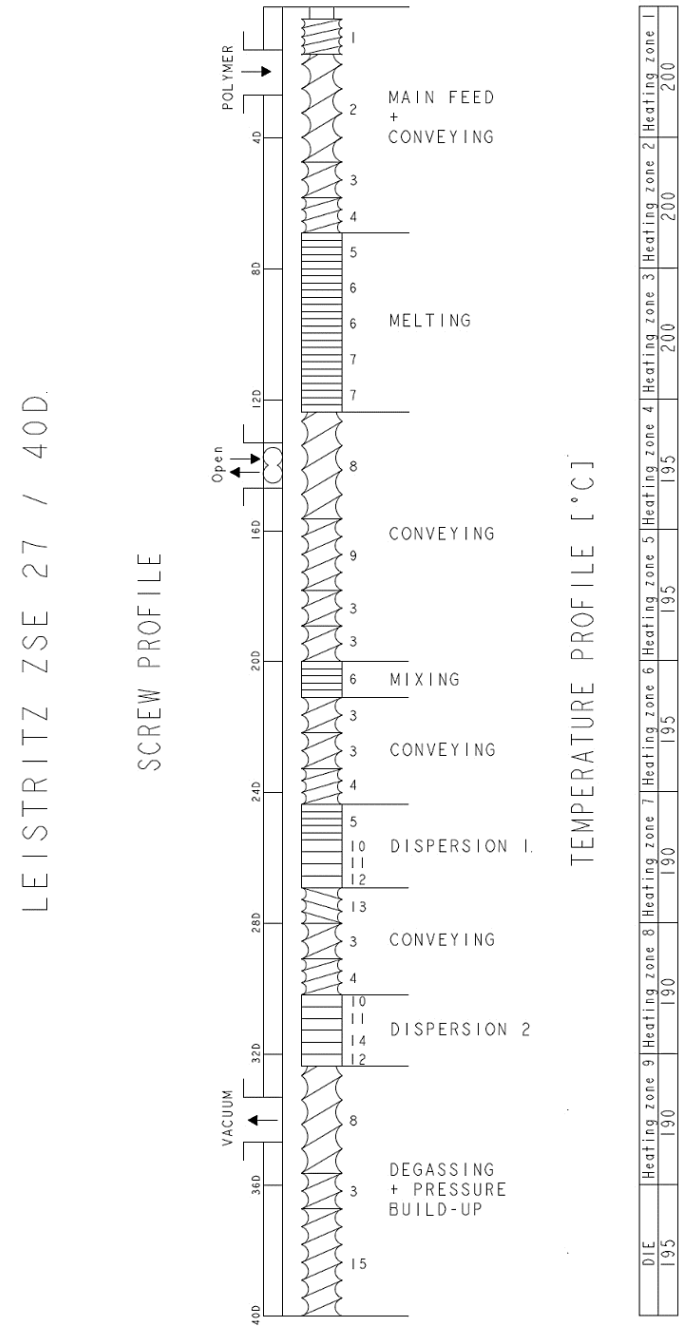

Figure 33: Temperature and screw profile, used for the melt mixing process. A legend with the codes of each element is reported in the image.

Polymer was fed through a Brabender gravimetric dosing unit at the beginning of the extrusion line through the main feeder, while MWCNTs were fed via the lateral side feeder, which is placed at two third of the screw length from the extrusion die. The screw speed was maintained constant and it was 220 rpm. The temperature profile was divided in 9 heating zones, from 200 to 190°C as reported in the figure above. The temperature of the die was set around 195°C.

Several formulations were prepared with MWCNTs, namely 1 - 7 wt%.

Two processing parameters were changed during melt mixing of MWCNT-based formulations. The temperature of the screw profile was increased of both 20°C and 40°C, starting from the standard temperature profile, described previously. Moreover, MWCNTs were fed through both the main hopper and the side-feeder. As already reported, different processing conditions could modify the aspect ratio of the fillers and the residence time in the extruder. Even though a longer residence time allows the matrix and the filler to be more in contact and to have a better dispersion, a longer path in the extruder could be detrimental for the MWCNTs length. This can lead to a decrease in the electrical conductivity of the final composite [158, 159].

2.2.2. Injection moulding and processing conditions

In order to be characterized in a second phase, the obtained nanocomposites were processed by injection moulding technique, using a Ferromatik K - Tec 200 press, with a screw diameter D of 50 mm. Rectangular-shaped samples (100x140x2 mm in size) were prepared and the processing temperature profile is reported in Figure 34 (a). The mould was precisely designed in order to minimize MWCNTs breakage during the filling process. It has a fan gate, which helps to uniform the flux of the molten material during the injection phase.

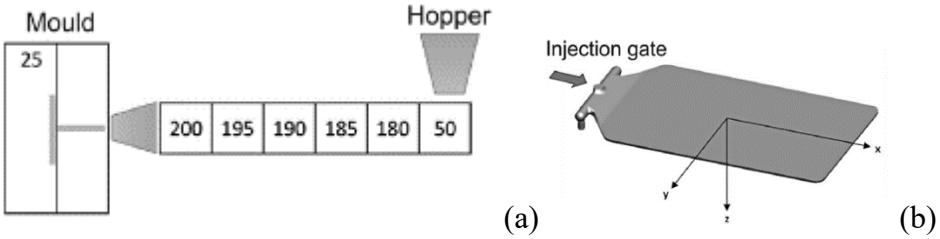

Figure 34: (a) Injection-moulding temperature profile, (b) injection-moulded specimen.

The samples were previously manufactured using a conventional injection moulding process. As standard conditions, the temperature of the mould was set at 30°C and the flow rate was 70 cm^3/s. These parameters were considered as standard

conditions hereinafter. The flow rate is directly linked to the injection rate, which matches the rotation speed of the screw. The velocity corresponds to the movement of a portion of the screw in a determined time. This movement is composed by a linear component due to the length of the screw and by a rotational component due to the diameter of the screw. Therefore, it is actually a volume (cm^3) displacement in a specific time (s) and so a flow rate (cm^3/s). The use of a flow rate as substitute of the injection rate leads to overcome the geometrical parameters of the screw (length and diameter), which change from one injection-moulding machine to another.

As previously reported, the modification of injection moulding conditions has been shown to strongly affect the final properties of the composites. For this reason, a series of specific injection-moulding tests on MWCNT-based compounds was performed, changing both the injection rate and the mould temperature. The set experimental conditions are reported in the Table 8 below:

Table 8: Modification in injection-moulding conditions.

Mould temperature (°C)	**Injection rate (cm^3/s)**		
30	**35**	**70**	**250**
70	**35**	**70**	**250**

In order to apply the H&C process to furtherly increase the mould temperature, a new injection moulding machine was used. It is an Engel VC 500/120 press, with a screw diameter D of 40 mm. The apparatus, used for this innovative technology, is assembled on this particular press, which shows some differences in the screw configuration if compared with the Ferromatik press, adopted in the first part of the experimentation part.

The heating and cooling circuit of the mould was specifically designed in order to exploit this particular injection moulding technique. The runners are positioned strictly near the surface cavity, in order to have an enhanced thermal exchange between the molten material and the steel surfaces of the mould. In this case, the temperature of the mould can be kept high during the injection and maintenance phases and then, it can be rapidly cooled during the cooling and ejection phases. An

HB Therm control unit controlled the changes in temperature. This control unit is made up of three different blocks, which work with water as mean to govern the heating cycle. These units can reach different maximum temperature, in particular 140°C and 180°C. The control unit does not directly control the cooling cycle. Using the H&C process modified the injection cycle time, increasing it. The MWCNT-based formulations were tested using the H&C process:

- increase of the mould temperature up to 100°C during the injection phase
- constant temperature during the maintenance phase
- cooling up to 60°C until ejection

The variation of these process parameters, as already said in the § *1.5.3. Heat&Cool,* which is directly related to the explanation of this process, implicates an increase of the cycle time of the global process. In this specific case, passing from a T mould near the room temperature (30°C) to a T mould of 100°C causes an increase of the cycle time of about 70%. This value is not affected by the filler content level and it remains more or less the same for each tested formulations. Nevertheless, this parameter has to be taken into account from an industrial point view, because it can mean an increase not only of the global cycle production time but also of the production costs. Probably, in the perspective of an industrial scale up, an optimization of this process has to be done.

In order to verify the impact of a change in melt temperature on the electrical properties of the final components, the temperature profile of the injection screw was increased of 20°C compared to the standard conditions.

Processing parameters were changed for all the MWNCT-based formulations around the percolation threshold (2 – 4wt %).

2.3. MWCNT characterization

Thermogravimetric analysis

MWCNTs were thermally tested using a thermogravimetric analysis (TGA) on a Q500 TA Instruments. The test was performed in a temperature range from 50°C to 800°C in both oxidative (air) and inert (nitrogen) atmospheres. The heating rate was 10°C/min with a gas flow of 60 mL/min. The collected data were T_{onset}, which corresponds to the temperature at which the material has a weight loss of about 5% of the initial weight, T_{max}, which is the temperature corresponding to the maximum rate of weight loss and the final residue at 800°C. As it can be seen in the thermograph in the Figure 35 below, the Nanocyl™ NC7000 are highly stable until

800°C, when they are tested in a nitrogen atmosphere (dash-dot blue line). At the end of the test, the MWCNTs have lost only the 3.5wt % of their initial weight. Different is their behaviour in the oxidative atmosphere. A quite complete thermal degradation occurs and a residue of 10.5wt % is present at 800°C.

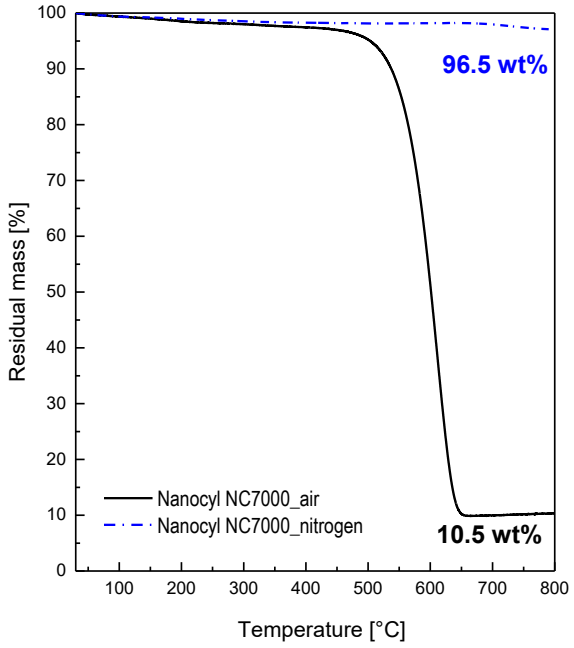

Figure 35: TGA in air and nitrogen atmosphere of Nanocyl™ NC7000.

For what concerns the morphology of MWCNTs, a TEM of the nanotubes producer has been reported in the following image (see Figure 36).

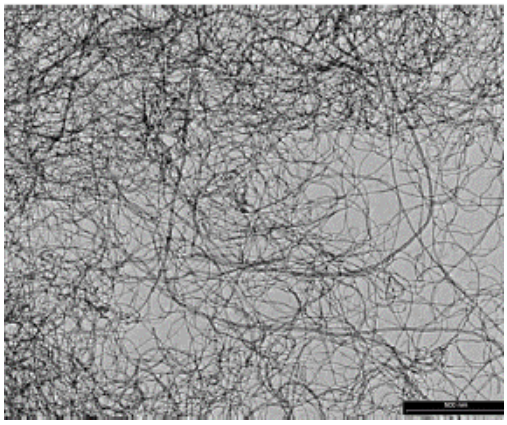

Figure 36: TEM of MWCNTs Nanocyl™ NC7000, performed by the producer (source: Nanocyl).

2.4. Nanocomposites characterization

2.4.1. Electrical characterization

Direct current characterization (DC)

DC electrical characterization was performed by the two-probe method. Electrical resistivity (Ohm cm) and percolation thresholds of samples were measured in the three main directions: longitudinal to the flow direction (X) of the molten material, transversal to the flow direction (Y) and in the through-thickness direction (Z).

The test setup adopted for the electrical measurements along the different directions are reported in Figure 37 (a) and (b).

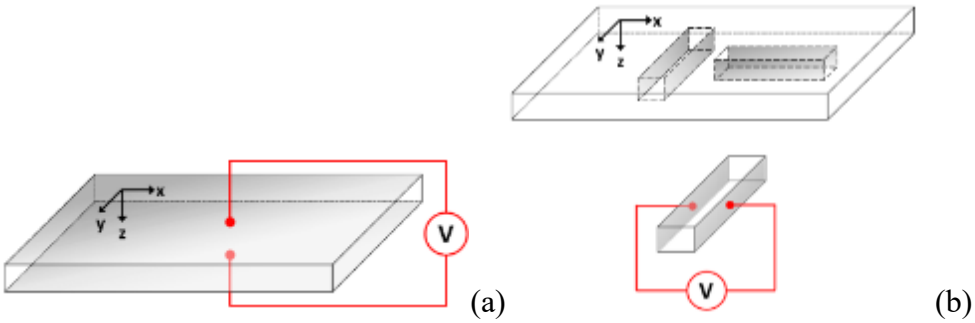

Figure 37: Test setup for electrical measurements in Z direction (a) and in X and Y directions (b) [167].

The volume electrical resistivity measurements in the Z direction were conducted using a Keithley 6517B electrometer (electrode dimensions: 20.971 cm^2) with a Keithley 8009 test fixture. The electrical properties along X and Y were measured using a digital multimeter Keithley 2420, applying a potential in a range of 1 ÷ 20 V. The specimens were cut from the injection moulded samples and their dimensions were 20 x 2 x 4 mm. A silver-based conductive paste was used to obtain two ohmic contacts with a low-resistance (A = 0.225x0.4 cm), 0.3 cm spaced.

A dedicated setup was then developed and implemented to measure the influence of the Z-coordinate in the electrical properties of a cross sectional area. Tests were performed using a Keithley 2420, using two microelectrodes, both perpendicular to Z. They are placed in contact with the specimen surface at regular intervals of 250 µm along the whole sample thickness, from the top to the bottom surface. This configuration setup is reported in Figure 38.

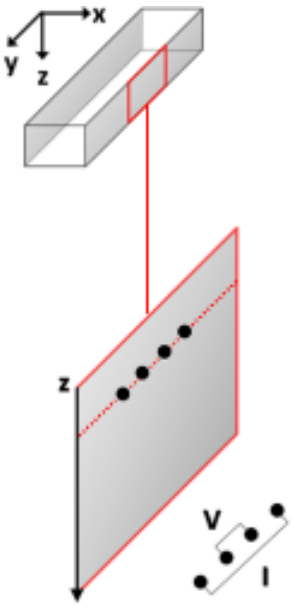

Figure 38: Setup for electrical measurements along the Z direction on *xy* plane [167].

The two tungsten carbide electrodes (100 µm in diameter) were separated by a distance of 1000 ± 10 µm and moved using a micrometre screw-driven XY-axes platform. Each of the electrodes in the backside is connected to a spring under a low loading (30 g) to prevent damage on the sample during the measurement. The spatial resolution during the measurements was estimated to be as low as 200 µm.

The surface resistivity (Ω/sq) was measured using the same instrument adopted for the bulk measurements in Z, a Keithley 6517B electrometer. The test configuration and the Keithley 8009 test fixture are reported in the Figure 39 below.

DC electrical tests were performed according to the ASTM D257-99 standard.

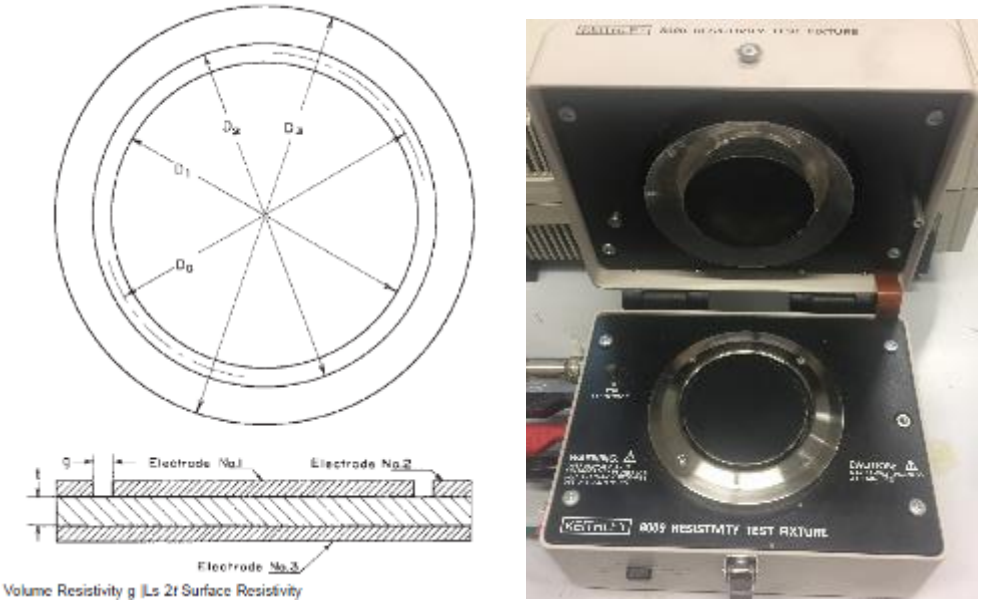

Figure 39: Electrode set-up for surface resistivity measurements on the left and Keithley 8009 test fixture on the right.

Alternating current characterization (AC)

AC dielectric characterization was performed in the through-thickness direction (Z):

- in the frequencies range $1 \cdot 10^6 \div 1 \cdot 10^9\, Hz$ in order to evaluate complex dielectric properties, the relative permittivity, ε' and the loss factor, ε''as a function of frequency. The test was performed using a HP 4291A software electrometer with a dielectric test fixture 16453 A.
- in the frequencies range $2 \cdot 10^1 \div 1 \cdot 10^6\, Hz$ in order to evaluate the AC electrical conductivity (σ_{AC}) and the impedance Z of the measured system. The σ_{AC}, derivable from the following formula, takes into account the geometrical parameters of each single specimen:

$$\sigma_{AC}(\omega) = \frac{1}{|Z(\omega)|}\frac{t}{A} \qquad (2.1)$$

where $|Z(\omega)|$ is the module of the impedance, t is the thickness of the specimen (in mm) and A is the area of the electrode used for the measurements (in mm^2).

The test was performed using a HP 4284A software electrometer. In this case the used test fixture was a homemade set-up, created specifically for this kind of test (A = 4.90 cm^2).

Moreover, a calculation of the complex impedance Z* was performed. Based on formulas reported in literature, this parameter was measured as:

$$Z^* = Z' - iZ'' = |Z|e^{-j\theta} \tag{2.2}$$

where, θ is the phase, Z' is the real part and Z'' is the imaginary part of the complex impedance. As previously described, $|Z|$ corresponds to the impedance module and it is calculated as:

$$|Z| = \sqrt{Z'^2 + Z''^2} \tag{2.3}$$

From these parameters, the complex dielectric constant, $\varepsilon^* = \varepsilon' - i\varepsilon''$, can be calculated as:

$$\varepsilon^* = \frac{1}{Z^* i\omega C_0} \tag{2.4}$$

where $C_0 = \varepsilon_0 \frac{S}{d}$ is the vacuum capacitance.

The real and imaginary parts of the dielectric constant can be calculated respectively as:

$$\varepsilon' = \frac{Z''}{|Z|^2 \omega C_0} \tag{2.5}$$

$$\varepsilon'' = \frac{Z'}{|Z|^2 \omega C_0} \tag{2.6}$$

The AC electrical parameters were measured in nine different positions of the injection-moulded samples, following the scheme reported below in Figure 40:

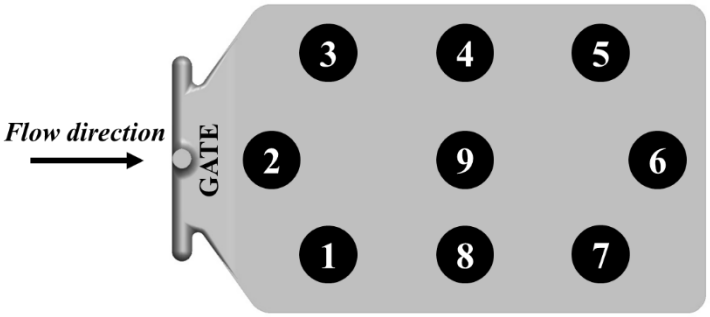

Figure 40: Test configuration in different positions on the injection-moulded samples.

2.4.2. Morphological characterization

Optical microscopy

An optical investigation was performed on the MWCNT-based formulations using an Axioskope 2 Zeiss microscope. The optical test was performed by means of polarized light on cryomicrotomed slices obtained from the injection-moulded samples. The tested specimens are 500 nm thick and they were obtained using an Ultracut E Reichert Jung ultracryomicrotome instrument and a Camera FC4 in order to achieve the correct cutting temperature.

Slices were cut from the entire samples and were obtained along the *z* direction. The observed section corresponds to *xz* and *yz* planes referring to a Cartesian coordinate system positioned in the gate point of the injection-moulded samples. A planar slice with the same thickness of the whole sample (2 mm) was difficult to realize and to observe under the microscope. For this reason, several slices of about 200-300 μm were cut in different zones of the samples thickness, considering the skin and the core layers. Moreover, specimens were taken from a cube cut in the central part of the specimen. Three different slices were obtained from three different positions of the cut cube, namely the two external layers and the core part.

Scanning electron microscopy

Part of the morphological analysis of the injection-moulded samples has been performed by means of a Zeiss Evo50 SEM instrument. In this case, samples were preventively cryofractured and chemically etched by a $KMnO_4/H_3PO_4/H_2SO_4$ etching treatment for 15 h [168]. For what concerns the morphological analysis of specimens injection-moulded with different process conditions, they were observed by a high resolution Field Emission Scanning Electron Microscope (FESEM, Zeiss Merlin 4248). The specimens were preventively cryofractured in liquid nitrogen and then coated with a thin layer (< 10 nm) of Chromium before observation. The differences between both the skin layers and the core region and the different positions of the sample were underlined using this morphological technique.

Two different techniques were used in order to investigate the morphological structure of the injection-moulded specimens at diverse depth levels. On the one hand, removing part of the polymer by means of a chemical etching let to evaluate better the structure and the morphological arrangement of the conductive network of MWCNTs. On the other hand, the global dispersion of the carbon-based filler in the whole thickness of the injection-moulded specimens in different processing conditions has been estimated using a powerful instrument as the high resolution FESEM.

2.4.3. Thermal characterization

Thermogravimetric analysis (TGA)

The formulations were thermally tested using a thermogravimetric analysis (TGA) on a Q500 TA Instruments. The tests were performed in a temperature range from 50°C to 800°C in an inert (nitrogen) atmosphere. The heating rate was 10°C/min with a gas flow of 60 mL/min. The collected data were T_{onset}, which corresponds to the temperature at which the material has a weight loss of about 5% of the initial weight, T_{max}, which is the temperature corresponding to the maximum rate of weight loss and the final residue at 800°C. Samples injected in standard conditions were tested.

Differential scanning calorimetry (DSC)

Differential scanning calorimetry (DSC) tests were carried out on a Q800 TA Instruments. The temperature range was set from 25 to 190 °C with a heating rate of 10°C/min. The method consists of a first heating cycle in order to eliminate the thermal history of the material, a second cooling cycle to study the crystallization of the nanocomposites and a third heating cycle in order to evaluate the melting temperature of the formulations. This test was performed on MWCNT-based formulations injection moulded in standard conditions (T mould 30°C and flow rate 70 cm^3/s).

2.4.4. Rheological characterization

Rheological test

Rheological properties of MWCNT-based nanocomposites were evaluated on a strain-controlled rheometer Ares TA Instruments, with a parallel-plate geometry. Test specimens were compression moulded in disks with 25 mm diameter and 1 mm thickness. Frequency sweeps ranging from 0.03 to 100 rad/s with a fixed strain of 5% (as determined by strain sweep tests). The temperature was controlled by a convection oven, equipped with the instrument and it was set at 200°C. The test was performed in nitrogen atmosphere.

Melt Flow Index test (MFI)

The melt flow index (MFI) was performed on the prepared formulations according to the ISO 1133 standard. The used test parameters were 230°C and 2.16 kg. This test was used to evaluate the possible degradation of the polymer formulations, due to the exacerbation of the processing parameters.

2.4.5. Mechanical characterization

MWCNT-based formulations were mechanically tested by means of the tensile test, performed according to UNI EN ISO 527-2 standard. The used dynamometer was a Zwick Roell Z010 model, equipped with a contact extensimeter. The load cell has a maximum capacity of 10 kN. The applied test conditions were speed test of both 1 mm/min until the 0.25% of deformation of the specimens and 50 mm/min until the breakage of the specimens. Test specimens were directly obtained from the injection-moulded samples, according type 5A of the defined standard.

Chapter 3

Relationship between morphology and electrical properties: anisotropic processing-induced percolation threshold

As it was well documented in literature and largely reported in the previous chapter, the morphological structure and the related properties of an injection-moulded plastic part are strongly affected by both processing conditions and process itself. The modification of morphology during the manufacturing process is even more influenced by adding a filler, as MWCNTs, in the polymer formulation. Anisotropic distribution and dispersion of polymer chains and fillers within the polymer matrix are induced. Consequently, a difference in the main spatial direction properties of the final component is observable. The first part of this thesis is focused on deeply studying the correlation between the morphology and the electrical properties of injection-moulded MWCNT-based nanocomposites. The DC and AC electrical behaviour of composites was studied and the morphological skin-core structure, induced by a conventional injection moulding process in standard conditions, was investigated.

Part of the results reported in this chapter is extracted from the published article "Relationship between morphology and electrical properties in PP/MWCNT composites: Processing-induced anisotropic percolation Threshold", F. Cesano, **M. Zaccone**, I. Armentano, S. Cravanzola, L. Muscuso, L. Torre, J.M. Kenny, M. Monti, D. Scarano, *Materials Chemistry and Physics 180 (2016) 284-290*.

3.1. DC electrical results

DC electrical properties of the PP/MWCNT composites were investigated in the three main directions, namely through-thickness direction (Z), longitudinal (X) and transversal (Y) to the flux directions. The percolation threshold of these directions and the electrical resistivity as a function of MWCNTs content are shown in Figure 41. The electrical percolation threshold in the Z-direction is compared with the X-Y-directions, which are very similar to each other. No significant differences can be observed into the X- and Y-directions, attesting that no filler orientation in the flow direction has been produced during the process. This aspect is in accordance with what is expected for medium viscosity melts obtained under medium or low shear rates [100, 169]. In the Z-direction, the percolation threshold is observable at higher MWCNTs content (between 2wt % and 3wt %), if compared with the values measured for the X- and Y-directions (in the range of 1wt% and 2wt %) [170]. Moreover, the electrical resistivity reaches different plateau values in the three spatial directions, being about 10^1 Ω cm (along X and Y) and 10^6 Ω cm (along the Z).

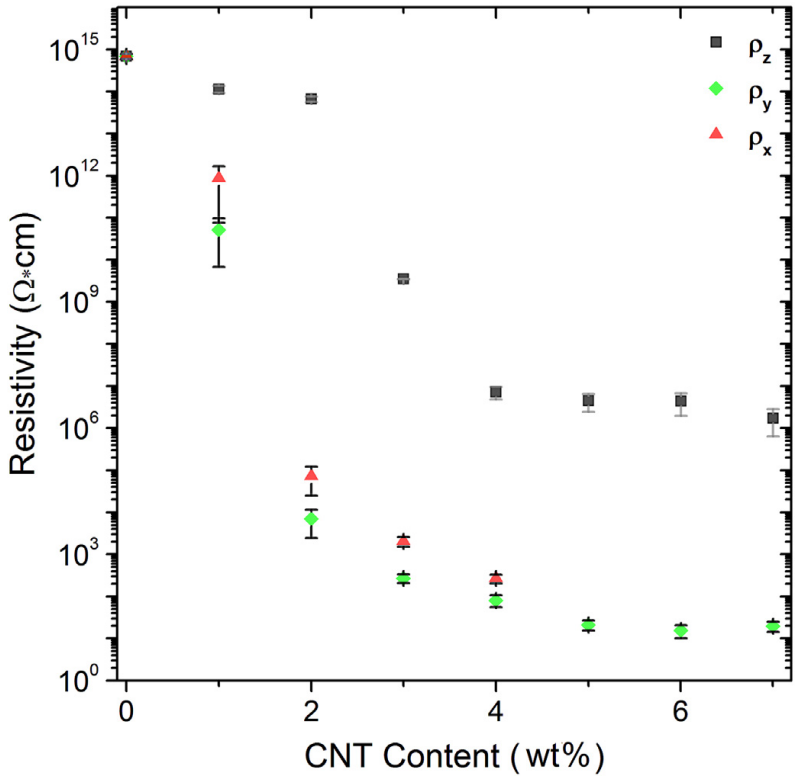

Figure 41: Percolation thresholds of MWCNT-based compounds in the three main spatial directions: *Z*- (black squares) *Y*- (green rhombus) and *X*-directions (red triangles), respectively [167].

Above the critical weight fraction (φ_c), the bulk conductivity σ (φ) takes the form of (1.13) and grows significantly. This behaviour, associated to the formation of a conductive network of particles, is described by the percolation theory, which is explained by several physical models, as previously reported in *Chapter 1 - §1.3.4 Percolation Theory*. The calculation of the critical exponent *t*, mainly dependent on the system dimensions, is a method to predict the three-dimensionality of the percolative network. Initially, it has been reported that in a 3D composite, the lattice percolation model predicts the critical exponent to take a universal value of 2 [14]. Then, it has been experimentally observed that this value is not universal and that it can deviate from the predicted one in many 3D percolation systems [171 - 175] and it can vary between 1.65 and 2 in 3D network [176, 177]. Theoretical explanations for the non-universality of *t* focus on the contacts between adjacent particles [178, 179 and 180].

In this study, the percolation behaviour in the Y-direction was fitted to the percolation equation. A power fitting formula (Belehradek function,$y = a(x - b)^c$) was used to fit the experimental results. The σ_0 value, which corresponds to the parameter *a*, has been set to 0.0032 [S/cm] for all the samples [181]. As it can be seen in the Figure 42 below, the calculated curve strictly fits the experimental data. The percolation threshold φ_c is set to the value around 2, which is coherent with the obtained experimental results. The calculated parameter *c*, referred to the *t* exponent and equal to 2.2, demonstrates that a 3D percolative network is created. Higher conductivity exponent indicates that the conductive fillers form a more uniform and connected path after percolation [182]. The formation of a segregated conductive network relies on the ability of the polymer to provide micro-domains, in which the conductive particles occupy a constrained volume [181].

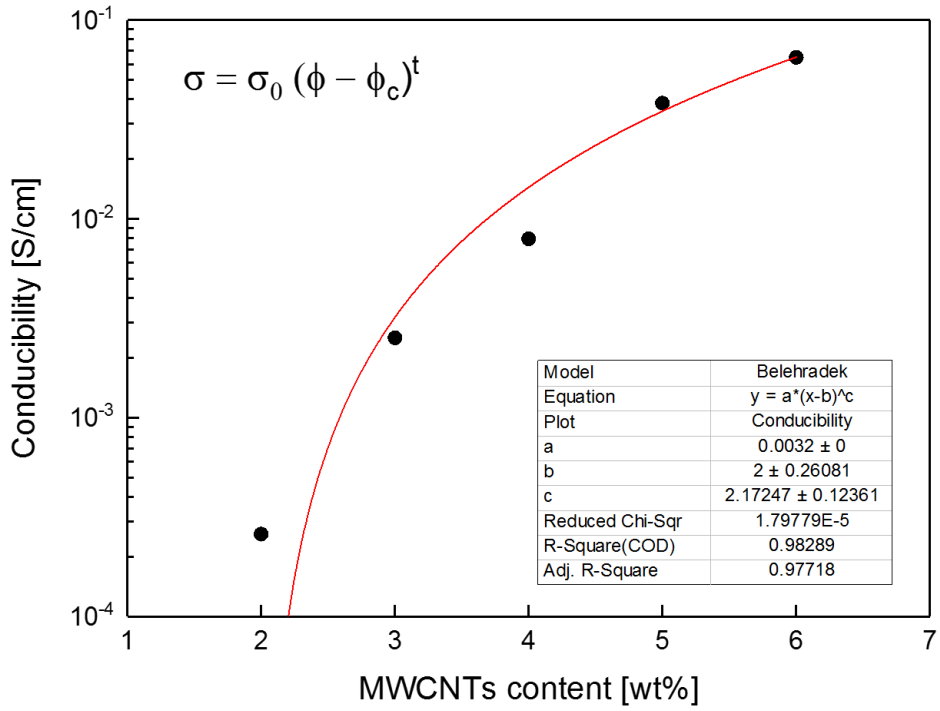

Figure 42: Fitting curve and formula of the Y-direction experimental conductive data.

In order to better understand the electrical behaviour in the three main directions, an extensive study about the influence of the *z*-coordinate on the electrical properties of the composites was performed. The surface electrical resistance was measured in the cross sectional area of the samples with 2-3-4wt % MWCNTs. These formulations were chosen because they are in the range of the electrical percolation threshold in the Z direction. Figure 43 reports the surface electrical resistance as a function of the position over the thickness. The top and the bottom parts of the graph (corresponding to the ordinate axis) represent the two external surfaces of the injection-moulded samples. Some values are missing due to the electrical resistance higher than the detectable limit of the used equipment (R_{max}: $2x10^7$ Ω).

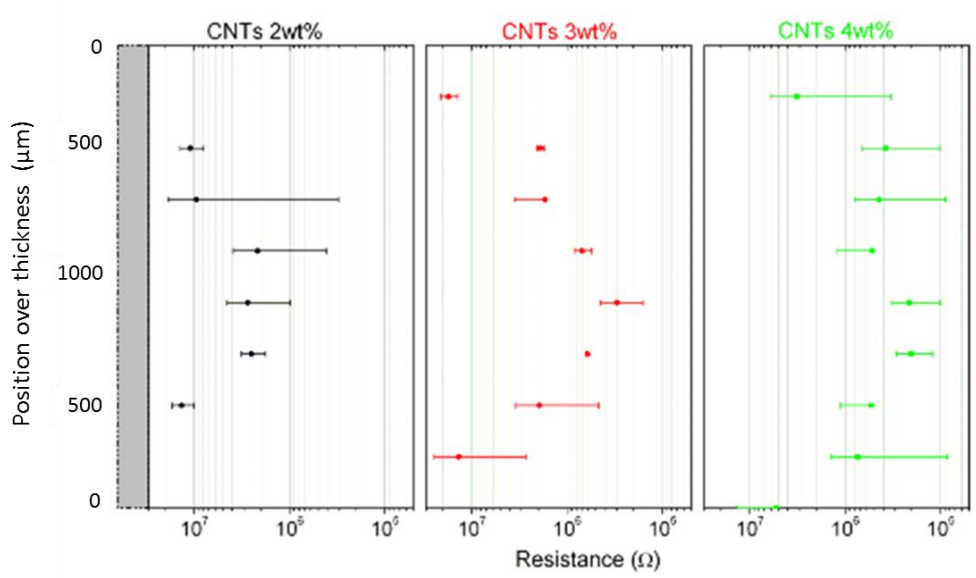

Figure 43: Surface resistance versus position over thickness: 2wt % (black points, left panel), 3w t% (red points, middle panel), 4wt % (green points, right panel) PP/MWCNT composites, respectively [167].

In every tested sample, an internal more-conductive region (*core*) and two external less-conductive layers (*skins*) are observable. In fact, a non-constant electrical resistance along the sample thickness is present and it increases moving towards the external regions. In particular, this behaviour is more marked for the lower content of MWCNTs (2wt %) in comparison with the other two (3-4wt %). In fact, as visible in the left panel of the above figure, the surface resistance grows from the order of 10^6 Ω in the internal region to 10^7 Ω and to values over the detectable limit of the instrument in the external layers. Likewise, in the 3wt % MWCNTs composite the surface resistance changes from the order of 10^5 Ω in the core region to 10^7 Ω in the skins. Although a resistance variation is also present in the 4wt % MWCNTs composite, it is worth underlining that in this case the more-conductive core region is wider than in the other studied nanocomposites and the conductance is nearly constant at about $2x10^5$Ω. In the 2wt % and 3wt % MWCNTs composites, the electrical surface resistance shows a parabolic-like semi-circular shape, with the maximum value of resistance in the middle of the sample thickness and the minimum at its surfaces. This behaviour corresponds to the flow lines of the melt polymer and it is consistent with what reported in literature [104, 150].

3.1.1. Morphological results

In order to explain the obtained results, a detailed morphological characterization was performed. Figure 44 shows SEM micrographs of 2, 3 and 4wt %, obtained from the skin layers (Figure 44 a, c, e) and from the core region (Figure 44 b, d, f). A non-homogeneous distribution of MWCNTs in the overall thickness of the samples seems to be present. The morphology of the 2wt % MWCNT-based composite, in fact, appears divided in filler-rich areas with agglomerates well impregnated by the polymer matrix in the core region, interconnected by resin-rich areas in the skin layers. Even though this structure is also visible in the other MWCNT-based composites, the 3wt % and the 4 wt % MWCNT-based composites are characterized by filler agglomerates, which look like to be well impregnated by the polymer matrix. Nonetheless, in all cases, the internal regions seem to be richer in MWCNTs content than the external layers. Like for the electrical resistance, which is a direct consequence of the morphological structure of the sample, this aspect is more evident for the lower content composite, while in the 4wt % MWCNTs formulation this difference is faded, although still detectable.

The possible explanation of this morphological and electrical behaviour is the formation of a conductive filler network (clustering or *secondary agglomeration state*), induced during the injection moulding process. This agglomeration, necessary for the electrical conduction, occurs at filler content higher than the percolation threshold and to a greater extent in the core regions and leads to conductive paths, which can explain the before-discussed electrical properties [100]. As a preliminary conclusion, it is possible to infer that the skin layers, induced by the manufacturing process, are characterized by a lower conductivity.

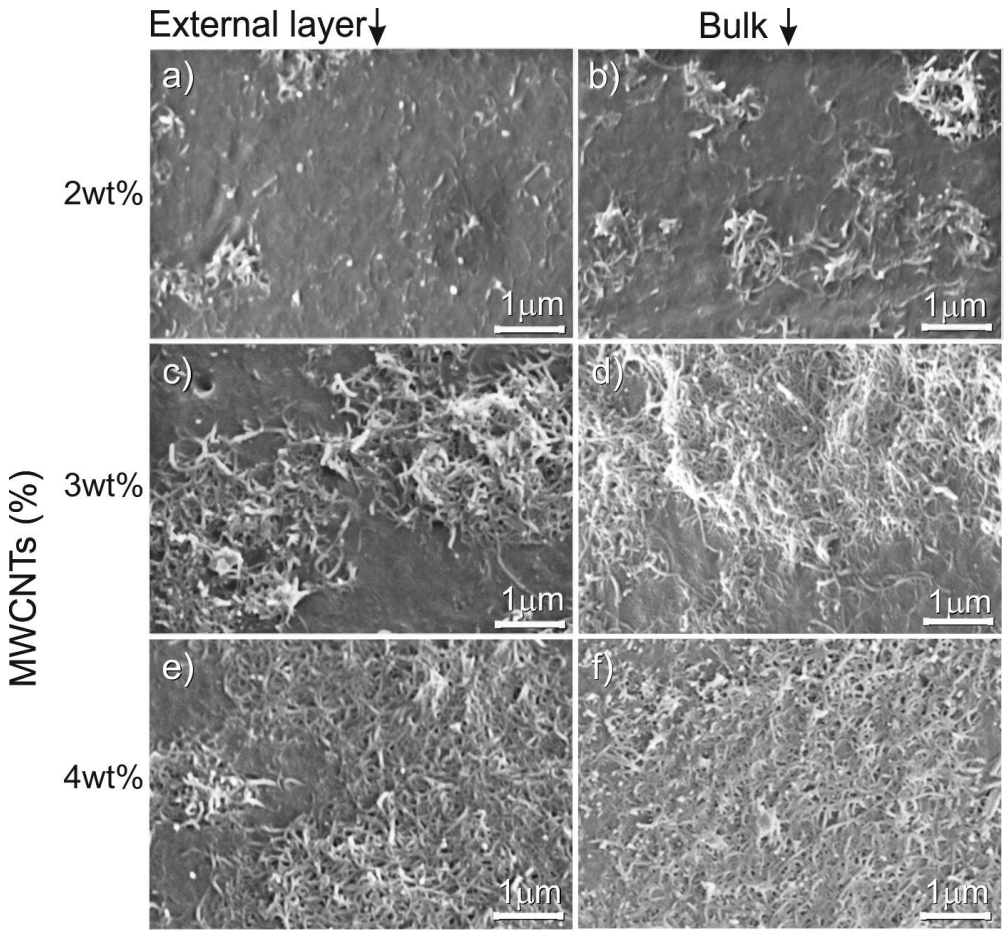

Figure 44: SEM images of the cross-section of the analysed MWCNT-based PP composites. The micrographs were obtained from the skin layers (a, c, e) and from the core regions (b, d, f), respectively [167].

In fact, during the injection moulding process, the molten material undergoes a shear-induced migration flux of the nanofillers from the outer surfaces to the inner ones (higher shear at the surfaces and lower in the centre of the sample). Surfaces of the moulded samples show a different distribution and morphological structure of the conductive nanofillers, which tend to align with the flux direction, extending and their shape in the skin layers and making difficult to create in these regions a strong conductive network [147, 170, 183 and 184]. As already anticipated, this leads to a structure in which the skins are less conductive and the core region is more conductive. This aspect is less evident in the 4wt % MWCNTs composite, most likely because the quantity of conductive fillers is entirely above the percolation threshold.

Consequently, a rough estimation of the thickness of both the skin and core layers can be determined directly by the reported graph. In the 2wt % MWCNT-based nanocomposite the thickness of the skin layers can be roughly estimated around 500 μm, while the core region is of about 1 mm. In the other two cases, the external less-conductive layers can be considered around 250 μm, with a resulting thickness of the more-conductive region of about 1.5 mm.

A confirmation of the described skin-core structure and of the related anisotropic electrical behaviour comes from the optical microscopy performed on ultracryomicrotomed slices of the injection-moulded components, which shows a different spatial orientation of MWCNTs within the polymer matrix.

Figure 45 shows an ultracryomicrotomed slice, obtained from the 3wt % MWCNT-based sample (from the previous discussed electrical results, this formulation seems to be the most suitable to be analysed more in detail). Slices were cut from the entire samples and were obtained along the *z* direction. The observed section corresponds to the *xz* plane. As it can be easily detected from the magnification reported on the Figure 45, the thickness of the micrograph (more or less 1.5 mm) does not exactly correspond to the global thickness of the injection-moulded sample (2 mm). It is a little shorter and this reduction in dimensions is due to the preparation of the specimen itself. The blade of the microtome instrument, in fact, tends to squeeze the first cut part of the sample, during the cutting procedure. For this reason, part of the specimen (in this case the larger side of the obtained trapezoid) results to be rolled up and not visible through the microscope. Therefore, precise considerations on the sizes of the skin and the core regions are not appropriate to be done. On the other hand, an appreciable evaluation of the morphological structure of the injection-moulded sample is possible.

As illustrated in the figure below, a difference in the morphological structure between the internal region and the two external layers are detectable. In both the skin zones, agglomerations of MWCNTs display an elongated and orientated shape. The structure of these layers is immediately frozen, when the molten polymer touches the surface of the mould. For this reason, it is presumably to infer that MWCNTs have not had enough time to organize themselves efficiently and a poor and weak conductive network has been created. Conversely, as it can be clearly seen from the image, in the core region, where the molten material has no contact with the surfaces of the mould, MWCNTs are organized as rounded agglomerates and no alignment is visible. It is reasonable to suppose that an agglomeration, induced by the injection moulding process, has taken place and a conductive

network has been created. Moreover, it seems that a higher quantity of MWCNTs is concentrated in the central region of the sample, if compared with the skin layers. This aspect is in line not only with the morphological results obtained with SEM, but also with the anisotropic electrical behaviour observed in the previous results.

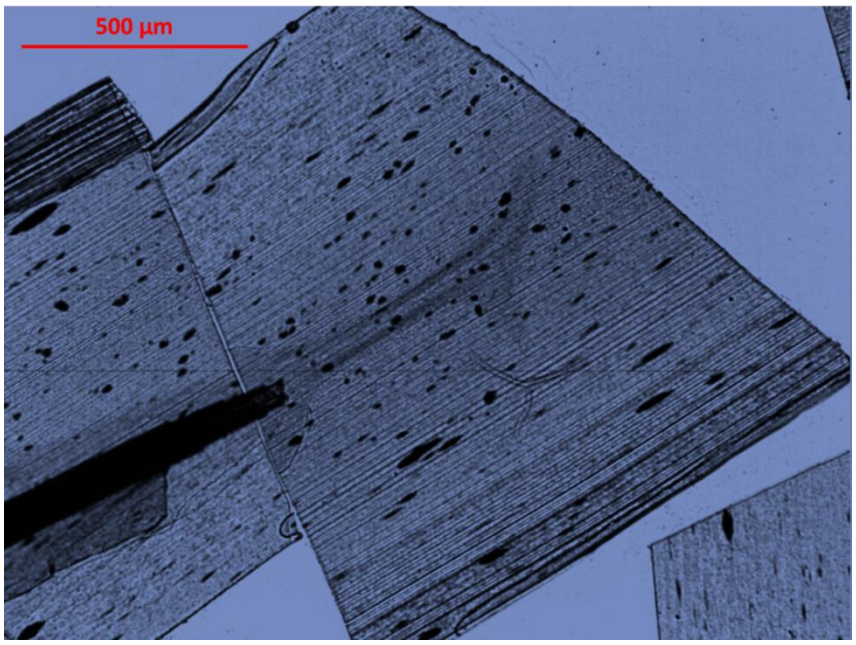

Figure 45: Ultracriomicrotomed slice of 3wt % MWCNT-based sample, obtained from the entire thickness of the *xz* plane of the injection-moulded component. The thickness of the slice is a little shorter than the thickness of the sample due to the cutting procedure. The sample was injection moulded in standard conditions, i.e. T mould 30°C and injection rate 70 cm^3/s.

In order to avoid the drawback of the rolling up of the specimen during the slicing process, smaller portions of samples were prepared. They were obtained from a portion of 3wt % MWCNT-based sample in the central part of the injection-moulded specimen. Slices from different positions over the thickness were obtained. In particular, the one reported in Figure 46 (a)) was cut from the skin layer of the sample, while the one reported in Figure 46 (b)) was cut from the core region of the sample. As expected, the micrograph of the skin layer (Figure 46 (a)) illustrates once again few elongated MWCNTs agglomerates, while the micrograph of the core region (Figure 46 (b)) shows a higher quantity of rounded MWNCTs agglomerates.

The micrographs referred to the *yz* plane are not here reported but they result very similar to the ones previously analysed (in the *xz* plane). This furtherly

confirms the electrical percolation data, which showed no difference in the electrical behaviour in the *x*- and *y*- directions, as discussed at the beginning of this chapter.

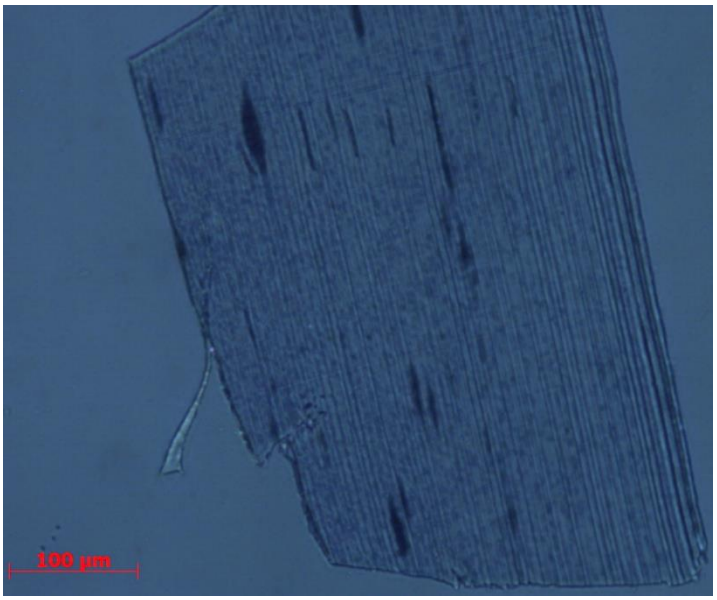

(a)

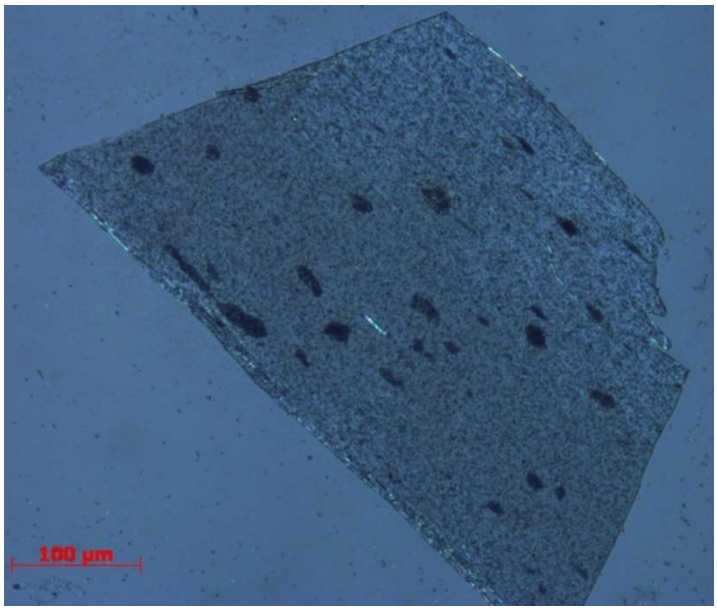

(b)

Figure 46: (a) Ultracriomicrotomed slice of 3wt % MWCNT-based sample, obtained from the skin layer of the sample. (b) Ultracriomicrotomed slice of 3wt % MWCNT-based sample, obtained from the core region of the injection-moulded component. The sample was injection moulded in standard conditions, i.e. T mould 30°C and injection rate 70 cm^3/s.

3.1.2. A proposed model for the electrical behaviour

As it was already said, the injection moulding process induces a non-homogeneous morphology of the MWCNT agglomeration over the thickness of the specimens. This results in the anisotropic electrical behaviour showed in *§ 3.1. DC Electrical results*, where different electrical percolation were obtained based on the test direction. This electrical behaviour can be explained and modelled by representing the injection-moulded samples as a multilayer system of conductive plies parallel to the *xy* plane.

More in detail, the proposed model is based on four layers stacked in the through-thickness direction, each one with its own electrical resistivity, symmetric with respect to the mid-plane (see Figure 47 a). The overall resistivity is affected by the electrical properties of the skin and of the core regions, as well as their relative sizes. In fact, the external layers (the skin) have proved to be less conductive and the internal region (the core) more conductive.

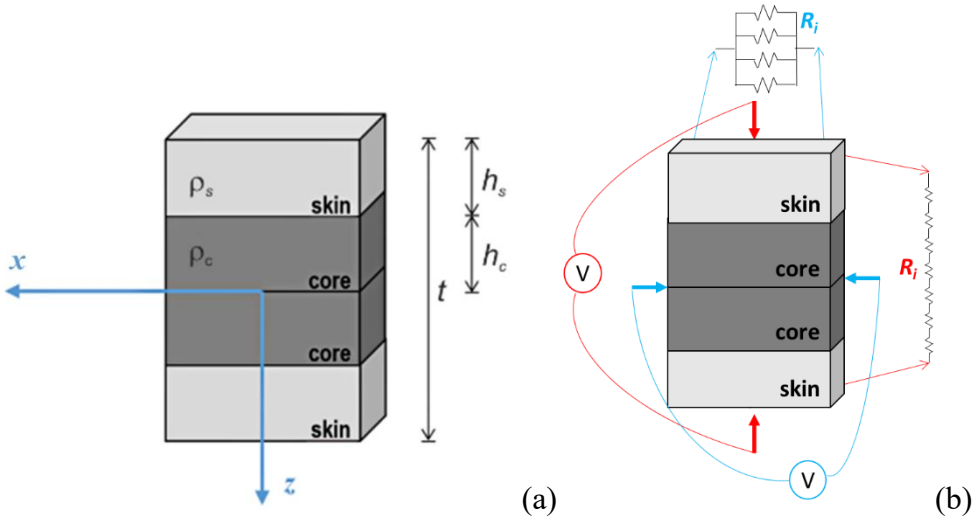

Figure 47: (a) Scheme of the injection moulded samples, described as four layers stacked in the thickness direction; (b) Resistors series (in red) and parallel (in blue), corresponding to the overall Z- and X- directions resistances respectively.

Therefore, according to this model, the *Z*-direction overall electrical resistance (R_z) is governed by a resistors series corresponding to the four layers, while a resistors parallel (see Figure 47 b) should govern the X-direction overall electrical resistance (R_x). This means that the system can be written, as follows (3.1):

$$\begin{cases} R_z = 2R_s + 2R_c \\ \frac{1}{R_x} = \frac{2}{R_s} + \frac{2}{R_c} \end{cases} \tag{3.1}$$

The system can be also written substituting R with the well-known equation $R = \rho \frac{l}{S}$, where l is the length of each resistor and S corresponds to the surface of the electrode (this parameter can be considered as a constant value in the system calculation). It results in the following system of equations (3.2):

$$\begin{cases} \frac{\rho_x}{t} = 2 \frac{\rho_s \rho_c}{\rho_s h_c + \rho_c h_s} \\ \rho_z t = 2(\rho_s h_s + \rho_c h_c) \end{cases} \quad (3.2)$$

where, ρ_x and ρ_z are the experimentally calculated electrical resistivity and t is the thickness of the sample (t = 2 mm). Subscripts s and c refer to the skin and the core layers respectively, as assumed for the proposed model; ρ_s and ρ_c correspond to the electrical resistivity, and h_s and h_c are the thicknesses of the skin and the core layers, respectively. The system (3.2) can be solved to calculate ρ_s and ρ_c, taking into account only the solution with a physical meaning (3.3 and 3.4):

$$\begin{cases} 4th_s\rho_s^2 + 2(\rho_x h_c^2 - \rho_x h_s^2 - \rho_z t^2)\rho_s + \rho_x \rho_z h_s t = 0 \\ \rho_c = \frac{\rho_z t - 2\rho_s h_s}{2h_c} \end{cases} \quad (3.3)$$

$$\begin{cases} \rho_s = \frac{-\rho_x h_c^2 + \rho_x h_s^2 + \rho_z t^2 + \sqrt{(\rho_x h_c^2 - \rho_x h_s^2 - \rho_z t^2)^2 - 4\rho_x \rho_z h_s^2 t^2}}{4th_s} \\ \rho_c = \frac{\rho_z t - 2\rho_s h_s}{2h_c} \end{cases} \quad (3.4)$$

The results of the system have been calculated for the three MWCNT contents (2-3-4wt %) and compared to the measured resistivity in the Z- and X-directions.

Table 9: Results of the proposed model.

MWCNT content [wt%]	**ρ_z [Ohm·cm]**	**ρ_x [Ohm·cm]**	**h_s [cm]**	**h_c [cm]**	**ρ_s [Ohm·cm]**	**ρ_c [Ohm·cm]**
2	6.65E+13	1.17E+05	5.00E-02	6.25E-02	1.50E+14	1.62E+04
3	3.49E+09	1.92E+03	2.50E-02	8.75E-02	1.57E+10	3.73E+02
4	4.82E+06	2.85E+02	2.50E-02	8.75E-02	2.17E+07	5.53E+01

The thickness of the two layers has been approximately evaluated by the micrographs reported in Figure 46. Indeed, a threshold can be detected and it can

be used to identify the non-conductive or nearly non-conductive area of the skins and the more conductive area in the core of the section.

The proposed theoretical model aims to explain the electrical behaviour of an injection-moulded MWCNT-filled component, taking into account the skin-core morphology of the sample. The advanced design of an electrically conductive injection-moulded component can lead to an optimization of the final performance. Therefore, the obtained results may provide a robust platform to gain insight into polymer-carbon nanotube dispersion, being an important step in the study and control of the morphology and of the electrical properties of the MWCNT-based nanocomposites.

3.2. AC electrical results

In this study, the electrical behaviour in alternating current at high and low frequencies in the Z-direction have been also studied. In particular, the electrical impedance spectroscopy was exploited to evaluate the frequency-dependence of the electrical properties of the MWCNT-based formulations [158, 185].

The first phase of the experimentation evaluates the effect of the MWCNTs content on the dielectric behaviour of the nanocomposites, produced at the same processing conditions. In Figure 48, AC conductivity, phase angle and dielectric permittivity as a function of frequency and MWCNTs content are reported. The AC conductivity (Fig. 48 (a)) of the 4wt % MWCNT-based formulation shows a plateau in the low frequency region, until a critical frequency. After this frequency the conductivity starts to increase linearly (log–log scale). In Figure 48 (b) the out of phase between current and voltage, theta (θ), is plotted as a function of the frequency. A theta value near to zero [rad] can be related to a conductive material with a resistive-like behaviour: this is true for the nanocomposite with the higher content of MWCNTs (4wt %), which is a percentage already over the percolation threshold. Conversely, a lower content of MWCNTs shows a frequency-constant theta value and it can be correlated to a more capacitive-like behaviour. Furthermore, these results confirm that in the range of frequencies of the test ($10^1 \div 10^6$ Hz), a conductive nature is leading at low frequencies, whereas at higher frequencies a capacitive nature occurs.

The described behaviour is representative of the samples over the percolation threshold and it can be explained by the current flow nearly totally through the MWCNTs network, which acts as a resistive path. On the other hand, when the frequency grows, the more capacitive parts, both the polymer matrix and the

nanotube/polymer/nanotube contact points, give their own contribution in the increase of the global conductance of the system. Finally, in Figure 48 (c) and (d), the real and imaginary parts of the dielectric constant are plotted as a function of the frequency. As it can be seen in the graphs, both these parameters increase when the amount of the MWCNTs grows and both decrease increasing the frequency. In the case of ε', this aspect can be explained with the electrical relaxation process [186]. On the other hand, in the case of ε'', the tendency to decrease can be due to the combination of three separate effects, namely the DC conductance, the interfacial polarization and the dipole orientation [176, 187].

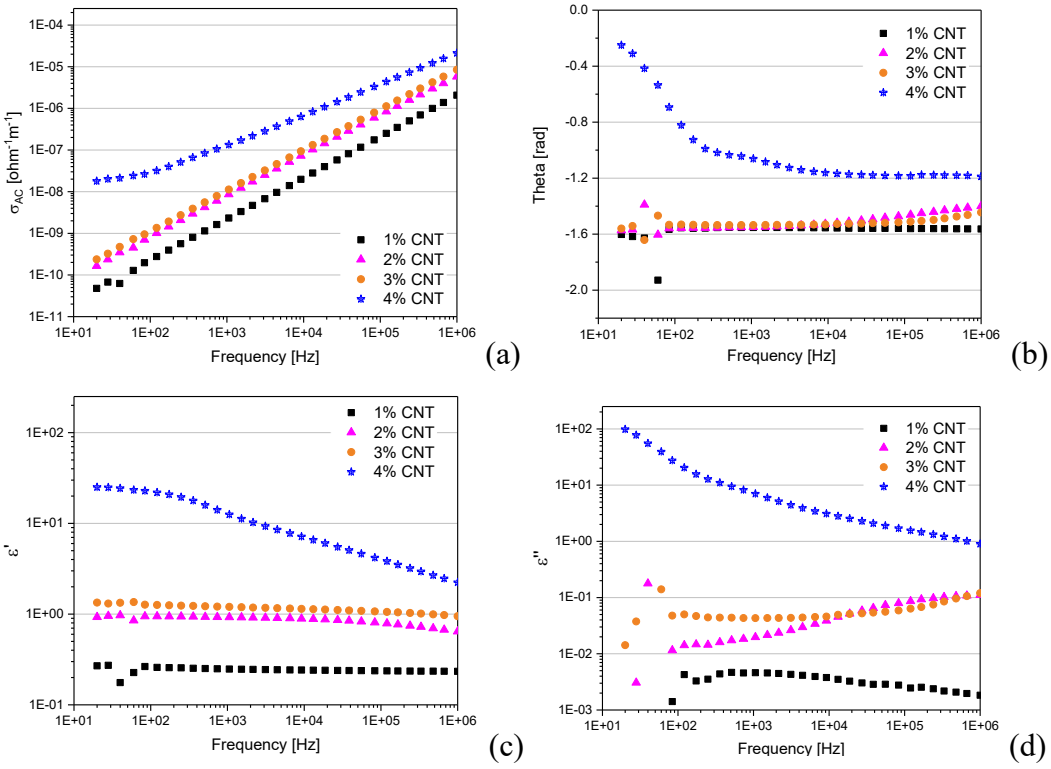

Figure 48: (a) Calculated electrical conductivity in AC ($\sigma_{AC}[\Omega^{-1}m^{-1}]$), (b) θ [rad], (c) ε' and (d) ε'' at low frequency ($10^1 \div 10^6$ Hz) for 1 to 4wt % MWCNTs formulations.

The overall behaviour of the σ_{AC} can be described as the superposition in the nanocomposites of both the capacitive and resistive components. This aspect has been already deeply investigated by Monti et al. [181], who in their work showed similar results related to thermosetting MWCNT-based nanocomposites. They proposed a graphical model, which tries to explain the simultaneous presence of both resistive and capacitive components (see Fig. 49 below).

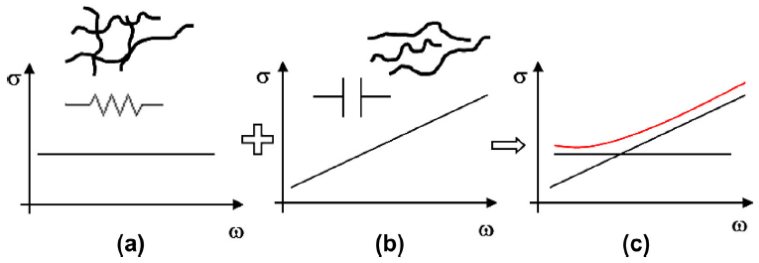

Figure 49: Scheme of the AC electrical conductivity of the systems. (a) Behaviour of a resistor related to the network of MWCNTs, (b) behaviour of a capacitor related to the structure polymer/nanotube/polymer, (c) superposition of resistive and capacitive behaviours, related to the global system. Credit for the picture from the article of Monti et al. [181]

A MWCNT-based nanocomposite can be schematise by an impedance with a resistive and a capacitive phase. The resistive part (Fig. 49 (a)) is mainly linked to the percolative network and it is due to the tube–tube contact resistance. At low frequencies, only this component contributes to conduction. On the other hand, the capacitive part (Fig. 49 (b)) can be described as the result of micro-capacitors, which are constituted by the nanotubes, separated one each other by a layer of insulating matrix. These components are the main responsible of conduction as frequency increases. Therefore, in a MWCNT-based nanocomposite, the conduction can be considered as the superposition of both the resistive-ohmic behaviour and the capacitive behaviour (which is relevant only at high frequency) (Fig. 49 (c)). A critical frequency value represents the change point between these two different behaviours. Conversely, no low frequency plateau is present in the curve when the material is completely insulating and the ohmic component of the conductivity is too low to be relevant in the global frequency range.

The AC electrical behaviour was measured also in the frequency region $10^6 \div 10^9$ Hz and the obtained data are reported in the Figure 50. The real part of the relative permittivity ε' as a function of the frequency for the 1 to 4wt % MWCNT-based formulations is shown. These results are consistent with what measured at low frequency. The 4wt % MWCNT-based formulation is further confirmed to be the most conductive among all the tested samples, but a change in the electrical behaviour is already observable in the 3wt% MWCNT-based formulation. These values correspond to the DC measured percolation threshold in the Z-direction.

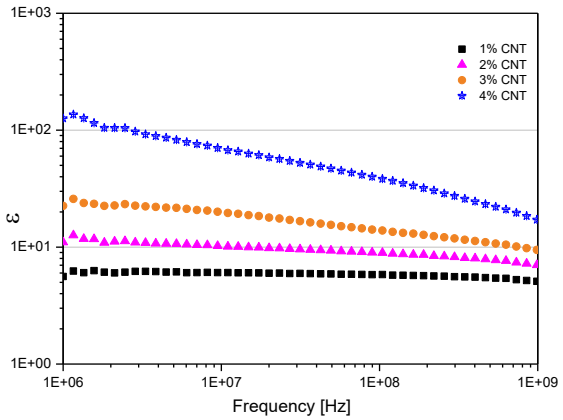

Figure 50: Relative permittivity ε' at high frequency ($10^6 \div 10^9$ Hz) for 1 to 4wt % MWCNTs formulations.

A deeper AC electrical investigation, in all the frequency range, was performed. The AC electrical parameters were globally measured in nine different positions of the samples, following the scheme reported in the Chapter 2. The aforementioned results are always referred to the position number 9, corresponding to the central part of the sample.

No significant dissimilarities are detectable in the 1wt % MWCNT-based formulation, because all the measured values (both σ_{AC} and ε') are completely superimposable. A clear change in the electrical behaviour in different positions is visible only in formulations with a higher MWCNTs content. Conversely, for the other AC electrical measured parameters, a difference is always present between position 2 and position 6, the nearest and the farthest to the gate in the injection-moulded sample, respectively. In the Figure 51 the σ_{AC} (for $10^1 \div 10^6$ range of frequency) and the ε' (for $10^6 \div 10^9$ Hz range of frequency) of some MWCNT-based formulations, measured in all the other positions, are reported as an example.

As a preliminary conclusion of the electrical and morphological characterization, it could be inferred that the injection moulding process induces a distribution of the MWCNTs in the cross sectional area of the sample, which influences not only the morphological structure but also the electrical behaviour of the injection-moulded components. The manufacturing process creates a non-homogeneous morphology, which consequently leads to an anisotropic electrical behaviour.

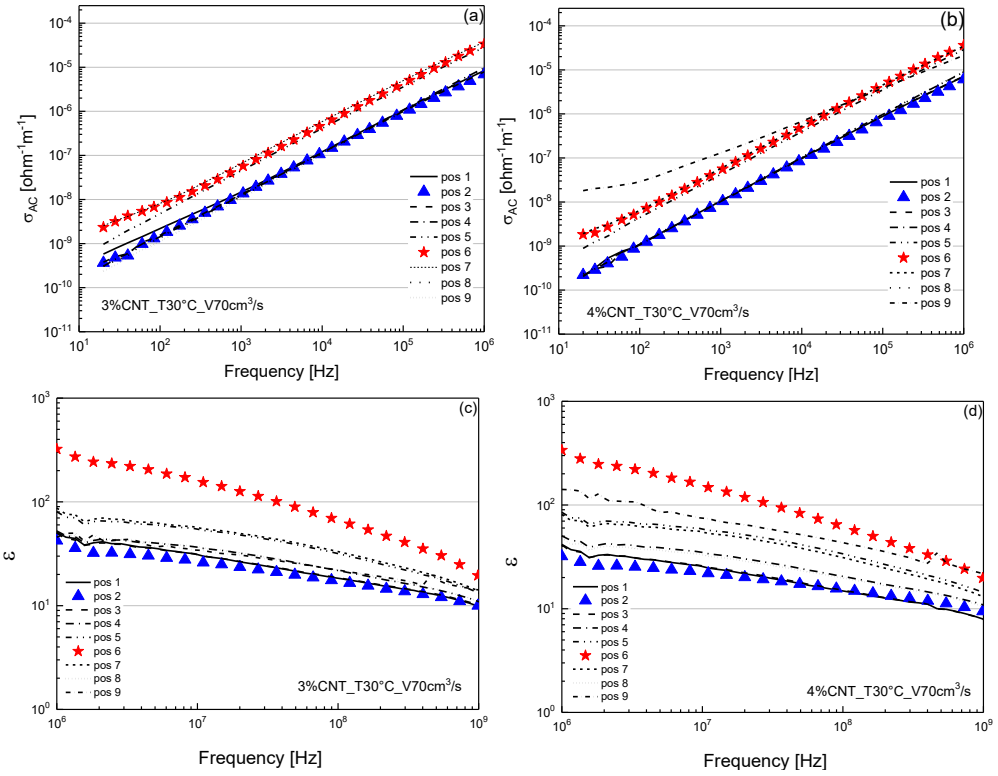

Figure 51: (a) Calculated electrical conductivity in AC ($\sigma_{AC}[\Omega^{-1}m^{-1}]$) at low frequency ($10^1 \div 10^6$ Hz) and (b) relative permittivity ε' at high frequency ($10^6 \div 10^9$ Hz) for 1 to 4wt % MWCNTs formulations, measured in different positions on the specimens: the number 2 corresponds to the position next to the gate, while the number 6 corresponds to the position further to the gate.

3.3. Thermal results

The injection-moulded samples were also characterized by means of thermogravimetric analysis and differential scanning calorimetry. These tests were performed in order to evaluate changes both in the overall thermal stability and in the degree of crystallinity of the matrix and nanocomposites respectively, induced by the presence of the MWCNTs.

In the DSC test, important parameters such as crystallization temperature Tc, melting temperature Tm, crystallization enthalpy ΔH_c, melting enthalpy ΔH_m, and degree of crystallinity X_c were obtained. In particular, this value was calculated as a function of temperature, using the following expression (3.5):

$$X_c(\mathrm{T}) = 100\left(\frac{\Delta H_f}{\Delta H_f^0}\right) \qquad (3.5)$$

where ΔH_f is the measured sample enthalpy, which changes during melting, while ΔH_f^0 is the thermodynamic heat of fusion at the melting point. It corresponds to the theoretical enthalpy value for a 100% random copolymer polypropylene and the used value during the test is 207 J/g [188].

The obtained data in the first heating, cooling and second heating cycles are reported in Table 10. The first heating step considers the effect of the manufacturing process on the thermal behaviour MWCNT-based composites, while the second heating step is necessary in order to evaluate the thermal behaviour of the plastic material itself. Then the cooling step gives information about the crystallization behaviour of the nanocomposites.

Table 10: Differential scanning calorimetry results for MWCNT/composites.

MWCNT content [wt%]	1st heating cycle			Cooling cycle		2nd heating cycle		
	Tm (°C)	ΔHm (J/g)	Xc (%)	Tc (°C)	ΔHc (J/g)	Tm (°C)	ΔHm (J/g)	Xc (%)
0	152	59	28.5	121	87	149	63	30.2
1	148	59	29.0	118	83	150	61	30.0
2	149	55	27.3	117	80	151	59	29.0
3	149	53	26.4	118	81	150	57	28.5
4	148	51	25.8	118	79	150	55	27.7

As evident from Figure 52, the melting temperature, in both heating cycles, remains nearly stable and no significant differences are detectable, due to the presence of the conductive filler. During the cooling phase, the crystallization rate of the MWCNT-filled samples is slightly slower, with the peak occurring at a low temperature in comparison with the neat polymer. Moreover, a slight reduction of the crystallinity with increasing the MWCNTs content is observable. This behaviour has been already seen, not only in the presence of MWCNTs [189] or SWCNTs [190], but also with other type of fillers like nano-clay [191]. Despite some researchers reported that MWCNTs acted as nucleating agents in polymers [192], it is reasonable to suppose that in this case the fillers operate as restriction sites for the polypropylene, impeding it from obtaining highly ordered spherulites.

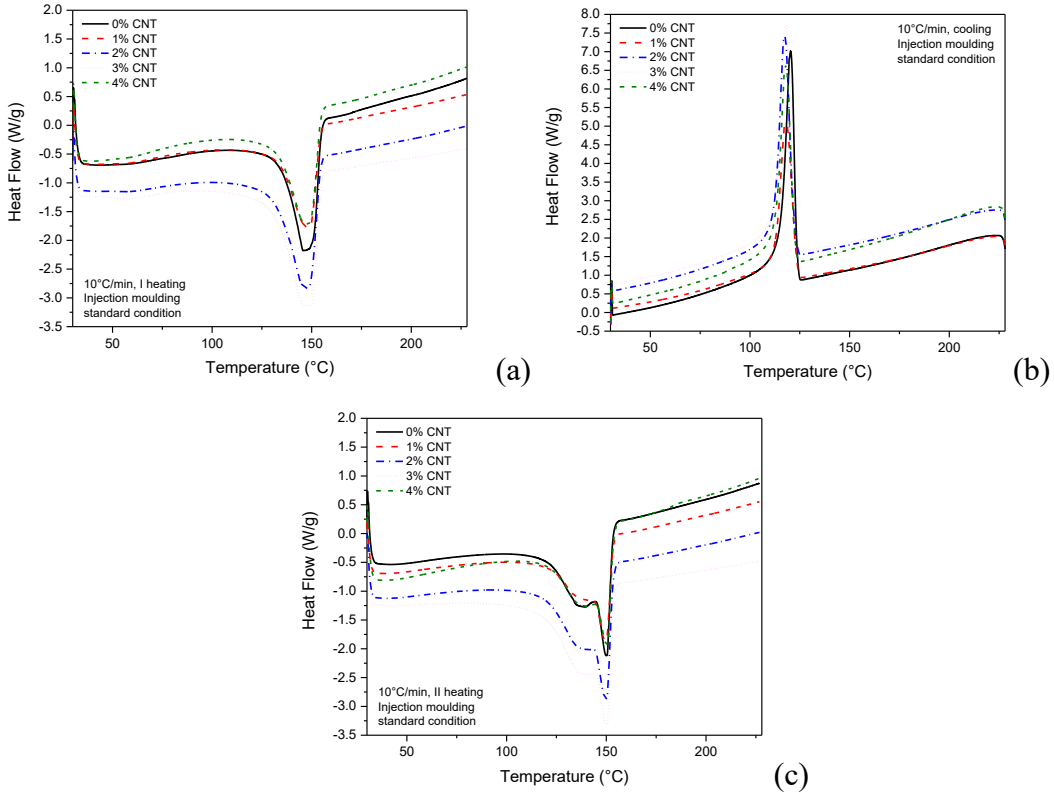

Figure 52: DSC graphs of MWCNT-based compounds, injection-moulded in standard conditions. (a) I heating cycle from 30°C to 230°C; (b) cooling cycle from 230°C to 30°C; (c) II heating cycle from 30°C to 230°C.

In Table 11, the results of the thermogravimetric analysis (TGA) in nitrogen atmosphere of the MWCNT-based mixtures are reported. The first three columns show the degradation temperatures of the samples at different percentages of mass loss in relation to the initial mass of the specimens. More in detail, T_{onset} represents the on-set degradation temperature, at which the thermal degradation of the material begins and it corresponds to the 5wt % mass loss of the initial mass of the analysed samples. The $T_{50wt\%}$ is the temperature at which the composite reduces its initial mass of 50wt %, while T max is the maximum peak of the derivative mass loss and corresponds to the maximum velocity of mass loss of the specimens. All these parameters are fundamental in order to understand the effect of the MWCNTs on the thermal stability of the neat polymer. The last column shows the residue of the samples at the end of the test, at 800°C. This value allows verifying the presence of the correct content of filler, added to the polymer during the melt mixing process. Moreover, in general, it is a valid instrument to prove the effect of the fillers with the polymer during their thermal degradation process.

Table 11: Thermogravimetric analysis results for MWCNT/composites.

MWCNT content [wt%]	$T_{5wt\%}$ (°C)	$T_{50wt\%}$ (°C)	T_{max} (°C)
0	394	433	438
1	416	442	446
2	419	445	449
3	421	446	449
4	421	446	450

In this case, an enhancement of the thermal stability of the polymer, due to the presence of the carbon nanotubes, is evident. The increase of the on-set temperature from the neat polypropylene to the 1wt % MWCNT-based compound confirms this aspect. In fact, an increment of about 20°C occurs in this formulation. Then, only a slight improvement in the thermal stability is observable in the other MWCNT-based formulations. The discussed results are also visible in the Figure 53 below, from which it can be deduced that the thermal degradation of both the neat PP and its nanocomposites takes place through a one-step process. The PP maximum decomposition temperature is around 440°C and this value is shifted towards higher temperatures in the MWCNT-based nanocomposites. This behaviour is reported in literature and it can be explained with the microstructure features of the nanocomposites, including the branching and the dispersing effect of MWCNTs [193 - 197]. Moreover, the higher thermal stabilization level could be attributed to the improved interfacial interactions between nanotubes and PP. This leads to an increase of the degradation's activation energy [193]. The final obtained residues at 800°C for each material is coherent with the amount of MWCNTs used to prepare the single formulations.

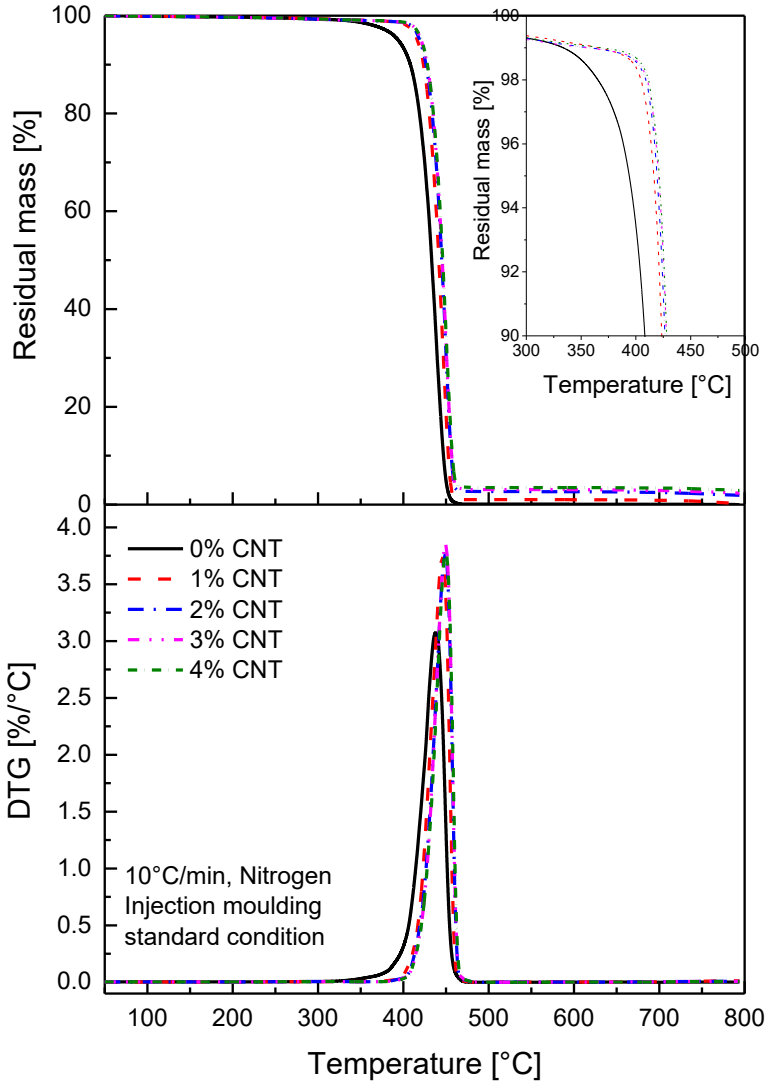

Figure 53: TGA graph of MWCNT-based compounds, injection-moulded in standard conditions. Residual mass and derivative of residual mass from 50°C to 800°C, 10°C/min, in nitrogen atmosphere. The inset graph shows the residual mass of the MWCNT-based compounds, in the temperature interval from 300°C to 500°C.

3.4. Mechanical results

Mechanical tensile tests were performed in the two main directions (parallel and transversal to the flux of the molten polymer direction, respectively MD and TD) on the injection-moulded specimens with a growing MWCNTs amount (from 1 to 4wt %), as reported in Figure 54.

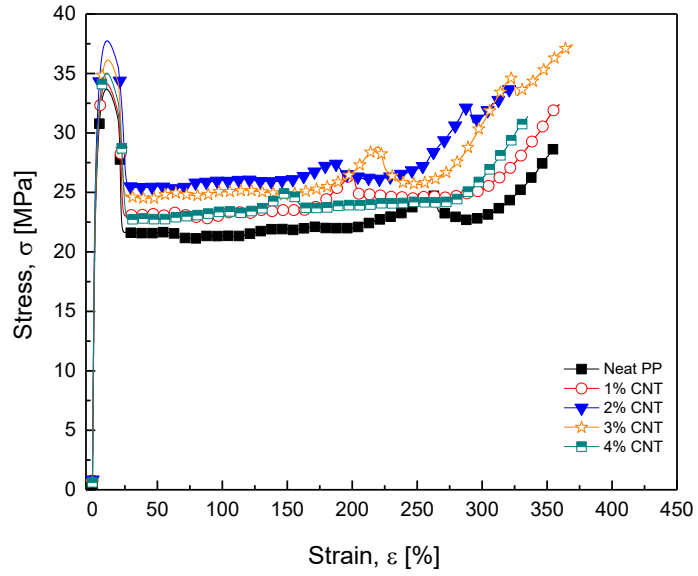

Figure 54: σ-ε graphs of MWCNT-based compounds. Specimens were obtained directly from the injection moulded parts in the directions both (a) parallel to the molten flow (MD) and (b) transversal to the molten flow (TD).

The measured data were compared with the neat polymer, as detailed in Table 12. It can be observed that the mechanical properties of the MWCNT-based formulations do not significantly vary in comparison with the behaviour shown by the neat polymer. The presence of the conductive fillers seems to have a negligible reinforcement effect for the thermoplastic matrix, most likely due to a weak physical interaction between polymer and fillers. It can be assumed that all the

reported data remain more or less the same and no evident modifications in the mechanical results can be detected within the experimental error of the measurements. The presence of secondary agglomerates of carbon nanotubes, which constitute the conductive network, is furtherly confirmed by these results. It could be inferred that, in order to create a conductive percolating network, such a degree of dispersion has been achieved. Anyway, this non-completely uniform level of dispersion is not still enough to achieve an efficient load transfer mechanism from the polymer matrix to the filler [76, 198]. It is also important to notice that the MWCNTs loading does not affect the final ductility of the nanocomposites, which remains similar to the one of the neat polypropylene. This can be considered remarkable for the mechanical properties of the MWCNT-based formulations [192].

Table 12: Tensile test results of MWCNT-based compounds. Test was performed in the directions parallel (MD) and transversal (TD) to the flux direction.

MWCNT content [wt%]	**Elastic modulus E (MPa)**		**Stress at yield σ_y (MPa)**		**Strain at yield ε_y (%)**		**Strain at break ε_b (%)**	
	Ave.	*Dev.St*	*Ave.*	*Dev.St*	*Ave.*	*Dev.St*	*Ave.*	*Dev.St*
Parallel to the flux direction								
0	1267	(43)	34.0	(1.2)	11	(1)	339	(24)
1	1307	(10)	34.4	(1.4)	11	(1)	380	(14)
2	1368	(70)	36.3	(1.8)	11	(1)	354	(20)
3	1303	(13)	35.9	(0.7)	12	(1)	379	(5)
4	1255	(31)	34.8	(0.2)	11	(1)	359	(21)
Perpendicular to the flux direction								
0	1313	(19)	32.1	(1.0)	9	(1)	337	(90)
1	1211	(48)	33.4	(1.9)	9	(1)	347	(89)
2	1222	(26)	31.9	(0.8)	10	(1)	347	(75)
3	1253	(13)	31.7	(0.4)	10	(1)	354	(100)
4	1310	(41)	33.3	(0.5)	10	(1)	250	(50)

Moreover, from the mechanical point of view no marked differences can be detected in the two main directions, parallel and transversal to the flux of the molten material during the process. This apparently could imply that the final injection-moulded samples are mostly isotropic. Conversely, the electrical and morphological characterization have demonstrated that the carbon nanotubes arrange differently in the skins or in the core region of the injection-moulded samples. This behaviour implies that a complete alignment of the fillers in the flow direction of the molten material during the process was not obtained [77, 190].

3.5. Rheological behaviour and correlation with the electrical properties

The rheological behaviour of the MWCNT-based mixtures compared with the neat polymer were analysed and the main results are reported in the Figure 55 (a-d).

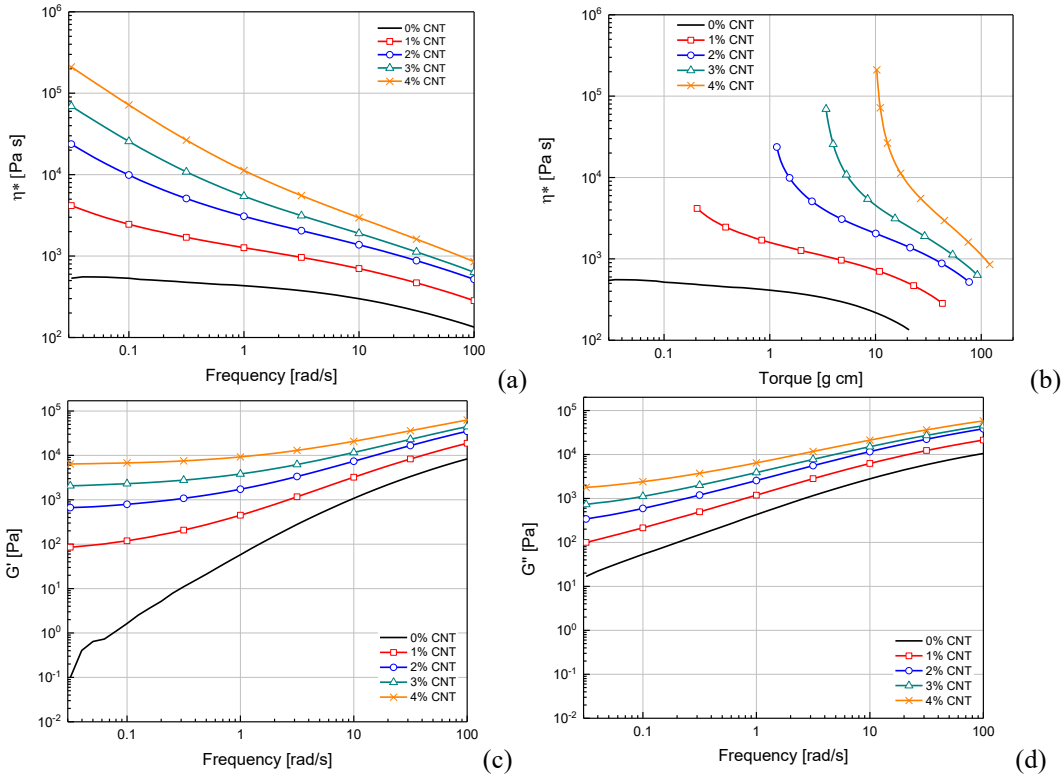

Figure 55: Rheological results of MWCNT-based compounds compared with the neat polymer. Strain-controlled tests were performed from 0.03 to 100 rad/s at 200°C. (a) Apparent viscosity vs applied frequency. (b) Apparent viscosity vs applied torque. (c) Shear storage modulus vs applied frequency. (d) Shear loss modulus vs applied frequency.

The first graph (Fig. 55 (a)) shows the complex viscosity η* as a function of the oscillation frequency during the test. As it can be observed, at low frequency the viscosity of the composites increases of some orders of magnitude with the MCWNTs content and in comparison with the neat PP. The tendency of the nanocomposites to change their rheological behaviour from a liquid-like to a solid-like material is evident and it can be due to the formation of a filler network, increasingly denser with the MWCNTs content [166, 192, 196, 199 and 200]. The increase is more pronounced in the low frequency region and it becomes less significant at higher frequency. Furthermore, all MWCNT-based samples show a shear-thinning behaviour. In fact, particle-particle interactions are reduced due to

the higher shear flow rate, and the effect of the carbon nanotubes on the rheological behaviour of the polymer is less evident in this frequency region. On the contrary, the neat polymer exhibits a lower frequency dependency and a pronounced Newtonian-like behaviour. This is in accordance with what is reported in literature [193, 199 and 201].

The formation of a filler network is also confirmed by the results reported in the second graph (Fig. 55 (b)), which shows the apparent viscosity as a function of the applied torque during the tests. These curves demonstrate that for the materials with the 2, 3 and 4 wt% of MWCNTs, a tendency to a yield stress is observed. This characteristic is associated with numerous kinds of complex fluids, whereby the material does not flow unless the applied stress exceeds a certain value. The tendency to a yield stress at the beginning of the flow can be explained, considering that at the higher MWCNTs amount, the percolation threshold could be reached. This parameter, which could be considered a problem from the manufacturing point of view, is present at different frequencies compared to which are really used in the injection moulding technique [202].

The viscosity growth is also directly linked with the marked increment of the storage modulus G', whose value increases of three orders of magnitude (from 10^{-1} to 10^{2} Pa) from the neat PP to the 1wt % MWCNT-based composite, as seen in the third graph (Fig. 55 (c)). This confirms the presence of a network, in which fillers have created an interconnected structure and the nanotube-nanotube contacts limit the motion of the polymer. Starting at about 1wt % MWCNTs, the storage modulus shows a plateau at low frequencies. This critical value may be assumed as a rheological percolation threshold, which is strictly correlated to the electrical percolation threshold [200, 201]. In this case, the rheological percolation threshold is lower than the electrical percolation threshold and it is between 0wt % and 1wt %. This is probably mainly due to the manufacturing process, which the MWCNT-based samples were prepared with, i.e. the compression moulding. It is widely reported in literature, in fact, that the use of this process lets to avoid an anisotropic displacement of the fillers in the polymer matrix and to obtain lower percolation threshold values. This behaviour is less evident for the loss modulus G'', which shows a slower growth tendency, in relation with the MWCNTs content (Fig. 55 (d)). Nevertheless, both moduli present a frequency dependency, more noticeable at low than at high shear rates [200]. Analysing more in detail the G' and G'' behaviour of each single formulation compared with the neat polymer, it is evident that at low frequencies, the molten material is more similar to viscous fluid, in which G''>>G'. Increasing the frequency values, G' passes over G'' and in this

case the polymer response is more similar to an elastic solid. The viscoelastic behaviour of a polymer is directly linked to its microstructure and in particular to the presence of entanglements and different amounts of fillers. The discussed behaviour is clearly visible in the graphs reported in the Figure 56. Increasing the amount of MWCNTs in the formulations leads to shift the polymer rheological properties closer to a material with a greater elastic component than a viscous one [203, 204].

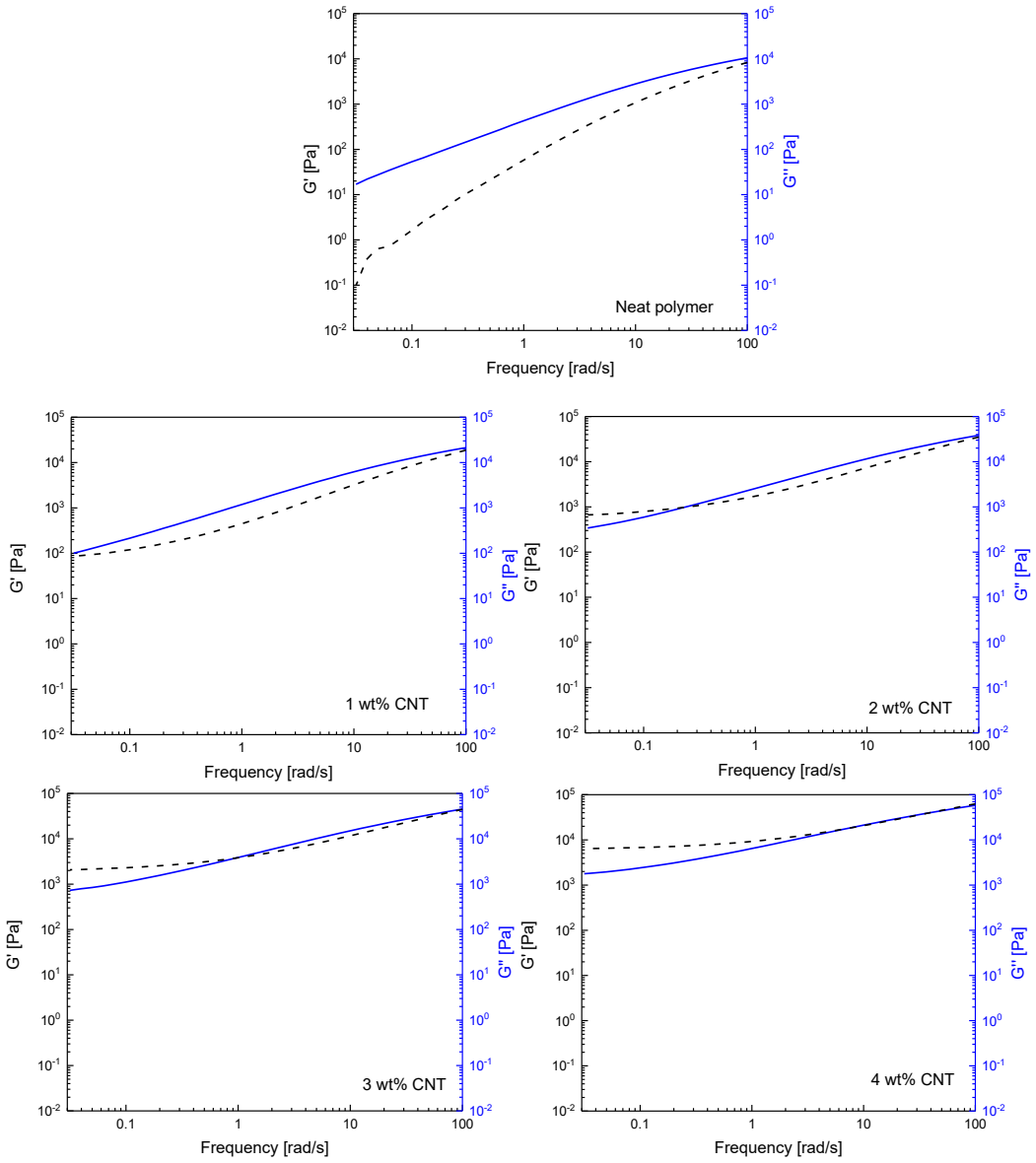

Figure 56: Comparison between G' and G'' for the 1 to 4wt % MWCNTs formulations in comparison with the neat polymer.

Finally, applying an industrial research technique as the Melt Flow Index (MFI), a qualitative evaluation of the grade of fluidity of the nanocomposites in comparison with the neat polymer, can be obtained. This parameter is directly correlated to the rheology of the system but, in addition, it takes into account the possible degradation of the polymer resulting from the used processing conditions.

As listed in Table 13, the MFI values for the neat polymer and the 3wt % MWCNT-based formulation, tested after different processing conditions (melt mixed and injection-moulded) and compared with the data stated in the technical datasheet of the polymer are reported. These data are consistent with the rheological results: increasing the amount of MWCNTs, a decrease in the MFI values occurs. This indicates a rising viscosity, due to the formation of the fillers percolative network in the polymer matrix. No degradation of the polymer occurs during the manufacturing processes, due to the presence of the carbon nanotubes: in fact, this phenomenon may be observed in some cases as a secondary effect in MWCNT-based formulation, tested under high shear rate conditions [205].

The neat polymer does not markedly change its chemical structure and the manufacturing processes seem not to affect their processability and rheological properties. The MFI values remain unchanged for both the melt mixed and the injection-moulded specimens, in comparison with the technical datasheet value. On the other hand, significant differences can be observed in the 3wt % MWCNTs samples, tested after the melt mixing and the injection moulding processes. Although the melt mixing helps to disperse the MWCNTs homogeneously in the polymer matrix, the presence of a filler, even in low amounts, can increase the viscosity and, consequently, decrease the fluidity of the final compound system. Then, during the injection moulding process, an agglomeration of the carbon nanotubes may occur and the fluidity of the system again strongly decreases, reaching the 5.5 g/10 min value.

Table 13: MFI 230°C/2.16 kg, injection moulding standard conditions (T mould 30°C, injection rate 70 cm^3/s)

MWCNT content [wt%]	**Technical datasheet of the neat polymer**	**Extruded sample**	**Injection moulded sample**
0	25.0	24.0	23.2
3	-	8.1	5.5

Chapter 4

Effect of processing conditions on the electrical behaviour and the morphology of injection-moulded PP/MWCNT nanocomposites

As investigated in the previous chapter, a conventional injection moulding process in standard conditions can induce an anisotropic distribution of MWCNTs in the polymer matrix and can create a related morphological skin-core structure in the PP/MWCNT nanocomposites. Consequently, a difference of the electrical behaviour in the three main spatial directions of the nanocomposites was found. Therefore, it can be reasonable to assume that a direct and marked correlation between electrical properties and manufacturing processes exists.

As aforementioned, not only the manufacturing process influences the final properties of the nanocomposites, but also the modification of the processing conditions seems to have a fundamental role on both the morphology and the electrical conductivity of the nanocomposites. Therefore, the aim of this second experimental part is to study the effect of variations of processing conditions on the electrical behaviour and morphology of the PP/MWCNT nanocomposites. For this reason, a modification of the parameters of both the melt mixing and the injection moulding processes and a non-conventional injection moulding technique were adopted. The obtained results of this part of thesis are reported in the present chapter.

4.1. Effect of melt mixing conditions

In order to verify the effect of melt mixing conditions and to understand the correlation of these changes on the morphology of the system, two key processing parameters were modified. In particular, the feeding conditions were changed and MWCNTs were fed both alone through the lateral side-feeder and together with the polymer matrix through the main hopper. Moreover, an increase of both 20°C and 40°C of the screw profile temperature, starting from the standard conditions profile, described in Materials & Methods section (see *Chapter 2*), was applied. The tested specimens were first melt-mixed with the previously mentioned different processing conditions and then injection-moulded in standard conditions. The DC electrical resistivity and the morphological structure of the nanocomposites were measured and observed on the injection-moulded samples.

4.1.1. DC electrical results

Figure 57 shows the electrical percolation curves in both Z- and Y- directions, as a function of the mixing layout (i.e. where the MWCNTs were fed, either the side-feeder or the main hopper). This modification of the feeding layout was adopted for the 4-5wt % of MWCNTs, formulations with resistivity values just beyond the percolation threshold. As it can be clearly seen from the graph, in both the Z- and Y- directions the measured resistivity values of the formulations in which MWCNTs were fed through the main hopper result much higher than the values obtained from the formulations in which MWCNTs were added through the lateral side-feeder. This behaviour is more marked in the 4wt % MWCNT-based formulation: in fact, the ρ_z of the main hopper fed formulation is eight orders of magnitude higher than the ρ_z of the lateral side-feeder fed formulation and the resulting final mixture is completely insulating. The same trend is observable for the two different ρ_y (both of the main hopper and of the lateral side-feeder): again, in the case of 4wt % when the nanofillers were fed through the main hopper, the resistivity value is nine orders of magnitude higher and it corresponds to a typically non-conductive material value (i.e. 10^{11} Ohm*cm).

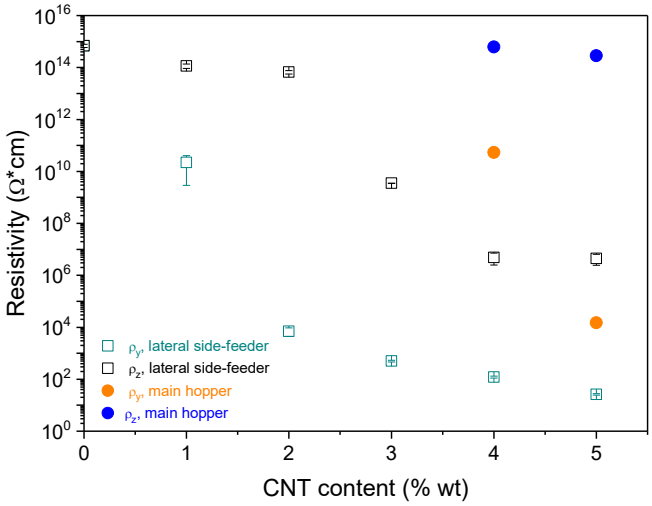

Figure 57: Comparison of bulk resistivity between compounds in which MWCNTs were fed through the main hopper (blue and orange filled circles for Z- and Y- directions respectively) and compounds in which MWCNTs were fed through the lateral side-feeder (black and green empty squares for Z- and Y- directions respectively).

Similar results have been observed in literature for compounds with polypropylene as polymer matrix and MWCNTs Nanocyl™ NC7000 as conductive nanofillers. Müller et al. [206], in fact, explained the worst electrical behaviour of materials in which the nanotubes were fed together with the unmolten polymer through the main hopper with the presence during the process of higher shear forces and longer residence times in the extruder. Moreover, these nanofillers show a quite low bulk density that makes their dispersion in the polymer matrix difficult, if they are not fed through the lateral side-feeder. For this reason, the unmolten pellets of polymer can easily compress them. Additionally, the formation of large agglomerates, more difficult to re-disperse, are favoured. All these aspects seem not to be favourable for the dispersion of carbon nanotubes in order to create a conductive network. It seems also plausible to consider that feeding the MWCNTs through the main hopper could bring to a reduction of the global length of the MWCNTs themselves. This length reduction, in turn, could be recognised as a possible cause for a worse dispersion of MWCNTs and a lower electrical conductivity of the PP/MWCNT nanocomposites.

The processing temperature was the other parameter, which was changed. The modification of temperature concerns the global screw profile, constituted by nine heating zones and the die. Table 14 lists the electrical results (i.e. surface resistivity and bulk resistivity in Z- and X- directions) of the 4wt % MWCNT-based formulation, melt mixed increasing temperature screw profile of 20°C and 40°C in

comparison with the standard conditions. This variation seems not to strongly affect the electrical behaviour of the MWCNT-based formulation [207], unlike changing the feeding conditions. Among all the electrical data, indeed, no substantial differences are detectable and the measured values stay in the order of a magnitude. Only a slight reduction of the electrical resistivity in X-direction is observable, when the melt temperature is increased of 40°C. Nevertheless, it is worth to note that this result is not completely in accordance with what reported in literature by some authors [208, 209], which on the contrary advice to increase the melt temperature in order to improve the electrical conductivity of the nanocomposites. This electrical invariance is also confirmed by the processing parameters, reported in the processing datasheet, where no dissimilarities occur during the melt mixing process (see Table 16). A decrement of about 23% of the applied torque and therefore of the applied shear stresses on the molten material (from the standard conditions to the higher temperature screw profile) demonstrates that an increment of the fluidity of the molten material occurs. Probably a larger dispersion of the nanofillers is present and therefore a weaker conductive network is formed.

Table 14: Comparison of R_s, ρ_z and ρ_x among specimens, melt-mixed with different screw profile temperature. All specimens were injection-moulded at T mould 30°C and injection rate 70 cm^3/s.

MWCNT content [wt%]	Melt mixing Conditions (Melt Temperature)	*Rs* [Ω/sq]	ρ_z [Ohm·cm]	ρ_x [Ohm·cm]
4	190 °C	6.50E+06	3.30E+07	1.04E+03
	210°C	1.11E+08	2.35E+08	2.73E+03
	230°C	4.52E+07	8.50E+07	8.13E+02

The melt temperature values, measured at the die, were used in the following fluidity tests (MFI). The tests confirm the expected increment of fluidity of the final compounds (as reported in Table 15) and the enhanced ability of the nanofillers to be dispersed in the polymer matrix [210]. Nonetheless, it seems that the successive injection moulding has a greater role in the conductive network formation in the PP/MWCNT samples.

Table 15: MFI results of melt-mixed specimens with different temperatures of screw profile (with a load of 2.16 kg). The tested formulation is with 4wt % MWCNTs.

Used temperature for MFI tests [°C]	Melt mixed sample MFI [g/10 min]
190	2.20
210	3.26
230	4.86

Table 16: Melt mixing condition datasheet of the tested formulations.

Melt mixing technical datasheet - Equipment Leistritz 27D

Material code	Screws peed	Amperage	Output	Melt Pressure	Melt Temperature	Barrel temperatures in °C										DIE
	rpm	%	kg/h	bar	°C		HZ 1	HZ 2	HZ 3	HZ 4	HZ 5	HZ 6	HZ 7	HZ 8	HZ 9	DIE		n x mm
PP0023	220	47	20	2	207	SET	200	200	200	195	195	195	190	190	190	195		3x4
						ACTUAL	200	200	200	195	195	195	190	190	190	195		
PP0023	220	34-39	20	2	229	SET	220	220	220	215	215	215	210	210	210	215		
						ACTUAL	220	220	220	215	215	215	210	210	210	215		
PP0023	220	30-34	20	1	252	SET	240	240	240	235	235	235	230	230	230	235		
						ACTUAL	240	240	240	235	235	235	230	230	230	235		
	Comp.1		Comp. 2		Comp. 3	Comp. 4			Comp. 5		Comp. 6	**Description of dosing units**						
No.1	PP		NC 7000									DOS 1		DOS 2		DOS 3		
%	96		4									PP		NC 7000				
No. 2	PP		NC 7000															
%	96		4															
No. 3	PP		NC 7000									Compound		Film		Screw profiles		
%	96		4									x				**A:**	Gentle	

4.2. Effect of injection moulding conditions

This technique induces an anisotropic morphology in the moulded parts structure, and when conductive fillers with a high aspect ratio like carbon nanotubes are used, such orientation leads to a poor network formation and to a shift of the percolation threshold towards higher filler contents. In order to minimize these orientations, which are unavoidable in moulded samples, an optimization of the injection moulding processing conditions is necessary in order to guarantee higher electrical performance. The variation of injection moulding parameters such as melt temperature, mould temperature and injection rate represents an important factor, which highly influences the degree of fillers orientation in injection-moulded parts and the optimization of the process [150, 162, 211].

4.2.1. Electrical characterization

Effect of the variation of the temperature of the melt.

Similarly to what was performed during the melt mixing process, the influence of the T melt was analysed. Table 17 shows the surface resistivity and the bulk resistivity measured in Z- and X- directions of the 4wt % MWCNT-based composite produced with an increase of 20°C of the T melt. The injection rate was maintained at 70 cm^3/s and the T mould was set up at 30°C. As it can be seen, no significant difference can be detected in the electrical results neither in the surface resistance nor in the bulk resistivity in the two main directions, when the processing parameters were changed. Again, only a slight decrease of one order of magnitude is observable in the resistivity of the Z-direction measurement, but it is in line with what obtained in literature. In that case, the effect of the T melt seemed to have a less relevant role on the electrical behaviour of the nanocomposites.

Table 17: Comparison of R_s, ρ_z and ρ_x among specimens with different screw profile temperature. All samples were injection moulded both with standard conditions (T mould 30°C; injection rate 70 cm^3/s).

MWCNT content [wt%]	Injection moulding Conditions			*Rs* [Ω/sq]	ρ_z [Ohm·cm]	ρ_x [Ohm·cm]
	T mould [°C]	Injection rate [cm^3/s]	T melt [°C]			
4	*30*	*70*	*200*	6.50E+06	3.30E+07	1.04E+03
	30	*70*	*+20*	6.50E+06	2.30E+06	1.01E+03

Effect of the variation of the temperature of the mould.

The effect of T mould seems to affect in a more relevant way the electrical behaviour of the MWCNT-based samples. The increase of this parameter, maintaining the injection rate constant and exploiting the Heat&Cool non-conventional injection moulding process, brings to an increment of the electrical conductivity. The table and the graphs below (Table 18, Figure 58 (a), (b) and (c)), indeed, show the effect of the increment of the temperature of the mould on both the bulk resistivity (ρ_z and ρ_x) and the surface resistivity of the 2 – 3 – 4wt % MWCNT-based formulations in DC electrical characterization.

Table 18: DC bulk resistivity in both Z- and X-directions (ρ_z and ρ_x, in Ohm*cm) and surface resistivity (Rs in Ω/sq) values of MWCNT-based formulations (2-3-4wt %) at different T mould (30°C, 70°C and 100°C) and at a constant injection moulding rate (70 cm^3/s).

ρ_z [Ohm·cm]				**ρ_x [Ohm·cm]**				**Rs [Ω/□]**			
	MWCNT content [wt%]				**MWCNT content [wt%]**				**MWCNT content [wt%]**		
T mould [°C]	**2**	**3**	**4**	**T mould [°C]**	**2**	**3**	**4**	**T mould [°C]**	**2**	**3**	**4**
30	8.40 E+14	1.36 E+12	1.26 E+07	**30**	5.51 E+05	2.53 E+05	1.87 E+03	**30**	7.80 E+12	1.13 E+11	5.35 E+06
70	4.26 E+14	2.13 E+08	1.12 E+06	**70**	9.48 E+05	3.23 E+04	5.98 E+02	**70**	2.69 E+13	3.36 E+07	4.09 E+06
100	3.06 E+06	3.84 E+06	3.83 E+05	**100**	3.63 E+02	4.27 E+02	2.01 E+02	**100**	5.41 E+06	3.71 E+06	1.93 E+05

The effect of the variation of parameters is more evident for formulation just below and around the percolation threshold [212]. Nevertheless, for the 2wt % and 3wt % MWCNT-based formulations, it is important to underline how the use of this innovative manufacturing technique, which allows reaching the highest T mould values, leads to a reduction of on average 7 orders of magnitude for all the measured electrical parameters. This tendency is more evident when the surface resistance and the electrical resistivity are measured in the through-thickness direction than in the X-direction.

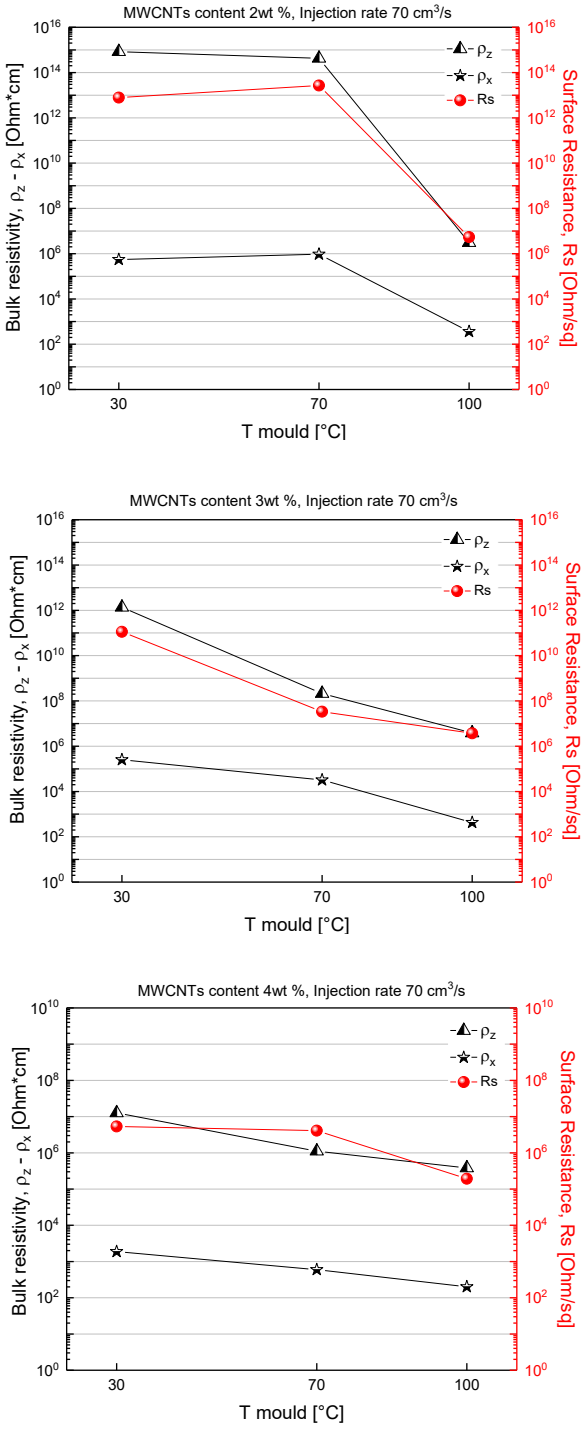

Figure 58: Effect of the T mould on the electrical properties of (a) 2wt % MWCNT formulation, (b) 3wt % MWCNT formulation and (c) 4wt % MWCNT formulation.

The positive effect of the high T mould on the electrical conductivity of the nanocomposites may be due to a chain relaxation process, which can favour the polymer chains reorientation and the nanotubes bundles recombination. In this way, this process may help the supposed re-agglomeration step and the formation of the conductive network. The MWCNTs producer supports this explanation. Moreover, in one of their experimental work Lew et al. [135] of Nanocyl attributed the beneficial effect of the high T mould to an annealing effect. In fact, the molten material, touching the high mould wall, does not freeze completely and immediately its morphological structure and a reorganization of the nanofillers agglomerates is possible. Besides this, using higher T mould brings to longer injection moulding cycle, in which the cooling phase and residence time in the molten state of the polymer are longer. This seems to favour the relaxation processes and a lower orientation of the nanotube network occurs [150].

Figure 59 (a), (b) and (c) presents again the effect of the increase of the temperature of the mould on the AC electrical behaviour of 2 – 3 – 4wt % MWCNT-based nanocomposites, in the central position (position 9). Also in this case, the samples were injection moulded with three different T mould, namely 30°C, 70°C and 100°C, using the Heat&Cool process. In these tests, the injection rate is considered as a constant parameter and its value is equal to 70 cm^3/s.

As it can be clearly observed in Figure 59, in the range of 10^1 -10^6 frequencies the nanocomposites with 2 and 3wt % of MWCNTs are insulating materials and, even the increase of the temperature of the mould, it seems not to modify their electrical behaviour. The improving active effect of the mould temperature can be observed in the 4wt % MWCNT formulation (see Figure 60). In this case, an increment of two orders of magnitude of the electrical resistivity can be measured in the samples, injection-moulded at T mould equal to 100°C. They are directly compared with the sample injection-moulded at T mould equal to 30°C, with the same MWCNTs content. The electrical conductive behaviour of this single formulation can be probably explained with the content of MWCNTs, which are present in an amount slightly over the percolation threshold. This statement can be considered valid taking into account the through-thickness direction as the measurement direction.

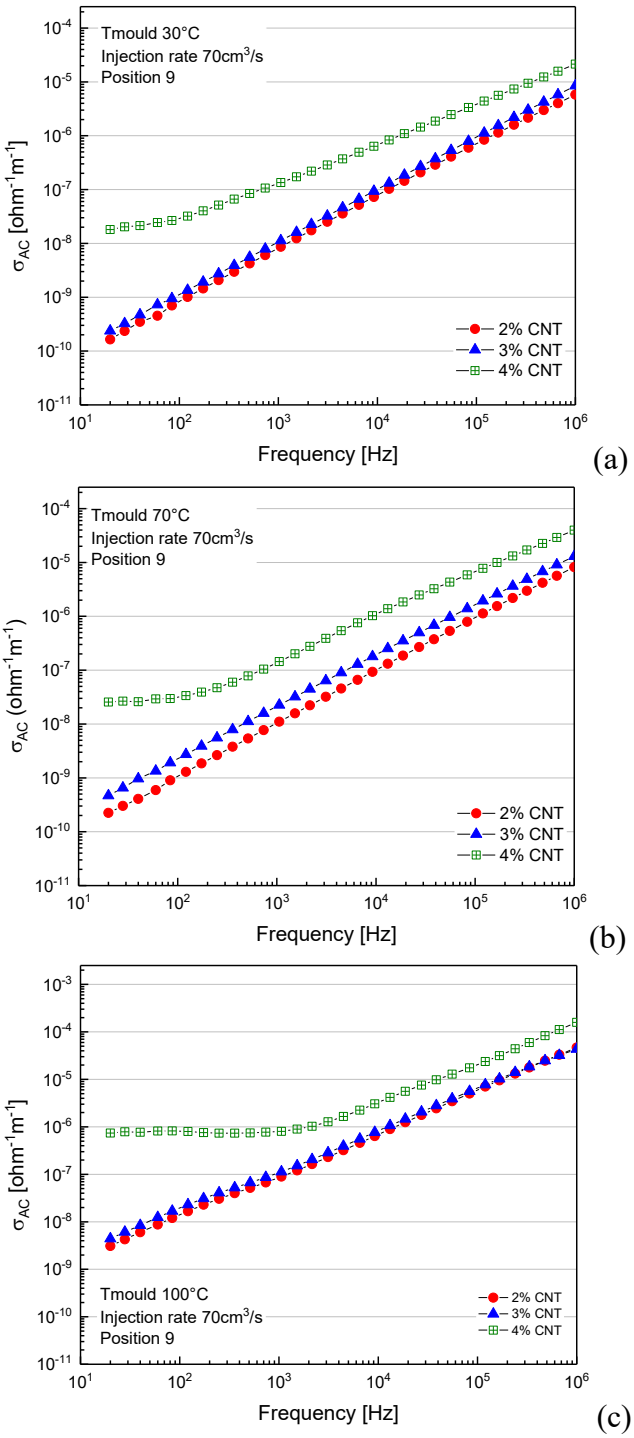

Figure 59: Calculated electrical conductivity in AC ($\sigma_{AC}[\Omega^{-1}m^{-1}]$) at low frequency ($10^1 \div 10^6$ Hz) for 2wt % to 4wt % MWCNTs formulations, injection-moulded at T mould (a) 30°C, (b) 70°C and (c) 100°C. Injection rate 70 cm^3/s (position 9).

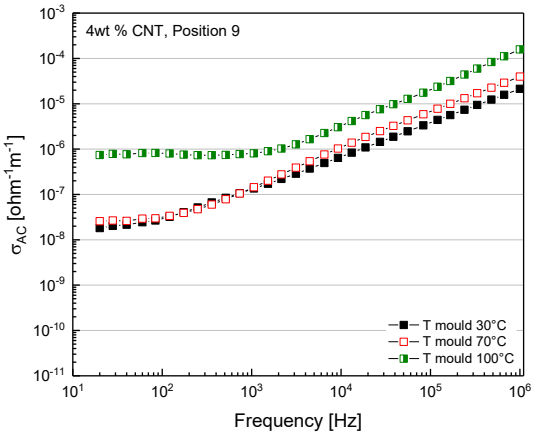

Figure 60: Calculated electrical conductivity in AC ($\sigma_{AC}[\Omega^{-1}m^{-1}]$) at low frequency ($10^1 \div 10^6$ Hz) for 4wt % MWCNTs formulation, injection-moulded at different T mould (position 9).

The positive influence of the increase of the T mould is also confirmed by the variation of other peculiar dielectric properties, such as the real and imaginary parts of electrical permittivity. As reported in literature, both the constituent parts of the complex permittivity increase with the increase of the electrical conductivity. In particular, the real permittivity ε', which is mainly correlated to the polarization of the material, tends to grow with increasing the electrical conductivity [213]. This is proved by the graphs reported in Figure 61 (a) and (b), which show the real permittivity trend in a wider range of frequencies, from $2 \cdot 10^1$ to $1 \cdot 10^9 Hz$. The pictures are referred to the 4wt % MWCNT-based formulation, injection-moulded with the three T mould (30°C, 70°C and 100°C). Mahmoodi et al. explained the increment of the real permittivity by decreasing the volume resistivity with the decrease in the distance between the MWCNTs and with the increase in the electric field between the nanofillers. This leads to a raise of the electronic polarization of the polymer. In fact, the MWCNT-based nanocomposites can be seen as a circuit, made by a capacitor (i.e. MWCNT-PP) in parallel to a resistor (i.e. MWCNTs). The chance for the electrons to move from one MWCNT to another powerfully grow with a more random distribution of the clusters of agglomerated nanofillers in the polymer matrix, which, from the first experimental results, seems to be favoured by the increment of the T mould during the process [213]. Finally, it can be observed that an increment of the T mould seems to favour a relaxation phenomenon inside the MWCNTs formulation. This is represented by the theta peaks, which shift at higher frequency values, increasing the temperature of the mould, as shown in Figure 61 (c).

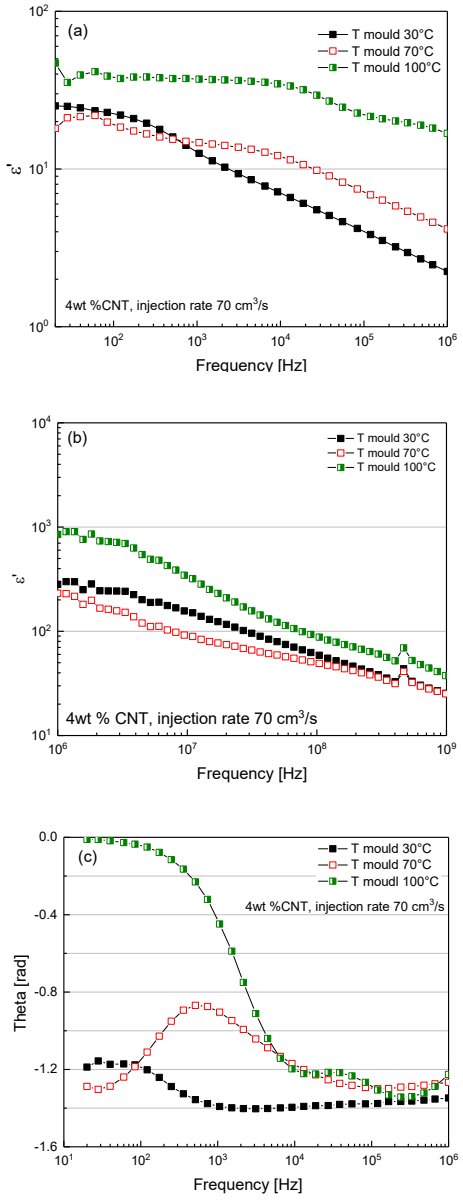

Figure 61: Real permittivity ε' (a) at low frequency range ($10^1 \div 10^6$ Hz), (b) at high frequency range ($10^6 \div 10^9$ Hz) and (c) theta values for 4wt % MWCNTs formulation, injection moulded at different T mould (position 9). All the specimens were injection moulded at 70 cm^3/s.

Considering this aspect more in detail, Figure 62 below shows the comparison between the 3wt % and 4wt % MWCNT-based injection-moulded formulations of the σ_{AC}, measured in areas located in different positions over the specimens in the AC frequency range $10^1 \div 10^6$ Hz. Both the graphs are referred to injection-moulded samples with T mould 100°C and injection rate 70 cm^3/s. The results are

consistent with the hypothesis of a not uniform distribution of the electrical conductivity along the injection-moulded samples. In fact, analogously to what has been obtained with the injection-moulded in standard conditions samples, the nearest position to the gate (i.e. position 2) seems to be the lowest conductive point in the samples. On the contrary, the farthest position from the gate (i.e. position 6) appears as the highest conductive area of the specimens [18, 214]. With the highest T mould (100°C), in the 3wt % MWCNT-based formulation (see Figure 62 (a)), the electrical properties pass from an insulating behaviour (position 2) to a completely conductive one (position 6) in the same sample. Moreover, on the 4wt % MWCNT-based formulation (see Figure 62 (b)), a variation of two orders of magnitude between the two considered positions is visible, even if in both cases a ohmic behaviour is shown in the low frequency region. This phenomenon could be explained with a higher fluidity and flowability of the molten material inside the die, also favoured by the use of a higher T mould. The higher temperature of the surfaces of the mould avoids immediately freezing the flowing molten material in aligned structures in the skin layers and, at the same time, leads to a simpler formation of agglomerated clusters of carbon nanotubes in the area farthest to gate and in the core region of the specimens. In fact, at higher T mould, the molten material has more time to create organized structures during the cooling cycle, increasing the clustering effect of the MWCNTs in the polymer matrix.

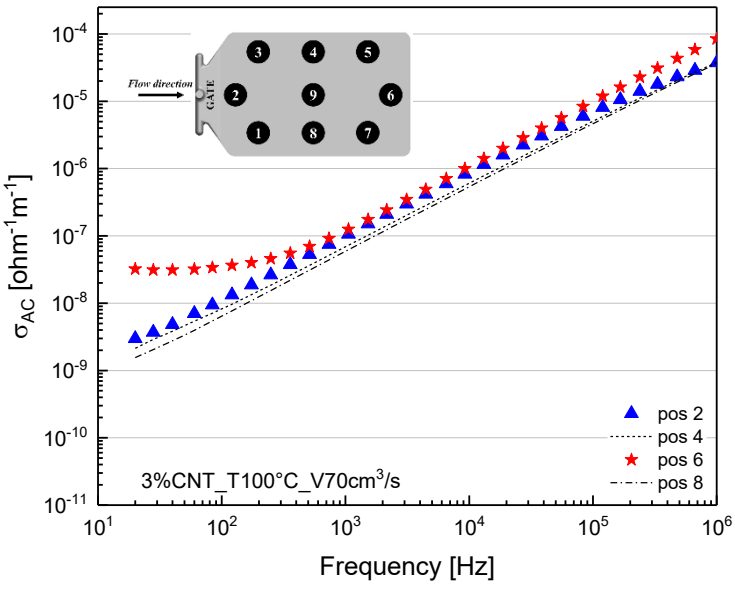

(a)

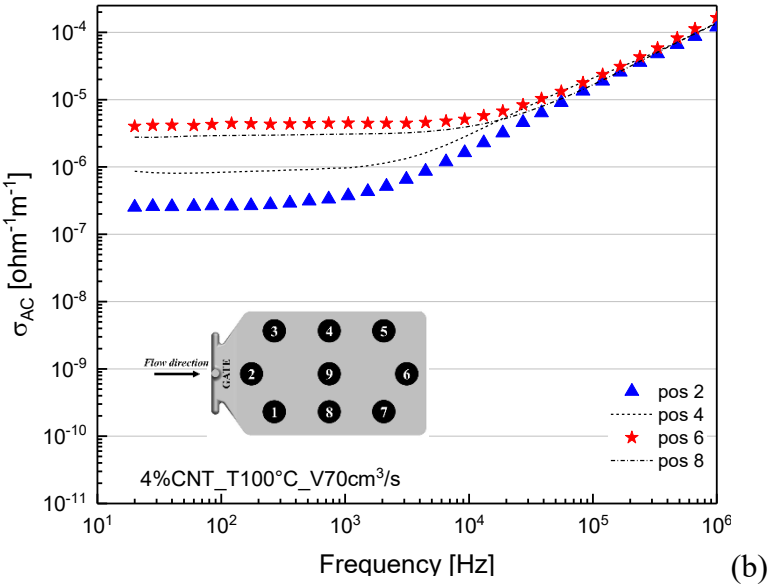

Figure 62: AC electrical conductivity for (a) 3wt % and (b) 4wt % MWCNTs formulations, measured in different positions on the specimens. Only the positions with the highest significance from the electrical point of view were reported, partly because they have an electrical behaviour symmetrical to the Y axe and partly in order to facilitate the reader in the interpretation of the data.

The literature partly confirms the formulated hypothesis. Wegrzyn et al. [131], in fact, explained the higher electrical conductivity in regions farthest from the injection gate with the presence of a shear gradient, which influences carbon nanotubes entanglement. They supposed that an increase of the MWCNTs content increasing distance from the gate occurs and they ascribe this aspect to flowabilities of fillers and molten polymer, different one to each other. Moreover, Chandra et al. [162] reported that the electrical conductivity is more uniform in regions farther from the gate, but they specified that this behaviour is more emphasised in determined conditions, namely at high melt temperatures and low injection rates.

Tests results reported in this thesis are in accordance with what has been reported in literature. A possible explanation can be ascribed to different factors. Firstly, a MWCNTs migration phenomenon in areas far from the gate or in the core region seems to occur. A migration effect, which is present and unavoidable, has to be attributed to the injection moulding process itself. This phenomenon is observable every time a filler is added to a polymer. An insulating skin effect due to nanofillers either migration towards the core or orientation may be expected. In fact, the oriented nanotubes may lead to an interruption of the tube-tube contacts. This behaviour may be actually considered as the direct result of the injection

moulding process, which - as already mentioned - creates a skin-core morphology with a decreasing fillers orientation towards the core region [150]. Therefore, a different distribution and organization of the MWCNTs agglomerated clusters in the skin-core structure and nearer or farther to the gate can be considered as a plausible occurrence. Nevertheless, these results are different from what reported by Villmow et al. [150], which affirmed that the lowest resistivity values were present in the zone near the gate and in the middle of the sample. They explained this behaviour with a modification of the network structure of MWNCNTs within the matrix during the injection moulding process, a phenomenon that would seem not to be active in the materials reported in this thesis.

As a preliminary conclusion, it can be affirmed that the variation of the temperature of the mould proved to have an important effect on the electrical behaviour of the PP/MWCNT nanocomposites. In fact, the increase of T mould helps to increase the electrical conductivity of the injection-moulded samples.

Effect of the variation of the injection rate.

The modification of the injection rate and its effect on the electrical properties was also investigated. In Figure 63 the AC electrical behaviour of the 4wt % MWCNT-based formulation with different injection-moulding parameters are reported. In particular, the samples were manufactured with a combination of injection moulding parameters, namely two different T mould (30°C and 70°C) at three different injection rate (35, 70 and 250 cm^3/s). Figure 66 shows the σ_{AC} (a), the phase angle (b) and the real and imaginary parts of dielectric permittivity (c – d) of the 4wt % MWCNT-based formulation.

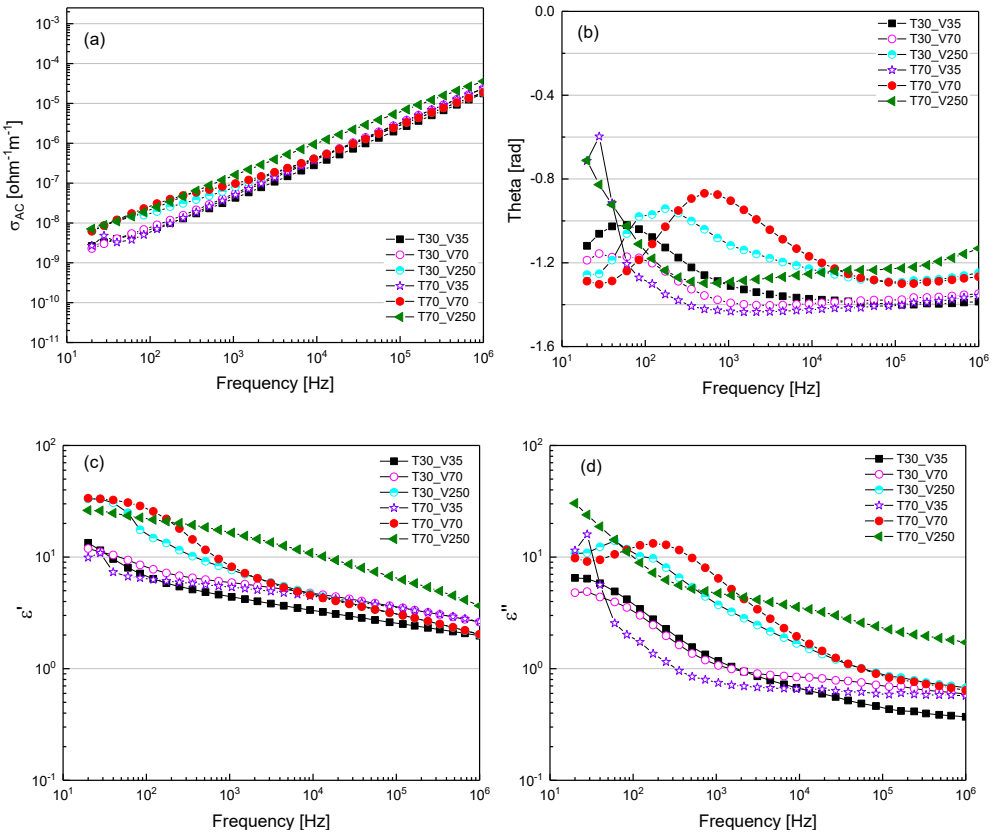

Figure 63: (a) Calculated electrical conductivity in AC ($\sigma_{AC}[\Omega^{-1}m^{-1}]$), (b) θ [rad], (c) ε' and (d) ε'' at low frequency ($10^1 \div 10^6$ Hz) for 4wt % MWCNT-based formulation, injection moulded at different processing conditions and in the same position 9.

No significant differences are detectable in the graph, reporting the AC conductivity. In fact, in all the combinations of parameters, no conductive plateau is visible. The same behaviour is observable for the phase angle ϑ, where none of the tested samples achieves 0 rad value, which indicates the conductive character of the compound. On the contrary, a difference however weak is shown in the real and imaginary parts of the dielectric permittivity. Both of them, even slightly, increase with the increase of the conductivity: this behaviour is more stressed when both the T mould and the injection rate are higher (70°C; 70 cm^3/s and 70°C; 250 cm^3/s respectively, red circles and green triangles in the graph). The improving effect on the electrical conductivity of the highest injection rate is also noticeable when the temperature of the mould remains around the room temperature. On the contrary, the lowest ε' and ε'', related to the highest resistivity values, are observed when the injection rate is lower (at 35 cm^3/s) with both the T mould. The other combinations of parameters produce intermediate results of conductivity. This behaviour is also visible analysing the real part of the permittivity in all the

frequencies measurement range (from 10^1 to 10^9 Hz). Again, as it can be seen in Figure 64, the permittivity increases rather on a small scale when the samples are injection-moulded at high injection rate (250 cm^3/s).

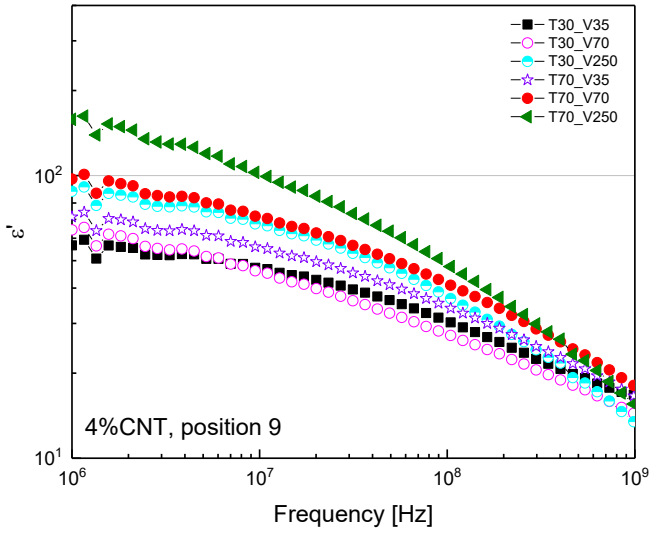

Figure 64: Real permittivity ε' at high frequency ($10^6 \div 10^9$ Hz) for 4wt % MWCNT-based formulation, injection-moulded with different conditions and measured in the same position.

The described impact of the temperature of the mould and of the injection rate on the electrical properties of the MWCNT-based formulations is observable not only in the AC electrical characterization but also in the DC measurements. The powerful effect of high injection rate on the electrical conductivity is not completely in accordance with what reported in literature by some authors [100, 133, 150, 162, 164 and 214], which on the contrary advice to adopt low injection rate values, in order to obtain high conductivity values. The following table (see Table 19) and graphs (see Figure 65 (a), (b) and (c)), indeed, are referred to the bulk resistivity in Z- and X- directions and surface resistance measurements of the 2wt %, 3wt % and 4wt % MWCNT-based samples, injection-moulded combining different processing parameters. In particular, Table 19 lists all the electrical data of the aforementioned formulations for all the used processing conditions. The data of the combinations of both the T mould (at 30°C and 70°C) and the injection rate (35, 70 and 250 cm^3/s) are reported. Considering each MWCNTs content, it is observable that mainly the 2wt % and 3wt % MWCNT-based formulations seem to be sensitive to the variation of the processing parameters. In fact, these contents are a little below and around the percolation threshold in the Z- and X- directions respectively. It seems plausible

to affirm that these formulations, in which a conductive network is not totally formed, are easily more affected by these changes.

Taking into account the variation of the T mould from 30°C to 70°C, it is evident that only little changes are present, more or less with all the MWCNTs contents and for all the measured parameters. Finally, regarding the increment of the injection rate, it is worth to mention the powerful effect of this parameter when it is moved to the highest value. Especially in the formulations around the percolation threshold, the bulk resistivity in the through-thickness direction and the surface resistivity values decrease of on average 4 – 5 orders of magnitude, passing from an insulating behaviour to a conductive one. This statement can be considered valid not only for the T mould at 30°C but also for the T mould at 70°C.

Table 19: ρ_z, ρ_x and Rs of MWCNT-based formulations for T mould at 30°C and 70°C, injection rate at 35, 70 and 250 cm^3/s.

ρ_z [Ohm·cm]									
	2 % MWCNT			**3 % MWCNT**			**4 % MWCNT**		
V / T	**35 cm^3/s**	**70 cm^3/s**	**250 cm^3/s**	**35 cm^3/s**	**70 cm^3/s**	**250 cm^3/s**	**35 cm^3/s**	**70 cm^3/s**	**250 cm^3/s**
30°C	4.04E+14	7.20E+11	1.26E+10	4.00E+10	1.70E+09	7.80E+08	9.80E+06	3.30E+07	6.60E+05
70°C	3.60E+15	3.15E+11	2.23E+09	1.60E+10	2.70E+08	3.50E+06	2.80E+06	2.60E+06	2.10E+05
ρ_x [Ohm·cm]									
	2 % MWCNT			**3 % MWCNT**			**4 % MWCNT**		
V / T	**35 cm^3/s**	**70 cm^3/s**	**250 cm^3/s**	**35 cm^3/s**	**70 cm^3/s**	**250 cm^3/s**	**35 cm^3/s**	**70 cm^3/s**	**250 cm^3/s**
30°C	7.02E+04	7.25E+04	4.47E+05	6.36E+04	9.74E+03	1.46E+03	2.38E+02	1.04E+03	3.09E+02
70°C	1.01E+07	1.47E+05	7.02E+04	2.02E+03	5.64E+03	5.26E+02	3.86E+02	2.41E+02	9.03E+01
Rs [Ω/sq]									
	2 % MWCNT			**3 % MWCNT**			**4 % MWCNT**		
V / T	**35 cm^3/s**	**70 cm^3/s**	**250 cm^3/s**	**35 cm^3/s**	**70 cm^3/s**	**250 cm^3/s**	**35 cm^3/s**	**70 cm^3/s**	**250 cm^3/s**
30°C	3.03E+12	3.60E+10	6.34E+10	2.09E+15	1.09E+10	1.70E+09	1.87E+07	6.50E+06	5.60E+07
70°C	2.28E+13	2.10E+11	3.41E+09	4.30E+14	2.53E+09	4.50E+08	8.60E+06	6.00E+06	3.30E+07

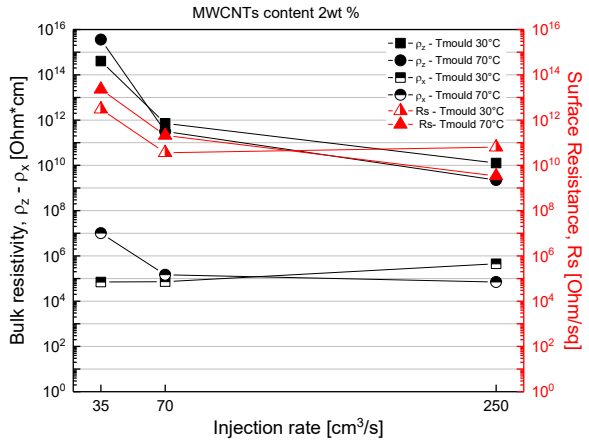

(a)

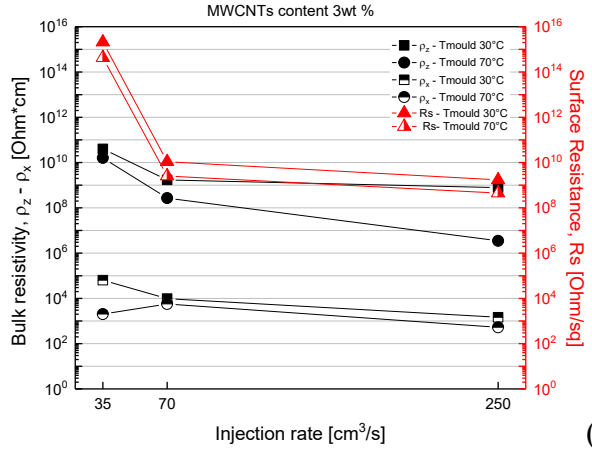

(b)

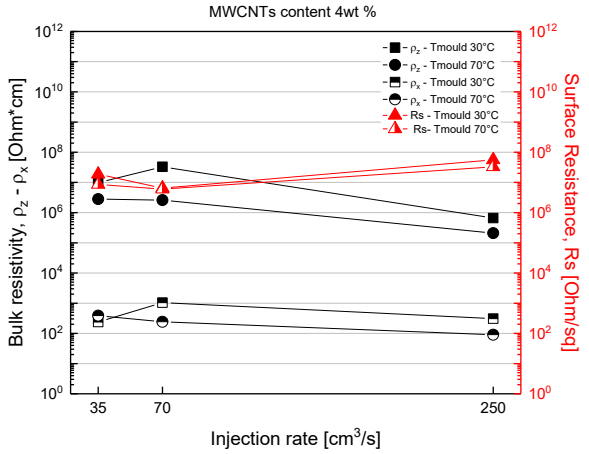

(c)

Figure 65: Effect of the T mould and injection moulding rate on the electrical properties of (a) 2wt % MWCNT formulation, (b) 3wt % MWCNT formulation and (c) 4wt % MWCNT formulation.

A possible explanation for these results has to be researched in the rheological behaviour of the MWCNT-based formulations. In fact, as reported in the previous chapter (see *Chapter 3*), the nanocomposites show a shear-thinning behaviour, in which a viscosity reduction occurs when an increase of the shear rate is adopted. Therefore, when high injection rates are used during the injection moulding process, an increase of the fluidity of the molten polymer can be detected. This leads to a more efficient diffusion of the polymer into the carbon nanotube bundles, resulting in higher electrical conductivities. Moreover, the decrease of melt viscosity may allow activating the agglomeration mechanisms, which brings to a better organization of the electrical conductive percolative network. It is well-known, indeed, that in order to achieve high conductivities values, the built-up of a network of MWCNTs, favoured by a higher fluidity of the polymer, is necessary.

Therefore, the variation of processing conditions has been demonstrated to be have a great impact on the electrical behaviour of the MWCNT-based nanocomposites. The percolation parameters, in particular percolation threshold φc and exponent *t*, obtained implementing the percolative power fitting law, are in accordance with the electrical results. In the Table 20 below, the fitted exponent *t* values are reported. As it can be seen, they are in the range of values of the 3D percolative network, as expected from the literature (i.e. 1.65 – 2). A 3D percolative network is almost always formed. Only in some cases, the values of the exponent *t* are lower than what expected and nearer to the *t* value typical for a 2D network [180].

Therefore, the obtained results can be explained considering that not a single nanotube is a percolating element, but agglomerated MWCNTs clusters constitute the percolating elements. The process itself induces these agglomerates and their intrinsic conductivity depends on processing conditions and on the interaction between polymer matrix and nanofillers [181].

Table 20: Fitted values of exponent *t*, referring to MWCNT-based formulations injection-moulded with different processing conditions.

T mould [°C]	**Injection rate [cm^3/s]**		
	35	**70**	**250**
30	1.2	2.2	1.5
70	2.1	1.2	1.7

The percolation thresholds are around the 2wt % of conductive nanofillers. A lower percolation threshold, equal to 1.5wt %, is observable for the formulation injection-moulded at T mould 100°C. The increase of the temperature causes the increase of the nanotubes mobility and it is linked with clustering and conducting phase segregation that are considered the reason for the lower percolation threshold [181]. The exponent *t* for this formulation was not calculated, because all the available electrical data are above the percolation and they could not be fitted with the percolative power fitting law.

As a preliminary conclusion, high T mould and high injection rate can be considered the processing parameters, whose variation has the main impact on the electrical properties of the injection-moulded samples. A possible explanation can be attributed to the action of these two conditions on the fluidity of polymer. The variation of these parameters induce a decrease in the viscosity of the polymer and help in the creation of nanotubes bundles and clusters.

From the shear rate point of view, carbon nanotubes collect other nanotubes on their way, sticking to each other when they are in a shear gradient. This agglomeration phenomenon can be considered one of the main cause of an increase of both the fluidity and the electrical conductivity [100]. A mixture of 'micro-fillers' (spherical-like) and 'nano-fillers' (individual MWCNTs or small agglomerates) are present and they are necessary to obtain a conductive pathway in the matrix with interconnected conductive particles.

Another possible explanation could be a shear-induced migration of particles, during the injection moulding process, developing gradients concentration across the flow direction. The concentration distribution of the particles can be modelled by a flux equation, in which several geometrical parameters related to the conductive particles (i.e. radius, volume fraction) and processing parameters (i.e. shear rate) are present. The great extent of migration depends on not only the particle size and concentration but also and in particular on the shear rate [104].

4.2.2. Morphological analysis

The morphological analysis were performed, using both Scanning Electron (SEM) and Optical Microscopy (OM), in order to correlate the electrical behaviour of the produced samples and their morphology, also considering the variation of processing conditions both during the melt mixing and injection moulding processes.

Starting from the melt mixing conditions point of view, fractured surfaces of the 4wt % MWCNT-based formulation, manufactured with different melt-mixing conditions, i.e. specimens in which the nanofillers were fed through the main hopper and the lateral side-feeder, respectively, were reported in Figure 66 (a) – (b) below. The SEM images are in accordance with the obtained electrical results and they have confirmed the relevant effect of feeding conditions during the melt-mixing process on the electrical behaviour of the MWCNT-based formulations.

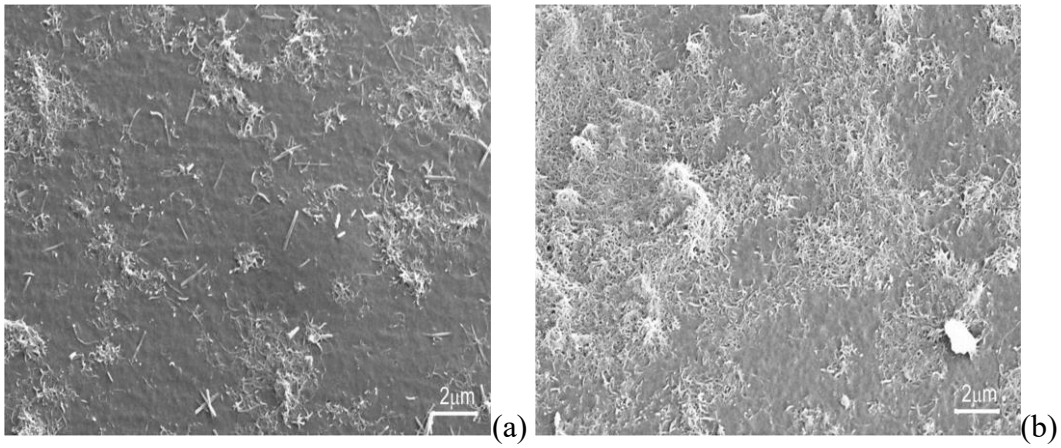

(a) (b)

Figure 66: SEM images of the cross sections of the analysed MWCNT-based nanocomposites. The micrographs were obtained from the injection-moulded sample, in which MWCNTs were fed through the main hopper (a) and from the lateral side-feeder (b).

As it can be seen, the micrograph (a) appears more resin-rich than the micrograph (b) and, although a higher level of dispersion of the nanotube is visible, a poorer agglomeration of the nanofillers is present. Carbon nanotubes appear more isolated in the polymer matrix and clusters of small dimensions and with weak tube-tube connections are observable. Wide areas, in which no nanotube is present, are visible. On the contrary, in the micrograph (b) a denser conductive network seems to occur. Larger carbon nanotubes clusters are distributed in the analysed surface and a wider connectedness among the nanofillers is present.

Apparently, therefore, changing the feeding conditions could modify the aspect ratio of the nanofillers, reducing the length of MWCNTs and the possibility to create a dense network. Moreover, when the fillers are fed together with the solid polymeric granules through the main hopper, the residence time in the extruder increases. Even though a longer residence time could be necessary to allow the matrix and the filler to be more in contact, a longer path along the twin-screw extruder could be detrimental for both the polymer degradation and the MWCNTs length. Consequently, a decrease in the electrical conductivity of the final nanocomposites occurs. Thus, a good balance between dispersion and shortening of the MWCNTs and degradation of the polymer should be found [100].

Considering the samples morphology from the injection moulding point of view, combined optical and scanning electron microscopy of the injection-moulded samples are observable in the following images. A comparison of the two different measuring technologies is reported for each samples, injection-moulded at a constant injection rate and with an increasing value of the temperature of the mould (namely, 30°C, 70°C and 100°C respectively).

The optical images were obtained from the observation of ultracryomicrotomed slices, cut directly from the injection-moulded samples. The thickness of these specimens does not exactly correspond to the global thickness of the injection-moulded part, because of the rolling-up effect of the blade during the cutting procedure. In fact, as explained in the Materials & Methods section (see *Chapter 2*), in order to obtain as thin as possible slices with such a wide thickness, a rolling up of the external layers is unavoidable. However, the morphology of these specimens can be considered representative of the morphology of the whole sample. The SEM images, instead, were performed analysing the samples surface, fractured in liquid nitrogen, in order to obtain a fragile fracture. In this case, the observed thickness corresponds precisely to the total thickness of the injection-moulded specimens.

A heterogeneous morphology clearly appears in the through-thickness direction of the samples. Elongated and oriented agglomerates of MWCNTs are observable in the skin layers of the samples. On the contrary, more circular and regular clusters are widespread in the core region of the samples. This morphology induced by the injection moulding process is documented in literature [100, 133 and 150]. A high orientation of MWCNTs in the skin layers may cause the increase of the electrical resistivity, while a clustering organization, taking place in the core region, may lead to a decrease of the electrical resistivity [150].

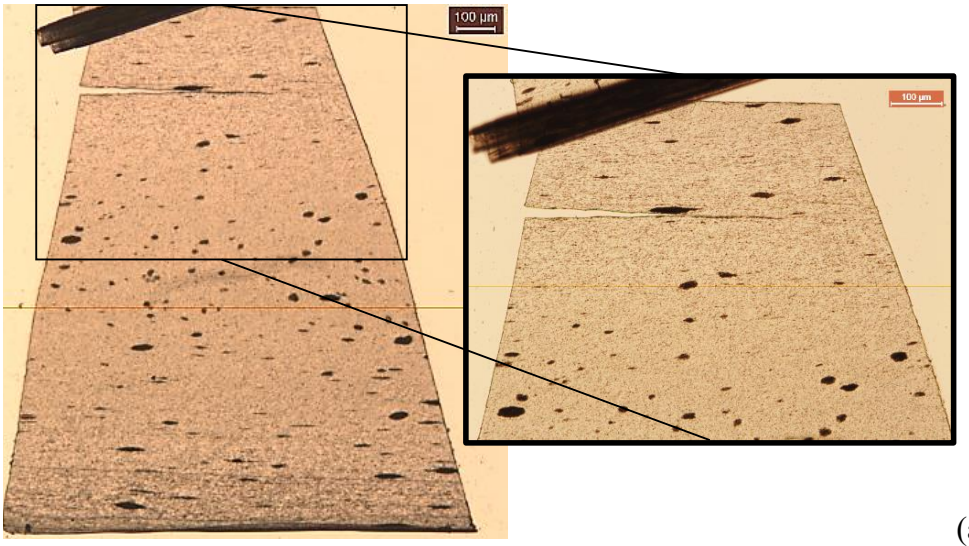

(a)

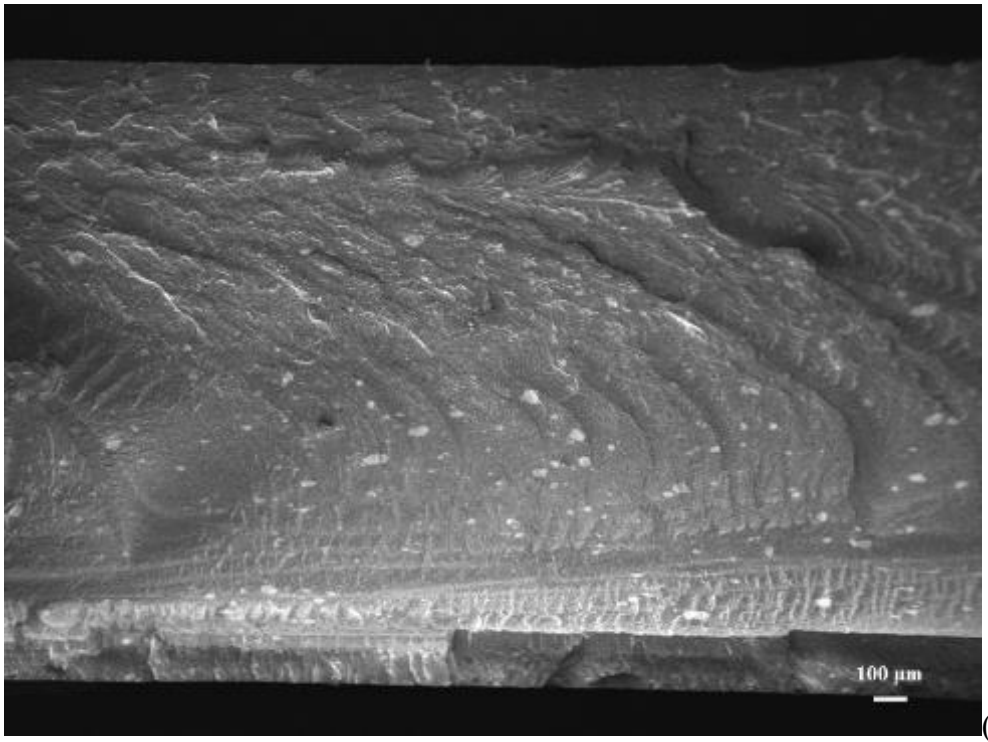

(b)

Figure 67: (a) Optical image of ultracriomicrotomed slice of 3wt % MWCNT-based formulation, measured thickness 1356 µm. The inset shows a portion of the specimens (with greater magnification), where the passage from skin layer to core region is visible. (b) SEM image of the fractured section of 3wt % MWCNT-based formulation, measured thickness 1.946 mm, magnification 90x. The sample was injection moulded in standard conditions, i.e. T mould 30°C and injection rate 70 cm^3/s.

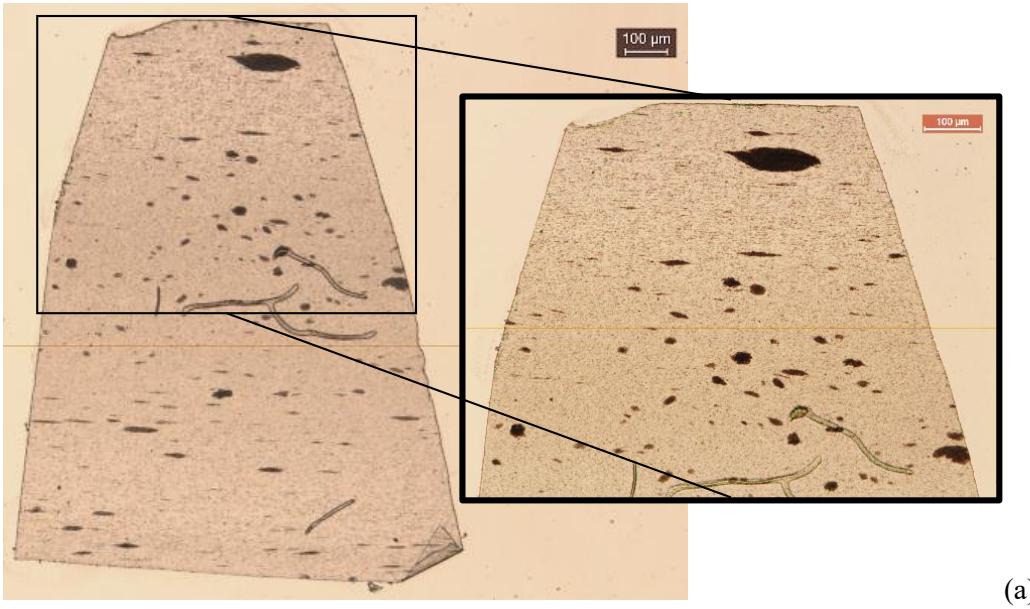

(a)

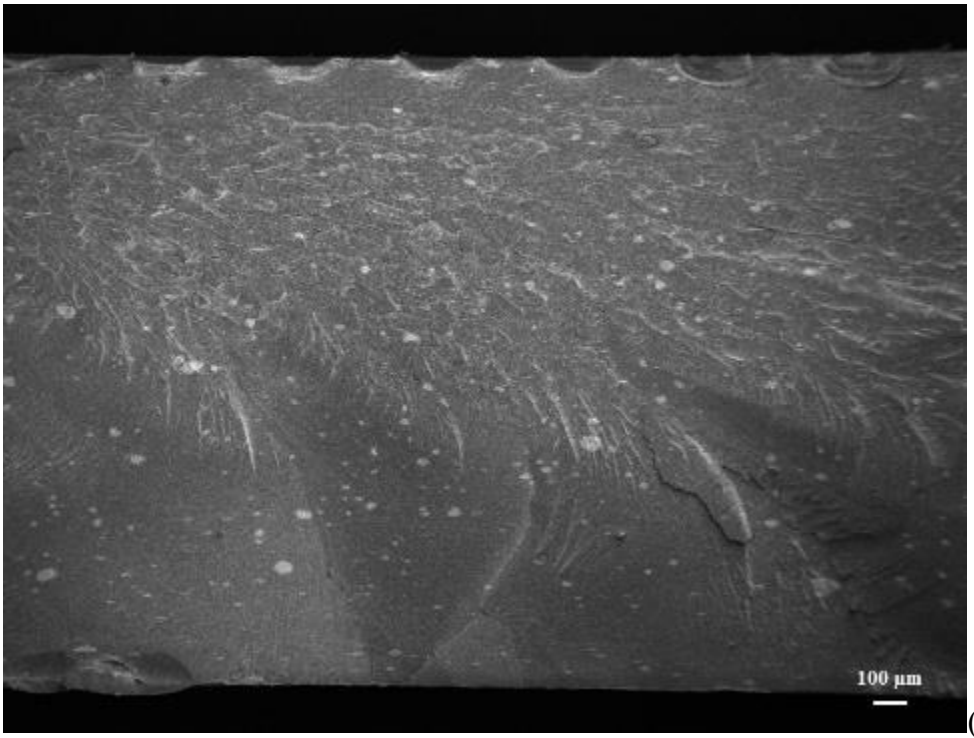

(b)

Figure 68: (a) Optical image of ultracriomicrotomed slice of 3wt % MWCNT-based formulation, measured thickness 1310 µm. The inset shows a portion of the specimens (with greater magnification), where the passage from skin layer to core region is visible. (b) SEM image of the fractured section of 3wt % MWCNT-based formulation, measured thickness 1.962 mm, magnification 90x. The sample was injection moulded at T mould 70°C and injection rate 70 cm^3/s.

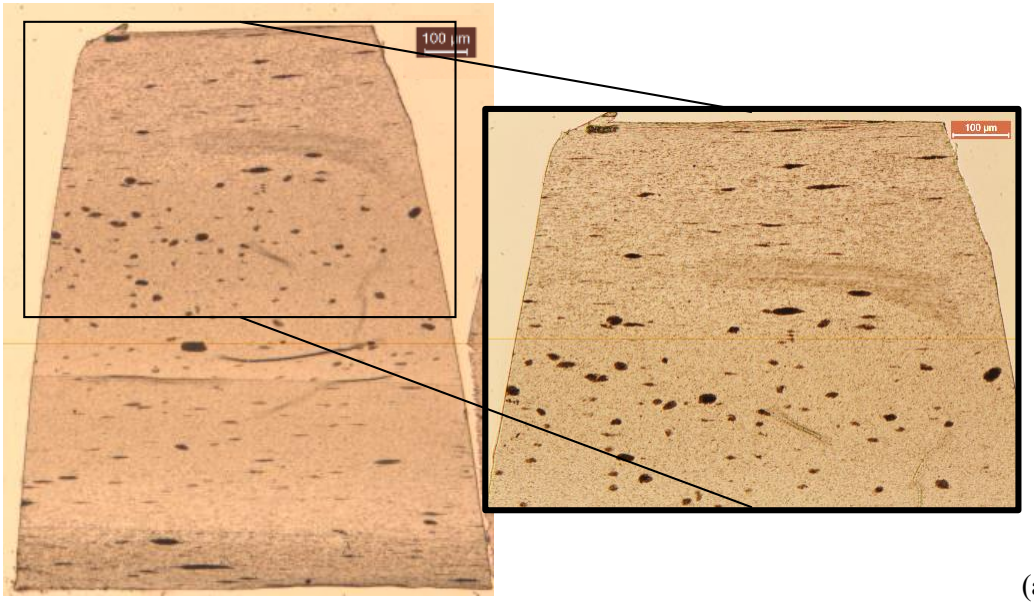

(a)

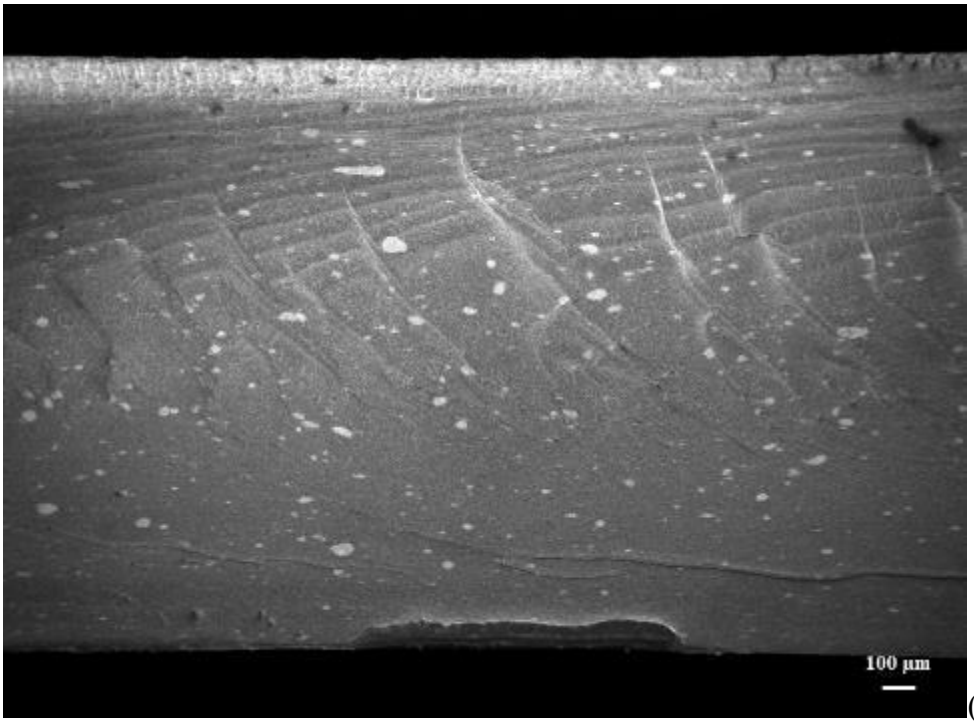

(b)

Figure 69: (a) Optical image of ultracriomicrotomed slice of 3wt % MWCNT-based formulation, measured thickness 1331 µm. The inset shows a portion of the specimens (with greater magnification), where the passage from skin layer to core region is visible. (b) SEM image of the fractured section of 3wt % MWCNT-based formulation, measured thickness 1.934 mm, magnification 90x. The sample was injection moulded at T mould 100°C and injection rate 70 cm^3/s.

Figures 67, 68 and 69 show the morphological structure of the injection-moulded samples at different T mould. In these images, passing from the skin layers to the core region, the variation of morphological structure is evident. This is valid and visible for all the three used T mould. Elongated and narrow agglomerates are observable in the skin layers, rounded and circular clusters are visible in the core regions. Elongated and rounded clusters are homogenously distributed in the skin layers and in the core region respectively. Micrometric clustering formations are present (around 50 – 100 microns), but a submicronic populations of agglomerates are also visible. This is confirmed by the SEM images reported in Figure 70 (a) - (b) below, where, as an example, a greater magnification of a portion of both the skin and the core areas is reported. As it can be clearly seen, not only the bigger micrometric clusters but also all the submicronic clustering formations are aligned in the skin layer, and similarly in the core region all the smaller clusters have a rounded and circular shape. This indicates that the dispersion of MWCNTs, even if with a different morphological structure, is present in the total surface of the sample.

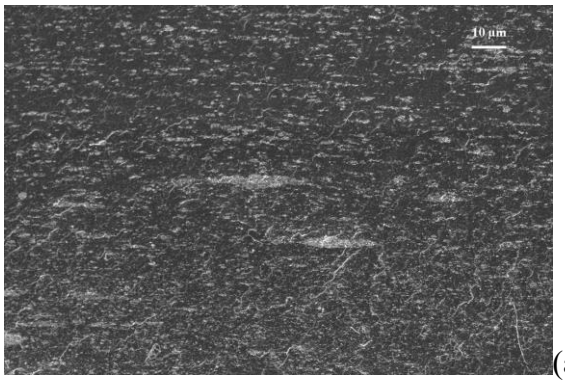

(a)

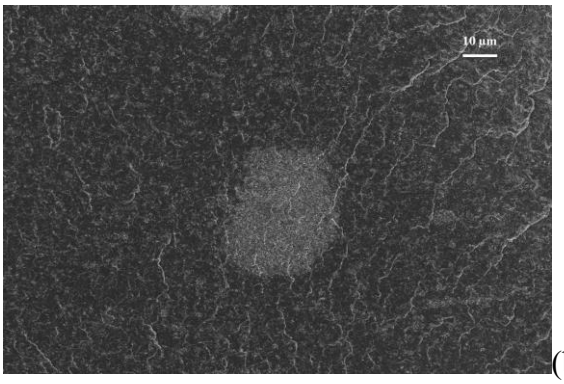

(b)

Figure 70: SEM images (2.0x magnification) (a) of the skin layer of a sample injection-moulded at T mould 70°C and (b) of the core region of a sample injection-moulded at T mould 100°C.

It can be also considered that a greater quantity of larger circular clusters are present in the specimen injection-moulded with the highest T mould. A more fluid polymer and a longer residence time inside the die in the molten state seem to favour the clustering phenomenon, helping the formation of a wider percolative conductive network. Chandra et al. explained this effect with the use of higher temperature during the injection moulding process [162].

Moreover, the bundles of MWCNTs appear completely immersed and penetrated by the polymer matrix. The clusters are not isolated and separated entities compared to the matrix, but the polymer is able to reach the internal areas of the nanotubes agglomerates. Probably, it can be stated that the conditions in which the polymer has higher fluidity (such as, higher injection rate or higher T mould), can favour the entry of the molten polymer inside the MWCNTs bundles. Nevertheless, this behaviour is true not only for both the skin layers and the core regions, but also for specimens injection-moulded with all the different T mould, as reported in the following Figures 71, 72 and 73. This aspect can help to create a real electrical percolative conductive network, in which the nanotubes are closer to each other and the strong tube-polymer-tube contacts are present. These contacts permit the transfer of electron and, as a consequence, the increment of the electrical conductivity in an insulating polymer matrix, like polypropylene.

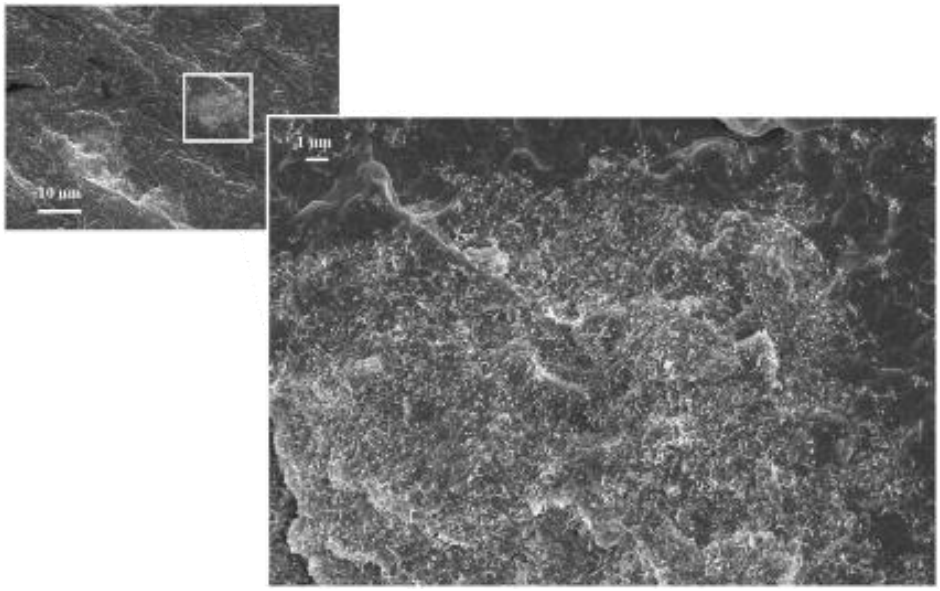

Figure 71: SEM image of the fractured section of 3wt % MWCNT-based formulation. Enlargement related to the core region of the analysed surface. The sample was injection moulded in standard conditions, i.e. T mould 30°C and injection rate 70 cm^3/s.

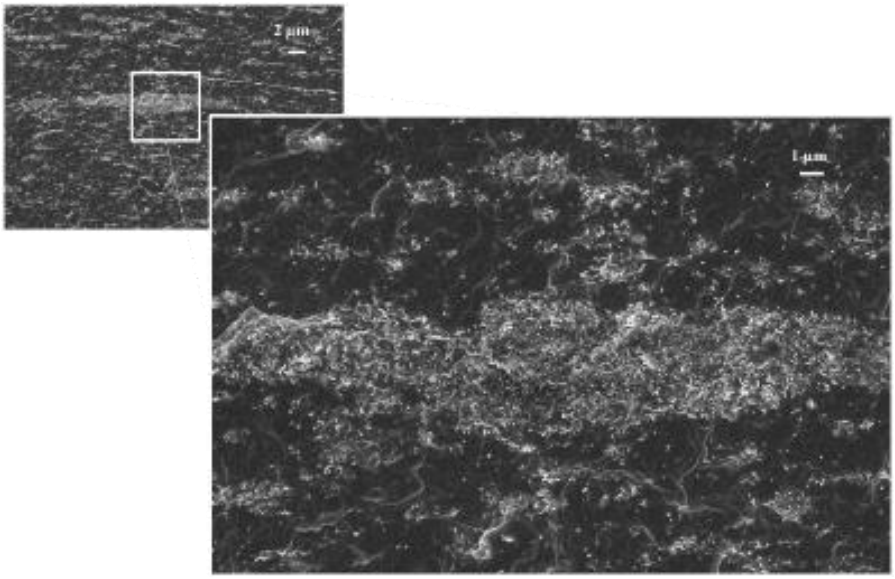

Figure 72: SEM image of the fractured section of 3wt % MWCNT-based formulation. Enlargement related to the skin layer of the analysed surface. The sample was injection moulded at T mould 70°C and injection rate 70 cm^3/s.

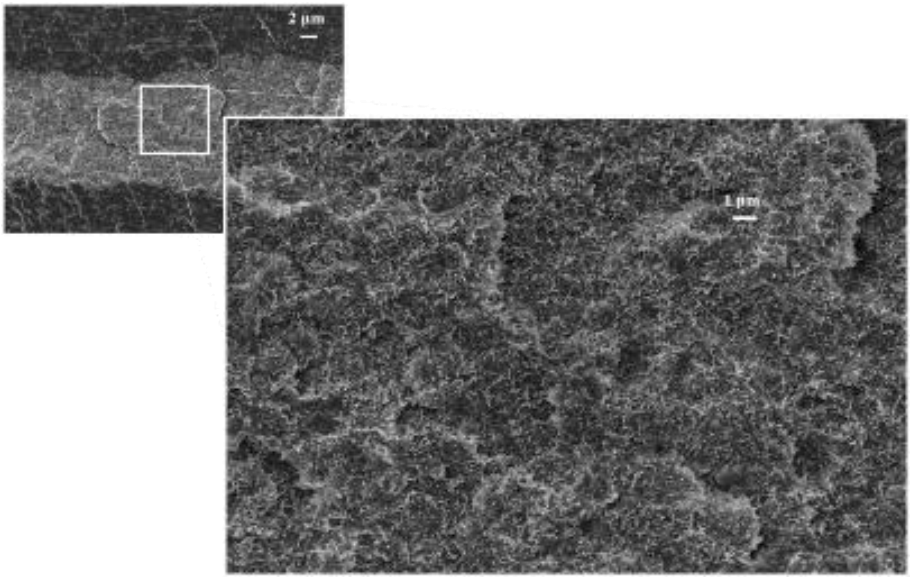

Figure 73: SEM image of the fractured section of 3wt % MWCNT-based formulation. Enlargement related to the core region of the analysed surface. The sample was injection moulded at T mould 100°C and injection rate 70 cm^3/s.

The morphological analysis has been also exploited to observe the structure of two different spatial positions of the 3wt % MWCNT-based formulation, injection-moulded at T mould equal to 100°C and with 70 cm^3/s as injection rate. In particular, the fractured surfaces of the least conductive and the nearest to the gate position (position 2) and the highest conductive and the farthest from the gate position (position 6) were observed. The global thicknesses of the observed specimens in the aforementioned positions are reported in Figure 74 and 75. It may be inferred that in the areas farer from the gate, if compared with the areas nearer to the gate, larger and circular shaped micro-clusters are present in the core region. These clusters assume a different shape in the skins, where more aligned and narrow agglomerates are visible. The alignment of the MWCNTs is not present inside each single bundle, where each single nanotube is randomly distributed and interconnected to the others (see Figure 76 and 77).

This physical and morphological arrangement is less visible in the image referred to the position 2. Apparently, smaller and more circular-shaped clusters are concentrated in the core region. As it can be clearly seen in the enlargements of the skin layers in Figure 76 and 77, a micro-clusters are not present. Nano-bundles and single multi-wall carbon nanotubes are visible. Probably, a weaker conductive percolation network is formed in this area of the specimen and this can be a reason of the lower electrical performance of the sample.

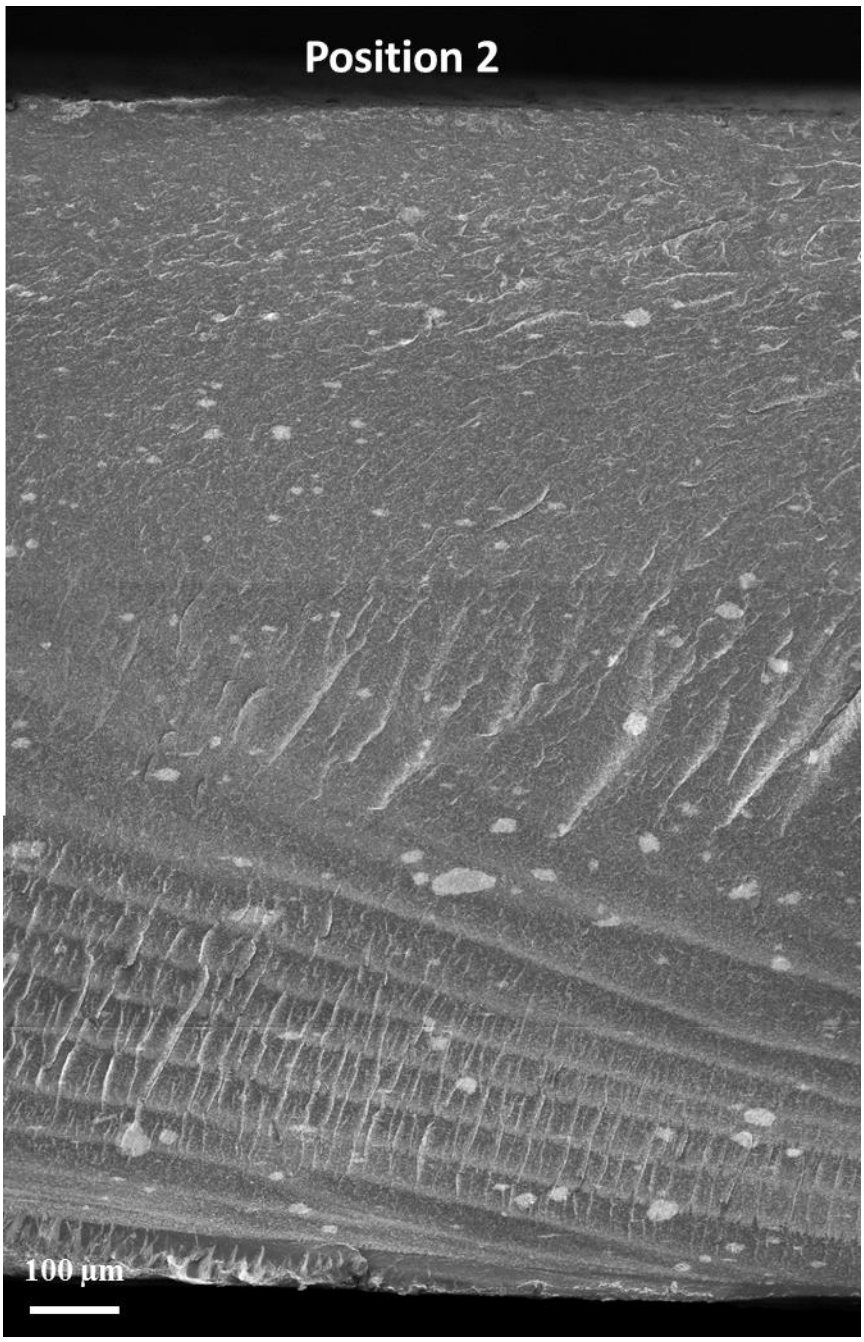

Figure 74: SEM image of the fractured section of 3wt % MWCNT-based formulation. Enlargement related to global thickness of the analysed surface in position 2. The sample was injection moulded at T mould 100°C and injection rate 70 cm^3/s.

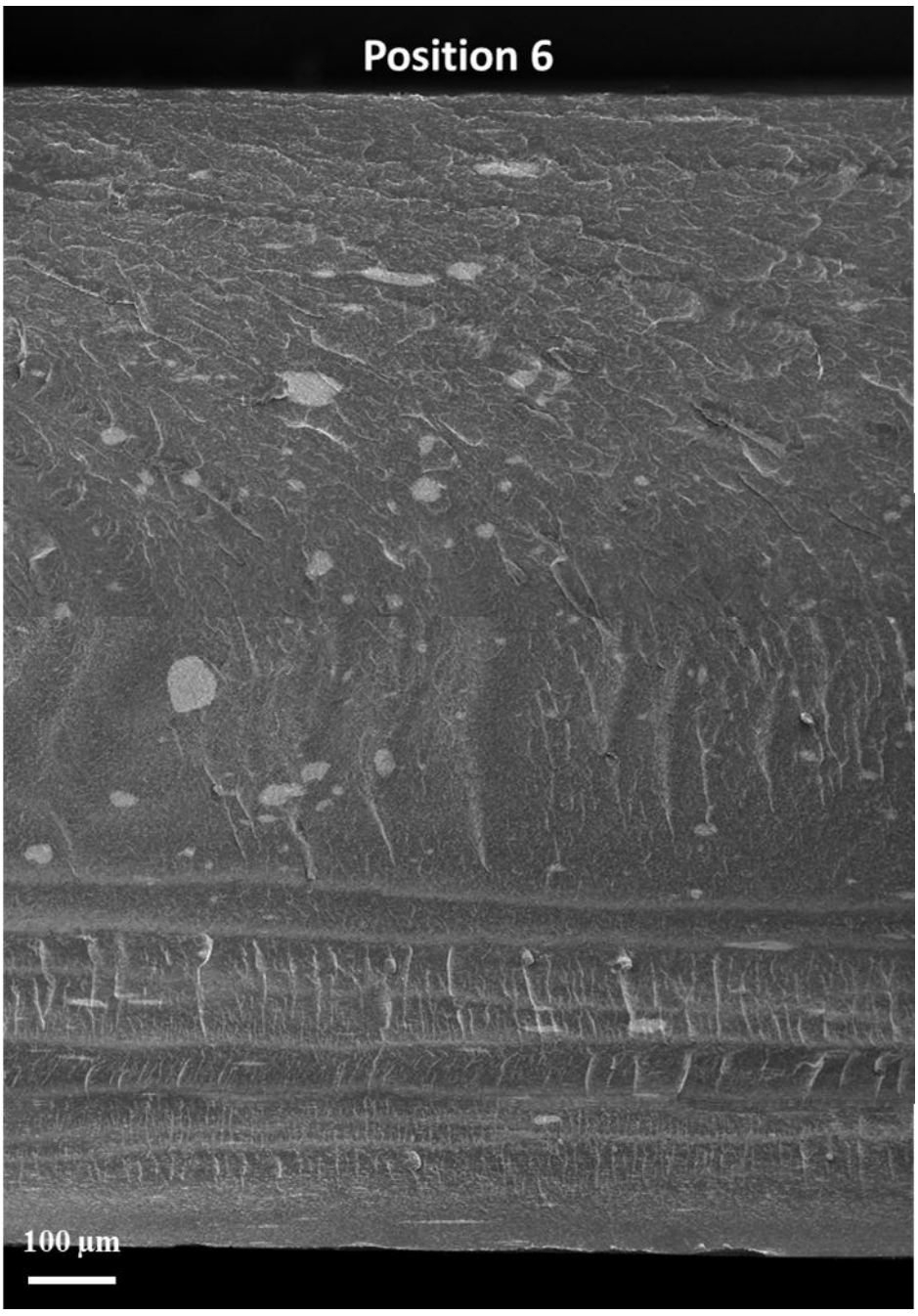

Figure 75: SEM image of the fractured section of 3wt % MWCNT-based formulation. Enlargement related to global thickness of the analysed surface in position 6. The sample was injection moulded at T mould 100°C and injection rate 70 cm^3/s.

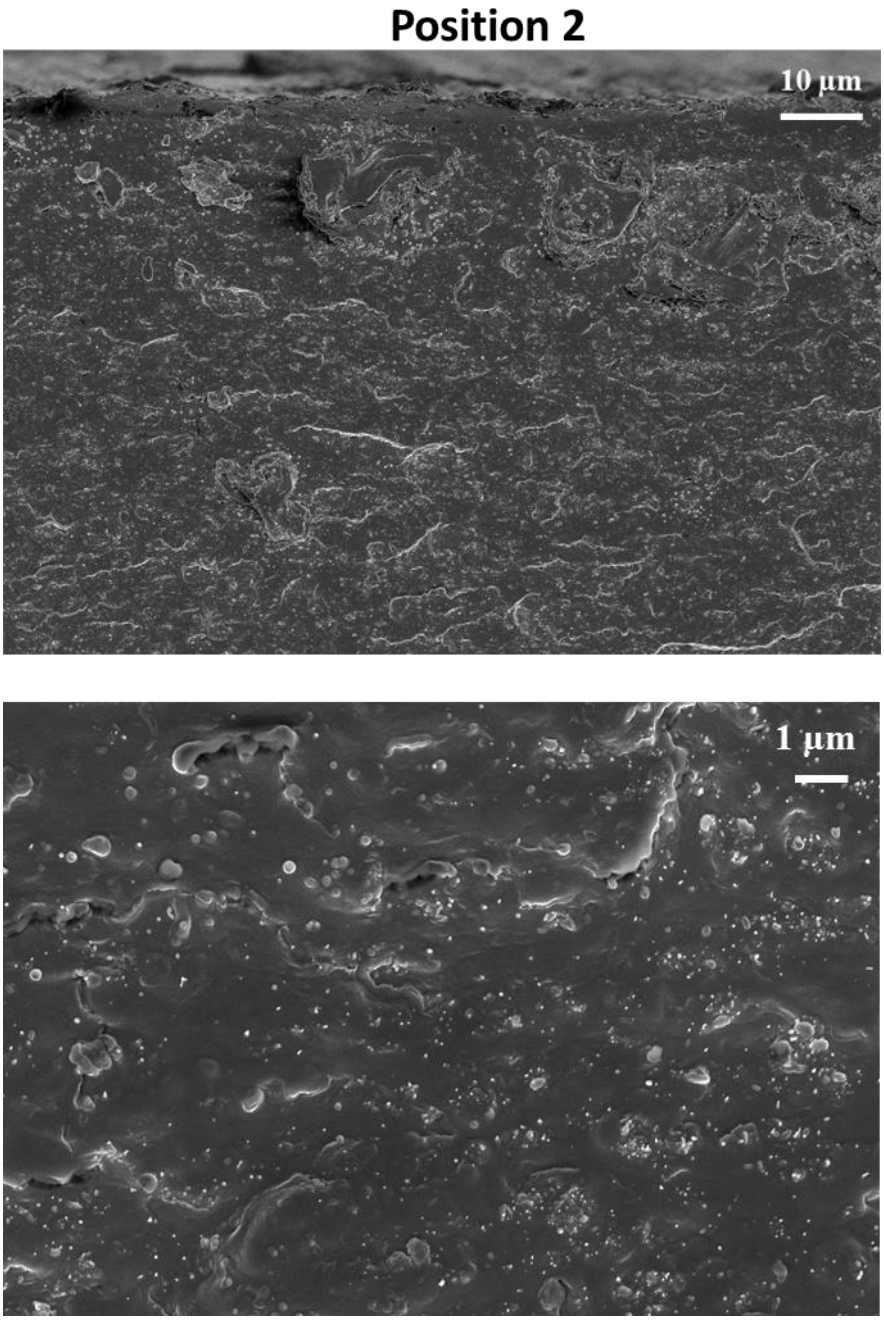

Figure 76: SEM image of the fractured section of 3wt % MWCNT-based formulation. Compared enlargements, related to the skin layer of the analysed surface in position 2. The sample was injection moulded at T mould 100°C and injection rate 70 cm^3/s.

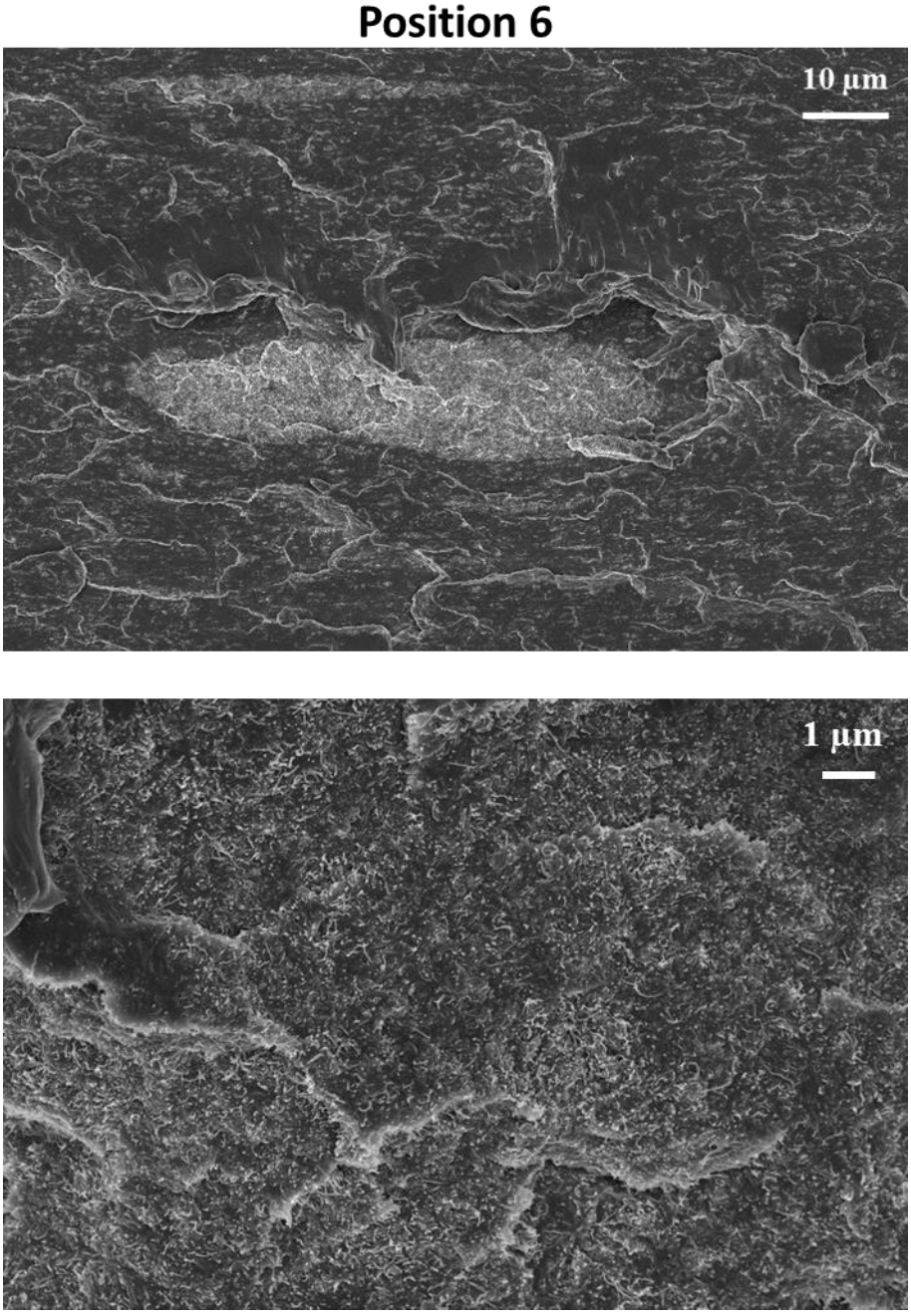

Figure 77: SEM image of the fractured section of 3wt % MWCNT-based formulation. Compared enlargements, related to the skin layer of the analysed surface in position 6. The sample was injection moulded at T mould 100°C and injection rate 70 cm^3/s.

Chapter 5

Conclusions

This thesis has studied the correlation between the morphology and the electrical behaviour of PP/MWCNT injection-moulded nanocomposites. In particular, the influence of the variation of the manufacturing parameters was deeply investigated. While the morphology has been studied with the traditional techniques such as optical and electron microscopy, special care was payed to the electrical characterization techniques. Indeed, several advanced approaches were utilized.

The multi-direction electrical testing was demonstrated to be a valuable approach to study indirectly the morphology of injection-moulded samples and to optimize the performance toward an advanced industrialization of a component.

The development of an electrical dedicated set-up allowed measuring the through-thickness electrical resistance in the cross-sectional area of the injection-moulded specimens. This has demonstrated to be a good method to evaluate the electrical behaviour at different depths of the samples. Moreover, this test gave an indirect information about the different morphology of the cross sectional area.

A thorough and complete AC dielectric study was performed on the MWCNT-based formulations. This characterization led to investigate the electrical ohmic-capacitive response of the nanocomposites undergoing a full range of frequency. The AC electrical measurements in different positions over the samples favored to examine the morphological structure of the nanocomposites in the through-thickness direction.

This advanced electrical characterization was necessary to thoroughly understand the effect of the specific morphology of the PP/MWCNT composites induced by tailoring the processing conditions of the injection moulding process. It is worth noting that the obtained results are in line with what is generally reported in literature (Figure 78).

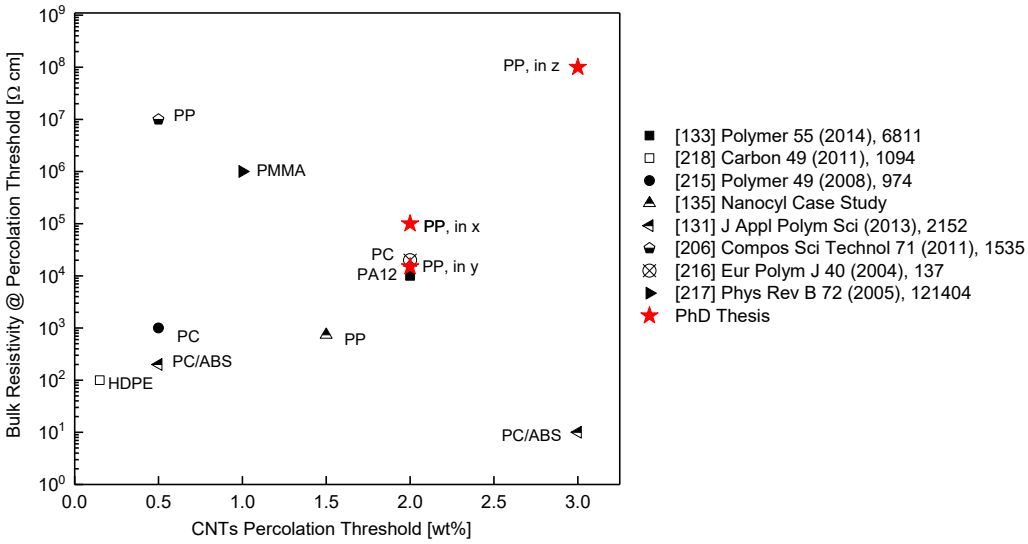

Figure 78: Percolation thresholds of several MWCNT-based nanocomposites, with different polymeric matrices, in comparison with the electrical results obtained in the experimental section of this thesis. The PP-based formulations were prepared in similar processing conditions and with materials, having comparable physical properties.

Skin-core structure. As a first step, the multidirectional electric test and the cross sectional electrical resistance measurements allow quantifying the effect of the skin-core morphology in the electrical behaviour. This leads to define a simple equivalent electric circuit, which takes into account this behaviour. This phenomenon, largely reported in literature and discussed in the previous Chapters, is mostly due to the shear flow, held up by the molten material inside the mould during the injection moulding process. Specifically, the carbon nanotubes, owning a micrometric length, behave as non-Brownian particles, when suspended in a polymeric matrix. On the other hand, their nanometric cross-section facilitates their deformation under flow. These hybrid dimensional properties seem to favour in the core internal region the migration of the conductive fillers and the formation of a disordered morphological structure, in which the nanotubes tend to create a self-sustaining structure within the polymer matrix. In this area, no preferential orientation, induced by the shear flow, is shown. On the contrary, a marked alignment of the micro-clusters of MWCNTs is observed in the skin layers, parallel to the flow of the molten material during the filling phase of the injection moulding process. The single MWCNTs, inside the clusters, assume a random configuration, with no preferential orientation.

This inhomogeneous MWCNTs distribution strongly affects the electrical behaviour of the injection-moulded samples. The results of the multi-direction electrical characterization allowed showing this anisotropic electrical behaviour in the three main directions. In fact, the electrical percolation threshold in the through-thickness direction occurs at higher MWCNTs content than in the in-plane directions, among which no significant differences were measured. Moreover, the electrical resistivity beyond the electrical percolation threshold in the through-thickness direction is two orders of magnitude higher than in the in-plane directions. The cross sectional area measurements favour the evaluation of the anisotropic electrical behaviour in the through-thickness direction. Indeed, the electrical resistance appears not constant from the external skins to the internal core region and the external layers are demonstrated to be less conductive than the internal area. Moreover, the electrical resistance seems to have a parabolic-like trend, with the maximum in the middle of the sample thickness. This trend is directly related to the fountain-flow phenomenon of the molten polymer during the filling phase of the injection moulding process and to its morphology.

Effect of the processing conditions. The main study of the present thesis was focused on the effect of the variation of the processing conditions in the morphology of the PP/MWCNT nanocomposites and the resulting electrical behaviour.

From the melt mixing point of view, two parameters were evaluated: the layout of the process, consisting in the feeding point of the MWCNTs, and the melt temperature. The change in the carbon nanotubes feeding point was demonstrated to have a high effect. Feeding the nanofillers through the main hopper with the solid polymeric granules strongly increases the electrical resistivity of the final component. In fact, even though a longer residence time allowed the matrix and the filler to be more in contact, a longer path in the extruder is detrimental for the MWCNTs length and for the formation of a solid 3D percolative conductive network. The SEM analysis has shown a lack in MWCNT clusters formation, when they are fed with the polymer at the beginning of the screw profile. This has also induced a strong decrease in the electrical conductive performance of the materials. On the other hand, the effect of the melt temperature in the electrical properties seems to be less significant and a clear trend related to the modification of this parameter was not observed. This is probably due to the fact that the mixing temperature, while modifying the viscosity of the molten polymer, can affect the morphology of the clusters. However, during the following injection moulding process, a further melt of the mixture occurs and this can fade the effect of the first melting phase.

From the injection moulding point of view, three parameters were modified, namely the mould temperature, the injection rate and the melt temperature. The increase of both T mould and injection rate shown the best electrical results, leading to a decrease of both the bulk and surface electrical resistivity of several orders of magnitude in both the through-thickness and the in-plane directions. Furthermore, the high increase of the temperature of the mould, made it possible by using the Heat&Cool technology, induces a change in the fluidity of the polymer, which favours an annealing effect in the nanocomposites. A similar result was obtained with an increment of the injection rate. It is widely known that the use of high injection rates during the filling phase could provide an increase of the shear stress, which could destroy the MWCNTs agglomerates. Nonetheless, at high shear rates, the rheological shear thinning behaviour of the nanocomposites, showed in *Chapter 3 § 3.5*, led to a decrease of the viscosity of the molten polymer during the injection phase and, consequently to a easier formation of circular shaped micro and nano bundles of carbon nanotubes, specifically in the core region of the sample. The lower viscosity of the molten polymer while filling the mould, regardless of the fact that it is due to an increase of the T mould or of the injection rate, allowed the carbon nanotubes to rearrange morphologically in clustered structures and an agglomeration during the cooling phase was facilitated. In this way, the molten polymer penetrated easily in the MWCNTs bundles creating a more efficient conductive structure.

It is worth to be noted that the effect of the processing conditions is more evident when the MWCNTs content is in the range of the electrical percolation. This can be easily justified because, at a significantly lower content, even the obtainment of most efficient morphology does not allow the formation of the conductive path. On the other hand, over the percolation threshold, even the achievement of worst morphology allows anyway the formation of a conductive path.

Table 21 and Figure 79 show a selection of the results reported in the scientific literature. As it can be seen, there is a general accordance to what was found in this thesis in terms of percolation threshold and electrical resistivity. Nonetheless, it can be noted that several authors reports a different trend by varying the processing conditions. This aspect can be mainly due to a difference in the used polymer matrix and to its viscosity, if compared with what used in this thesis.

In fact, the majority of the reported literature results are referred to amorphous matrices, which have a different rheological and processability behaviour from the used copolymer polypropylene.

Table 21: Influence of processing parameters in literature, compared with this thesis results. The "-" symbol indicates a negative effect on the electrical conductivity. On the contrary, the "+" symbol indicates a positive effect on the electrical conductivity.

Ref	Polymer matrix	Increasing Injection rate	Increasing T Melt	Increasing T Mould
[219]	PC		++	
[150]	PC	--	++	-
[220]	PC	--	++	
[133]	PA12	--		
[131]	PC/ABS	--	++	
[164]	PC – PA12	--	++	+/-
[135]	PP	--	++	++
[162]	PC	--	++	
[213]	PS	--	++	+/-
[221]	PC	--	++	+/-
[197]	PC	--	++	
[132]	PC	--	++	++
[165]	POM	+/-	+/-	++
[166]	TPU			++
[184]	PS	++	++	
PhD thesis	**PP**	**++**	**+/-**	**++**

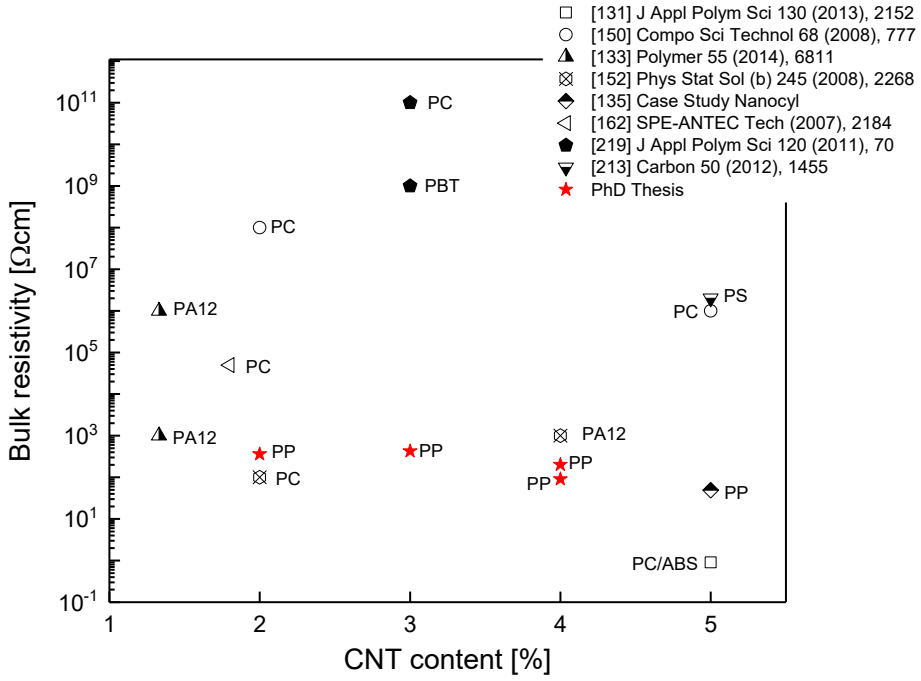

Figure 79: Comparison of electrical resistivity as a function of the MWCNTs content of several data reported in literature and the results, obtained in this thesis project. The reported values are referred to electrical resistivity obtained after a modification of the injection moulding parameters (i.e. T melt, T mould and injection rate mainly).

Position over the sample. In this thesis, the electrical behaviour was evaluated also as a function of the measurement position over the sample, with respect to the injection gate. As a result, a difference in the electrical resistivity was observed.

In particular, it is worth to be noted that a significant difference is present if the measurement was performed in the nearest position to the gate or in the farthest position from the gate. This can be explained by the fact that the observed migration of the nanotubes from the skin toward the core region during the filling phase leads to an increasingly higher filler concentration while the front of the molten polymer moves from the gate to the end of the mould cavity. In this way, a higher concentration of the MWCNTs is expected to be found in the farther position from the gate. Moreover, the part of the sample close to the gate obviously does not undergo to the same shear stress of all the other positions, and this can also affect the particular morphological structure of this position, which is apparently less efficient.

In conclusion, the injection moulding process induces an inhomogeneous morphology of the MWCNTs in both the cross sectional area and over the position of the component, which is influenced by the processing condition and which influences the electrical behaviour. The advanced design of an electrically conductive injection-moulded component can lead to an optimization of the final performance. Therefore, the results obtained in this thesis may provide a robust platform to gain insight into polymer-carbon nanotube dispersion, being an important step in the study and control of the morphology and electrical properties of the MWCNT composites.

References

[1] PlasticEurope, Association of Plastic Manufacturers, Plastics – the Facts 2016. An analysis of European plastics production, demand and waste data

[2] M. H. Al-Saleh, U. Sundararaj, A review of vapor grown carbon nanofiber/polymer conductive composites, Carbon 47 (2009) 2 –22

[3] S. H. Voldman, A review of electrostatic discharge (ESD) in advanced semiconductor technology, Microelectronics Reliability 44:1 (2004) 33-46

[4] B. Lee, Electrically conductive polymer composites and blends, Polymer Engineering and Science 32:1 (1992) 36–42

[5] W.D. Greason, Electrostatic discharge: a charge driven phenomenon, Journal of Electrostatics 28:3 (1992) 199-218

[6] D.D.L Chung, Electromagnetic interference shielding effectiveness of carbon materials, Carbon 39:2 (2001) 279–285

[7] S. Geetha, K. K. S. Kumar, C. R. K. Rao, M. Vijayan, D. C. Trivedi, EMI Shielding: Methods and Materials—A Review, Journal of Applied Polymer Science 112 (2009) 2073–2086

[8] J. M. Thomassin, C. Jérôme, T. Pardoen, C. Bailly, I. Huynen, C. Detrembleur, Polymer/carbon based composites as electromagnetic interference (EMI) shielding materials, Materials Science and Engineering: Reports 74:7 (2013) 211–232

[9] J.C. Huang, EMI shielding plastics: A review, Advances in polymer technology 14:2 (1995) 137–150

[10] http://www.regione.piemonte.it/innovazione/notizie/nanocontact-2.html

[11] https://www.crf.it/IT/Pages/Projects/20151223_progetto_drapo.aspx

[12] Process for producing conductive and/or piezoresistive traces on a polymeric substrate, European Patent Application EP 2448 383 A1

[13] E. F. Northrup, Methods of Measuring Electrical Resistance, New York, Graw-Hill, 1912

[14] D. Stauffer, Introduction of Percolation Theory, Taylor and Francis: London, UK, (1985)

[15] Electrical properties of polymers, Academic Inc Press, Edited by D. Seanor, 1982

[16] J. Mijovic, B. D. Fitz, Dielectric Spectroscopy of Reactive Polymers, Application Note Dielectrics 2, Material Science (1998)

[17] R. H. Cole, K. S. Cole, Dispersion and Absorption in Dielectrics I. Alternating Current Characteristics, Journal of Chemical Physics 9 (1941) 341

[18] A. Ameli, Y. Kazemi, S. Wang, C.B. Park, P. Pötschke, Process-microstructure-electrical conductivity relationships in injection-moulded polypropylene/carbon nanotube nanocomposite foams, Composites: Part A 96 (2017) 28–36

[19] Intrinsically Conducting Polymers: An Emerging Technology, Editors M. Aldissi, Springer Netherlands, Nato Science Series E: Series 246 (1993)

[20] H. S. Nalwa, Handbook of Organic Conductive Molecules and Polymers, Volume 2, Conductive Polymers: Synthesis and Electrical Properties, Editor Wiley publisher (1997)

[21] F. Lux, Models proposed to explain the electrical conductivity of mixtures made of conductive and insulating materials, Journal of Materials Science 28:2 (1993) 285–301

[22] H. Shirakawa, E. J. Louis, A. G. MacDiarmid, C. K. Chiang, A. J. Heeger, Synthesis of electrically conducting organic polymers: halogen derivatives of polyacetylene, $(CH)_x$, Journal of the Chemical Society, Chemical Communications 16 (1977) 578-580

[23] L. Paganin, Sintesi e proprietà di nuovi polimeri tiofenici per applicazioni opto-elettroniche, Dottorato di Ricerca in Chimica Industriale - XVIII Ciclo

[24] F. P. Di Nicola, Sintesi e caratterizzazione di polimeri coniugati per l'ottenimento di piste conduttive mediante tracciatura laser, Corso di laurea specialistica in Chimica Industriale (2011)

[25] R. Holzea, Y.P. Wub, Intrinsically conducting polymers in electrochemical energy technology: Trends and progress, Electrochimica Acta 122 (2014) 93– 107

[26] Handbook of conducting polymers, third edition, Conjugated polymers Processing and Applications, T.A. Skotheim and J. R. Reynolds Editors, CRC Press, Taylor and Francis group

[27] A. J. Epstein, Electrical conductivity in conjugated polymers, Conductive Polymers and plastics in industrial applications, L. Rupprecht Editor, Society of plastic engineers, Plastic design library (1999) 1

[28] W.K. Lu, R. L. Elsenbaumer, The Corrosion Protection of Metals by Conductive Polymers. II. Pitting Corrosion, Conductive Polymers and Plastics in Industrial Applications, A volume in Plastics Design Library (1999) 195–200

[29] D. E. Tallman, Y. Pae, G. Chen, G. P. Bierwagenz, B. Reems, V. Johnston Gelling, Studies of Electronically Conducting Polymers for Corrosion Inhibition of Aluminum and Steel, Conductive Polymers and Plastics in Industrial Applications volume in Plastics Design Library (1999) 201–207

[30] D. Kumar, R. C. Sharma, Advances in conductive polymers, European Polymer Journal 34:8 (1998) 1053-1060

[31] D. T. McQuade, A. E. Pullen, T. M. Swager, Conjugated Polymer-Based Chemical Sensors, Chemical Reviews 100 (2000) 2537-2574

[32] J. H. Burroughes, D. D. C. Bradley, A. R. Brown, R. N. Marks, K. Mackay, P. L. Burns, A. B. Holmes, Light-emitting diodes based on conjugated polymers, Nature 347 (1990) 539

[33] S. Soenmezoglu, R. Tas, S. Akın, M. Can, Polyaniline micro-rods based heterojunction solar cell: Structural and photovoltaic properties, Applied Physics Letters 101 (2012) 253301

[34] J. G. Drobny, Polymers for Electricity and Electronics: Materials, Properties, and Applications, Polymeric Materials Chapter 2 (2012)

[35] Metal-filled polymers, Properties and applications, edited by S. K. Bhattacharya, Chapter 3 (1986) 165

[36] D. M. Bigg, Thermal and Electrical Conductivity of Polymer Materials Advances in Polymer Science 119 (1995)

[37] Z. Han, A. Fina, Thermal Conductivity of Carbon Nanotubes and their Polymer, Nanocomposites: A Review, Progress in Polymer Science 36: 7 (2011) 914 – 944

[38] A. Boudennea, L. Ibosa, M. Foisa, J.C. Majeste, E. Ge´hina, Electrical and thermal behaviour of polypropylene filled with copper particles, Composites: Part A 36 (2005) 1545–1554

[39] D. Bloor, K. Donnelly, P.J. Hands, P. Laughlin, D. Lussey, A metal-polymer composite with unusual properties, Journal of Physics D: Applied Physics, 38:16 (2005) 2851-2860

[40] A.S. Luyt, J.A. Molefi, H. Krump, Thermal, mechanical and electrical properties of copper powder filled low-density and linear low-density polyethylene composites, Polymer Degradation and Stability 91 (2006) 1629-1636

[41] Y.P. Mamunya, V.V. Davydenko, P. Pissis, E.V. Lebedev, Electrical and thermal conductivity of polymers filled with metal powders, European Polymer Journal 38 (2002) 1887–1897

[42] H. S. Tekce, D. Kumlutas, I. H. Tavman, Effect of Particle Shape on Thermal Conductivity of Copper Reinforced Polymer Composites, Journal of reinforced plastics and composites 26:1 (2007) 113-121

[43] http://www.carbonblack.jp/en/cb/tokusei.html

[44] Y. W. Wong, K. L. Lo, F. G. Shin, Electrical and thermal properties of composite of liquid crystalline polymer filled with carbon black, Journal of Applied of polymers science 82:6 (2001) 1549–1555

[45] N. Abdel-Aal, F. El-Tantawy, A. Al-Hajry, M. Bououdina, Epoxy resin/plasticized carbon black composites. Part I. Electrical and thermal properties and their applications, Polymer Composites 29 (2008) 511–517

[46] J. A. King, F. A. Morrison, J. M. Keith, M. G. Miller, R. C. Smith, M. Cruz, A. M. Neuhalfen, R. L. Barton, Electrical Conductivity and Rheology of Carbon-Filled Liquid Crystal Polymer Composites, Journal of Applied Polymer Science 101 (2006) 2680–2688

[47] N. Probst, E. Grivei, Structure and electrical properties of carbon black, Carbon 40 (2002) 201–205

[48] http://carbon-black.org/index.php/what-is-carbon-black

[49] F. Gubbels, R. Jerome, Ph. Teyssie, E. Vanlathem, R. Deltour, A. Calderone, V. Parente, J. L. Bredas, Selective Localization of Carbon Black in Immiscible Polymer Blends: A Useful Tool To Design Electrical Conductive Composites, Macromolecules 27:7 (1994) 1972–1974

[50] H. Tang, X. Chen, A. Tang, Y. Luo, Studies on the Electrical Conductivity of Carbon Black Filled Polymers, Journal of Applied Polymer Science 59 (1996) 383-387

[51] J. C. Huang, Carbon black filled conducting polymers and polymer blends, Advances in polymer technologies, 21:4 (2002) 299–313

[52] I. Balberg, A comprehensive picture of the electrical phenomena in carbon black–polymer composites, Carbon 40 (2002) 139–143

[53] M. H. Al-Saleh, U. Sundararaj, An innovative method to reduce percolation threshold of carbon black filled immiscible polymer blends, Composites: Part A 39 (2008) 284–293

[54] R. Tchoudakov, O. Breuer, M. Narkis, A. Siegmann, Conductivity/Morphology Relationships in Immiscible Polymer Blends: HIPS/SIS/Carbon Black, Conductive Polymers and plastics in industrial applications, Larry Rupprecht Editor, Plastic Design Library 51 (1999)

[55] K. S. Novoselov, A. K. Geim, S. V. Morozov, D. Jiang, Y. Zhang, S. V. Dubonos, I. V. Grigorieva, A. A. Firsov, Electric Field Effect in Atomically Thin Carbon Films, Science 306 (2004)

[56] S. Stankovich, D. A. Dikin, G. H. B. Dommett, K. M. Kohlhaas, E. J. Imney, E. A. Stach, R. D. Piner, S. T. Nguyen and R. S. Ruoff, Graphene-based composite materials, Nature 442 (2006) 282-286

[57] A. K. Geim, Graphene: Status and Prospects, Science 324: 5934 (2009) 1530-1534

[58] A. A. Balandin, S. Ghosh, W. Bao, I. Calizo, D. Teweldebrhan, F. Miao, C. N. Lau, Superior Thermal Conductivity of Single-Layer Graphene, Nano Letters 8:3 (2008) 902–907

[59] C. Lee, X. Wei, J. W. Kysar, J. Hone, Measurement of the Elastic Properties and Intrinsic Strength of Monolayer Graphene, Science 321 (2008) 385

[60] D. Varshney, B. R. Weiner, G. Morell, Growth and field emission study of a monolithic carbon nanotube/diamond composite, Carbon 48:12 (2010) 3353-3358

[61] Z-S. Wu, W. Ren, L. Gao, B. Liu, C. Jiang, H-M. Cheng, Synthesis of high-quality graphene with a pre-determined number of layers, Carbon 47:2 (2009) 493-499

[62] L. M. Viculis, J. J. Mack, O. M. Mayer, H. T. Hahn, R. B. Kaner, Intercalation and exfoliation routes to graphite nanoplatelets, Journal of Materials Chemistry 15 (2005) 974-978

[63] J. Du, H-M. Cheng, The Fabrication, Properties, and Uses of Graphene/Polymer Composites, Macromolecular Chemistry and Physics 213:10-11 (2012) 1060 - 1077

[64] A. Bianco, H-M. Cheng, T. Enoki, Y. Gogotsi, R. H. Hurt, N. Koratkar, T. Kyotani, M. Monthioux, C. R. Park, J. M. D. Tascon, J. Zhang, All in the graphene family – A recommended nomenclature for two-dimensional carbon materials, Carbon 65 (2013) 1 – 6

[65] Y. Sun, H.D. Bao, Z.X. Guo, J. Yu, Modeling of the electrical percolation of mixed carbon fillers in polymer-based composites, Macromolecules 42 (2009) 459–63

[66] S.M. Zhang, L. Lin, H. Deng, X. Gao, E. Bilotti, T. Peijs, Q. Zhang, Q. Fu, Synergistic effect in conductive networks constructed with carbon nanofillers in different dimensions, Express Polymer Letters 6 (2012) 159–68

[67] K.C. Etika, L. Liu, L.A. Hess, J.C. Grunlan, The influence of synergistic stabilization of carbon black and clay on the electrical and mechanical properties of epoxy composites, Carbon 47:3 (2009) 128–36

[68] C.R. Yu, D.M. Wu, Y. Liu, H. Qiao, Z.Z. Yu, A. Dasari, X.S. Du, Y.W. Mai, Electrical and dielectric properties of polypropylene nanocomposites based on carbon nanotubes and barium titanate nanoparticles, Composites Science and Technology 71 (2011) 1706–12

[69] R.H.J. Otten, P. van der Schoot, Continuum percolation of polydisperse nanofillers, Physical Review Letters 103 (2009) 225704/1-4

[70] M. G. Jang, C. Cho, W. N. Kim, Synergistic effects of hybrid conductive fillers on the electrical properties of carbon fiber pultruded polypropylene/ polycarbonate composites prepared by injection moulding, Journal of Composite Materials 51:7 (2017) 1–13

[71] S. Iijima, Helical microtubules of graphitic carbon, Nature 34 (1991), 56-58

[72] M. Kumar, Y. Ando, Chemical Vapor Deposition of Carbon Nanotubes: A Review on Growth Mechanism and Mass Production, Journal of Nanoscience and Nanotechnology 10 (2010) 3739–3758

[73] M. F. L. De Volder, S. H. Tawfick, R. H. Baughman, A. J. Hart, Carbon Nanotubes: Present and Future Commercial Applications, Science 339 (2013) 535

[74] D.S. Bethune, C.H. Kiang, M.S. Devries, G. Gorman, R. Savoy, J. Vazquez, et al, Cobalt-catalyzed growth of carbon nanotubes with single atomic-layer walls, Nature 363: 6430 (1993) 605–7

[75] S Iijima, T. Ichihashi, Single-shell carbon nanotubes of 1-nm diameter, Nature 363: 6430 (1993) 603–5

[76] J. N. Coleman, U. Khan, W. J. Blau, Y. K. Gun'ko, Small but strong: A review of the mechanical properties of carbon nanotube–polymer composites, Carbon 44 (2006) 1624–1652

[77] R. H. Baughman, A. A. Zakhidov, W. A. de Heer, Carbon Nanotubes—the Route Toward Applications, Science 297 (2002) 787

[78] M. Paradise, T. Goswami, Carbon nanotubes – Production and industrial applications, Materials and Design 28 (2007) 1477–1489

[79] W. Liang, M. Bockrath, D. Bozovic, J.H. Hafner, M Tinkham, H. Park, Fabry - Perot interference in a nanotube electron waveguide, Nature 411:6838 (2001) 665-9

[80] S. Frank, P. Poncharal, Z. L. Wang, W. A. de Heer, Carbon Nanotube Quantum Resistors, Science 280 (1998)

[81] P.G. Collins, P. Avouris, Nanotubes for electronics, Scientific American 283:6 (2000) 62-9

[82] V. N. Popov, Carbon nanotubes: properties and application, Materials Science and Engineering R 43 (2004) 61–102

[83] M. Dresselhaus, G. Dresselhaus, P. Eklund, Science of Fullerenes and Carbon Nanotubes, 1st Edition, Their Properties and Applications, Academic Press (1996)

[84] P. Kim, L. Shi, A. Majumdar, and P. L. McEuen, Thermal Transport Measurements of Individual Multiwalled Nanotubes, Physical Review Letters 87:21 (2001)

[85] E.W. Wong, P.E. Sheehan, C.M. Lieber, Nanobeam mechanics: elasticity, strength, and toughness of nanorods and nanotubes, Science 277 (1997) 1971–5

[86] M. Yu, O. Lourie, M.J. Dyer, T.F. Kelly, R.S. Ruoff, Strength and breaking mechanism of multiwalled carbon nanotubes under tensile load, Science 287 (2000) 637–40

[87] J.P. Salvetat, G.A.D. Briggs, J.M. Bonard, R.R. Bacsa, A.J. Kulik, T. Stockli, et al., Elastic and shear moduli of single-walled carbon nanotube ropes, Physical Review Letters 82:5 (1999) 944–7

[88] M.F. Yu, B.S. Files, S. Arepalli, R.S. Ruoff, Tensile loading of ropes of single wall carbon nanotubes and their mechanical properties, Physical Review Letters 84:24 (2000) 5552–5

[89] Y. Liu, L. Gao, A study of electrical properties of nanotube–$NiFe_2O_4$ composites: effect of surface treatment of carbon nanotubes, Carbon 8 (2005) 47–52

[90] R. G. Ding, G. Q. Lu, Z. F. Yan, M. A. Wilson, Recent Advances in the Preparation and Utilization of Carbon Nanotubes for Hydrogen Storage, Journal of Nanoscience and Nanotechnology 1:7 (2001) 7-29

[91] C. Journet, P. Bernier, Production of carbon nanotubes, Applied Physics A-Materials Science & Processing 67:1 (1998) 1–9

[92] B. Izaskun, F. Ingio, G. Ainara, M. Belsue, M. Roberto, Synthesis purification and characterization of carbon nanotubes, Poster (2004)13–7

[93] C. Chen, W. Perry, H. Xu, Y. Jiang, J. Phillips, Plasma torch production of macroscopic carbon nanotube structures, Carbon 41:13 (2003) 2555–60

[94] Massachusetts Technology Collaborative and The Nano Science and Technology Institute, Nanotechnology and its impact on industry. Industry Summaries, (1997)

[95] J.P. Delmotte, A. Rubio, Mechanical properties of carbon nanotubes: a fibre digest for beginners, Carbon 40:10 (2002) 1729–34

[96] F. H. Gojny, M. H. G. Wichmann, U. Kopke, B. Fiedler, K. Schulte, Carbon nanotube-reinforced epoxy-composites: enhanced stiffness and fracture toughness at low nanotube content, Composites Science and Technology 64:15 (2004) 2363

[97] L.S. Schadler, S.C. Giannaris, P.M. Ajayan, Load transfer in carbon nanotube epoxy composites. Applied Physics Letters 73:26 (1998) 3842–4

[98] T. Kuzumaki, K. Miyazawa, H. Ichinose, K. Ito, Processing of carbon nanotube reinforced aluminum composite, Journal of Materials Research 13:9 (1998) 2445–9

[99] A. Peigney, C. Laurent, A. Rousset, Synthesis and characterization of alumina matrix nanocomposites containing carbon nanotubes, Key Engineering Materials 132–136 (1997) 743–6

[100] I. Alig, P. Pötschke, D. Lellinger, T. Skipa, S. Pegel, G. R. Kasaliwal, T. Villmow, Establishment, morphology and properties of carbon nanotube networks in polymer melts, Polymer 53 (2012) 4 - 28

[101] M. Klüppel, The Role of Disorder in Filler Reinforcement of Elastomers on Various Length Scales Advances in Polymer Science 164 (2003) 1-86

[102] O. Meincke, D. Kaempfer, H. Weickmann, C. Friedrich, M. Vathauer, H. Warth, Polymer 45:3 (2004) 739-48

[103] M. L. Clingerman, E. H. Weber, J. A. King, K. H. Schulz, Development of an Additive Equation for Predicting the Electrical Conductivity of Carbon-Filled Composites, Journal of Applied Polymer Science 88 (2003) 2280–2299

[104] C-M. Hong, J. Kim, S. C. Jana, Shear-Induced Migration of Conductive Fillers in Injection Moulding Polymer Engineering and Science 44:11 (2004)

[105] R. Struèmpler, J. Glatz-reichenbach, Conducting Polymer Composites, Journal of Electroceramics 3:4 (1999) 329-346

[106] I. Chodak, I. Krupa, "Percolation effect" and mechanical behaviour of carbon black filled Polyethylene, Journal of Materials Science Letters 18 (1999) 1457 – 1459

[107] K. Kalaitzidou, H. Fukushima, L. T. Drzal, A Route for Polymer Nanocomposites with Engineered Electrical Conductivity and Percolation Threshold, Materials 3 (2010) 1089-1103

[108] A. Belashi, Percolation modeling in polymer nanocomposites, The University of Toledo (2011)

[109] A. Hunt, Percolation theory for flow in porous media, New York: Springer (2005)

[110] R. Zhang, M. Baxendale, T. Peijs, Universal resistivity-strain dependence of carbon nanotube/polymer composites, Physical Review B 76:195433 (2007) 1-5

[111] H. Deng, L. Lin, M. Ji, S. Zhang, M. Yang, Q. Fu, Review Progress on the morphological control of conductive network in conductive polymer composites and the use as electroactive multifunctional materials, Progress in Polymer Science 39 (2014) 627–655

[112] W. Zhai, S. Zhao, Y. Wang, G. Zheng, K. Dai, C. Liu, C. Shen, Segregated conductive polymer composite with synergistically electrical and mechanical properties Composites: Part A 105 (2018) 68–77

[113] P. Pötschke, M. Abdel-Goad, I. Alig, S. Dudkin, D. Lellinger, Rheological and dielectrical characterization of melt mixed polycarbonate-multiwalled carbon nanotube composites, Polymer 45:26 (2004) 8863-70

[114] A.V. Kyrylyuk, P. van der Schoot, Continuum percolation of carbon nanotubes in polymeric and colloidal media, PNAS 105 (2008) 8221–6

[115] R. D. Sherman, L. M. Middleman, S. M. Jacobs, Electron Transport Processes in Conductor-Filled Polymers, Polymer Engineering and Science 23:1 (1983)

[116] X. Jing, W. Zhao, L. Lan, The effect of particle size on electric conducting percolation threshold in polymer/conducting particle composites, Journal of Materials Science Letters 19(2000) 377

[117] H. S. Gokturk, T. J. Fiske, D. M. Kalyon, Effects of particle shape and size distributions on the electrical and magnetic properties of nickel/polyethylene composites, Journal of Applied Polymer Science 50 (1993) 1891

[118] J. Y Yi, G. M. Choi, Percolation Behaviour of Conductor-Insulator Composites with Varying Aspect Ratio of Conductive Fiber, Journal of Electroceramics 3 (1999) 361

[119] P. Calvert, Nanotube composites: A recipe for strength, Nature 399 (1999) 210–211

[120] H. Cruz, Y. Son, Effect of aspect ratio on electrical, rheological and glass transition properties of PC/MWCNT nanocomposites, Journal of Nanoscience and Nanotechnology 18:2 (2018) 943-950

[121] D.M. Bigg, D.E. Stutz, Plastic composites for electromagnetic interference shielding applications, Polymer Composites 4 (1983) 40

[122] M. Zilberman, G.I. Titelman, A. Siegmann, Y. Haba, M. Narkis, D. Alperstein, Conductive Blends of Thermally Dodecylbenzene Sulfonic Acid-Doped Polyaniline with Thermoplastic Polymers, Journal of Applied Polymer Science 66:243 (1997)

[123] Q. Zhang, H. Xiong, W. Yan, D. Chen, M. Zhu, Electrical conductivity and rheological behaviour of multiphase polymer composites containing conducting carbon black, Polymer Engineering Science 48:11 (2008) 2090–2097

[124] T. Wu, Y. Pan, L. Li, Highly electrically conductive and injection mouldable polymeric composites, Journal of Applied Polymer Science 121(2011) 2969

[125] C. Zhang, X.S. Yi, H. Yui, S. Asai, M. Sumita, Morphology and electrical properties of short carbon fiber-filled polymer blends: High-density polyethylene/poly(methyl methacrylate), Journal of Applied Polymer Science 69 (1998) 1813

[126] I.C. Finegan, G.G. Tibbetts, Electrical conductivity of vapor-grown carbon fiber/thermoplastic composites, Journal of Materials Research 16:6 (2001) 1668-1674

[127] Y. Liu, S. Kumar, Recent Progress in Fabrication, Structure, and Properties of Carbon Fibers, Polymer Reviews 52 (2012) 234

[128] B. Krause, P. Poetschke, E. Ilin, M. Predtechenskiy, Melt mixed SWCNT-polypropylene composites with very low electrical percolation, Polymer 98 (2016) 45-50

[129] M. H. Al-Saleh, Carbon nanotube-filled polypropylene/polyethylene blends: compatibilization and electrical properties, Polymer Bulletin 73 (2016) 975–987

[130] K. Kalaitzidou, H Fukushima, P. Askeland, L.T. Drzal, The nucleating effect of exfoliated graphite nanoplatelets and their influence on the crystal structure and electrical conductivity of polypropylene nanocomposites, Journal of Materials Science 43 (2008) 2895–2907

[131] M. Wegrzyn, S. Juan, A. Benedito, E. Gimenez, The Influence of Injection Moulding Parameters on Electrical Properties of PC/ABS-MWCNT Nanocomposites, Journal of Applied Polymer Science 130 (2013) 2152-2158

[132] J. Qiu, L. Wang, K. Uchiya, E. Sakai, Effects of Injection Moulding Conditions on the Electrical Properties of Polycarbonate/Carbon Nanotube Nanocomposites, Polymer Composites 37:11 (2016) 3245-3255

[133] S. Versavaud, G. Regnier, G. Gouadec, M. Vincent, Influence of injection moulding on the electrical properties of polyamide 12 filled with multi-walled carbon nanotubes, Polymer 55 (2014) 6811-6818

[134] S. Zhou, A. N. Hrymak, M. R. Kamal, Electrical, morphological and thermal properties of microinjection moulded polyamide 6/multi-walled carbon nanotubes nanocomposites, Composites: Part A 103 (2017) 84–95

[135] C. Y. Lew, M. Claes, F. Luizi, The Influence of Processing Conditions on the Electrical properties of Polypropylene Nanocomposites Incorporating Multiwall Carbon Nanotube, Nanocyl

[136] B. Afrinaldi, A.L. Juwono, C. Liza, S.J.A. Nasiri, Effect of Multi Wall Carbon Nanotube Content on The Electrical and Rheological Properties of Polypropylene-based Nanocomposites, MATEC Web of Conferences 78 (2016) 01092

[137] S. Almuhamed, N. Khenoussi, L. Schacher, D. Adolphe, H. Balard, Journal of Nanomaterials, 2012:1 (2011)

[138] P. Riviere, T. E. Nypelo, M. Obersriebnig, H. Bock, M. Muller, N. Mundigler, R. Wimmer, Unmodified multi-wall carbon nanotubes in polylactic acid for electrically conductive injection-moulded composites, Journal of Thermoplastic Composite Materials 30:12 (2017) 1615-1638

[139] J. Sandler, M.S.P. Shaffer, T. Prasse, W. Bauhofer, K. Schulte, A.H. Windle, Development of a dispersion process for carbon nanotubes in an epoxy matrix and the resulting electrical properties, Polymer 40:21 (1999) 5967–71

[140] R.J. Crawford, Plastics Engineering (Third Edition), Chapter 4 – Processing of Plastics (1998) 245–342

[141] Z. Tadmor, C. Gogos, A. Spe, Principles of polymer processing, Second Edition, Chapter 13 Moulding, Technical Volume A, John Wiley & Sons Inc. Publication, 753

[142] J.H. DuBois, Plastics History U.S.A., Catmers Books (1972)

[143] A.M. De Filippi, Fabbricazione di componenti in materiali polimerici, Chapter 3, Hoepli

[144] A. Ciaperoni, A. Mula, Chimica e tecnologia delle poliammidi, Chapter 4, PACINI editore

[145] W. Rose, Fluid-Fluid Interfaces in Steady Motion, Nature 191 (1961) 242–243

[146] J. Vlachopoulos, D. Strutt, Overview Polymer processing, Materials Science and Technology, 19 (2003) 1161

[147] M. Vincent, T. Giroud, A. Clarke, C. Eberhardt, Description and modeling of fibre orientation in injection moulding of fibre reinforced thermoplastics, Polymer 46 (2005) 6719–6725

[148] T.D. Papathanasiou, Flow-induced alignment in injection moulding of fibre-reinforced polymer composites. In T.D. Papathanasiou, D.C. Guell, editors. Flow-induced alignment in composite materials, Cambridge: Woodhead Publishing Ltd (1997) 113–65

[149] J. Tiusanen, D. Vlasveld, J. Vuorinen, Review on the effects of injection moulding parameters on the electrical resistivity of carbon nanotube filled polymer parts, Composites Science and Technology 72 (2012) 1741–1752

[150] T. Villmow, S. Pegel, P. Poetschke, U. Wagenknecht, Influence of injection moulding parameters on the electrical resistivity of polycarbonate filled with multi-walled carbon nanotubes, Composites Science and Technology 68 (2008) 777–789

[151] I. Alig, T. Skipa, M. Engel, D. Lellinger, S. Pegel, P. Pötschke, Electrical conductivity recovery in carbon nanotube–polymer composites after transient shear Physica Status Solidi B, Basic Solid State Physics 244:11 (2007) 4223-6

[152] I. Alig, T. Skipa, D. Lellinger, M, Bierdel, H. Meyer, Influence of the injection moulding conditions on the in-line measured electrical conductivity of polymer–carbon nanotube composites, Physica Status Solidi B, Basic Solid State Physics 245:10 (2008) 2264-7

[153] I. Alig, T. Skipa, D. Lellinger, P. Pötschke, Destruction and formation of a carbon nanotube network in polymer melts: Rheology and conductivity spectroscopy, Polymer 49:16 (2008) 3524-32

[154] I. Alig, D. Lellinger, M. Engel, T. Skipa, P. Pötschke, Destruction and formation of a conductive carbon nanotube network in polymer melts: In-line experiments, Polymer 49:7 (2008) 1902-9

[155] T. Skipa, D. Lellinger, M. Saphiannikova, I. Alig, Shear-stimulated formation of multi-wall carbon nanotube networks in polymer melts Physica Status Solidi B, Basic Solid State Physics 246:11-12 (2009) 2453-6

[156] T. Skipa, D. Lellinger, W. Böhm, M. Saphiannikova, I. Alig, Influence of shear deformation on carbon nanotube networks in polycarbonate melts: Interplay between build-up and destruction of agglomerates, Polymer 51:1 (2010) 201-10

[157] D. Lellinger, T. Skipa, W. Böhm, I. Alig, Spatial decorrelation of the conductive nanotube network in a polymer melt , Physica Status Solidi B, Basic Solid State Physics 246:11-12 (2009) 2667-70

[158] P. Pötschke, S.M. Dudkin, I. Alig, Dielectric spectroscopy on melt processed polycarbonate—multiwalled carbon nanotube composites, Polymer 44 (2003) 5023–30

[159] B. Krause, R. Boldt, P. Pötschke, A method for determination of length distributions of multiwalled carbon nanotubes before and after melt processing, Carbon 49:4 (2011) 1243-7

[160] M. H. Al-Saleh, Effect of processing conditions on the dispersion, electrical, and mechanical properties of carbon nanotube/ polypropylene nanocomposites, Journal of Reinforced Plastics and Composites 34:9 (2015) 742–749

[161] V. Dudler, M. C. Grob, D. Merian, Percolation network in polyolefins containing antistatic additives Imaging by low voltage scanning electron microscopy, Polymer Degradation and Stability 68 (2000) 373-379

[162] A. Chandra, A. J. Kramschuster, X. Hu, L-S. Turng1, Effect of injection moulding parameters on the electrical conductivity of polycarbonate/carbon nanotube nanocomposites, Antec (2007) 2184

[163] M. Claes, M. Hurtgen, V. Lison, Importance of processing and converting conditions on the use of carbon nanotubes in thermoplastic applications, SPE-ANTEC (2014) 2190

[164] D. Lellinger, D. Xu, A. Ohneiser, T. Skipa, I. Alig, Influence of the injection moulding conditions on the in-line measured electrical conductivity of polymer–carbon nanotube composites, Physica Status Solidi B, Basic Solid State Physics 245:10 (2008) 2268–2271

[165] V. Bellantone, R. Surace, I. Fassi, Effects of injection moulding parameters on dimensional accuracy of POM/MWCNT micro parts, Proceedings of the ASME 2014 International Design Engineering Technical Conferences & Computers and Information in Engineering Conference IDETC/CIE (2014), DETC2014-35083

[166] D. Li, T. Zhai, Q. Gong, G. Fei, H. Xia, Effect of processing temperature on structure and properties of microinjection moulded thermoplastic polyurethane/multiwalled carbon nanotube composites, Plastics, Rubber and Composites 44:5 (2015) 197

[167] F. Cesano, M. Zaccone, I. Armentano, S. Cravanzola, L. Muscuso, L. Torre, J.M. Kenny, M. Monti, D. Scarano, Relationship between morphology and electrical properties in PP/MWCNT composites: Processing-induced anisotropic percolation Threshold, Materials Chemistry and Physics 180 (2016) 284-290

[168] F. Cesano, I. Rattalino, F. Bardelli, et al., Structure and properties of metal-free conductive tracks on polyethylene/multiwalled carbon nanotube composites as obtained by laser stimulated percolation, Carbon 61 (2013) 63-71

[169] Kang DW, Ryu SH. Orientation of carbon nanotubes in polypropylene melt. Polymer International 62:2 (2013) 152-7

[170] S. Zhou, A. N. Hrymak, M. R. Kamal, Electrical and morphological properties of microinjection moulded polypropylene/carbon nanocomposites, Journal of Applied Polymer Science 134:43 (2017) 45462

[171] D. S. McLachlan, M. Blaszkiewicz, and R. E. Newnham, Electrical Resistivity of Composites, Journal of the American Ceramic Society 73, 2187 (1990)

[172] S. I. Lee, Y. Song, T.W. Noh, X. D. Chen, and J. R. Gaines, Experimental observation of non-universal behaviour of the conductivity exponent for three-dimensional continuum percolation systems, Physical Review B 34, 6719 (1986)

[173] G. E. Pike, Conductivity of thick film (cermet) resistors as a function of metallic particle volume fraction, AIP Conference Proceeding 40, 366 (1978)

[174] F. Carmona, P. Prudhon, F. Barreau, Percolation in short fibres epoxy resin composites: Conductivity behaviour and finite size effects near threshold, Solid State Communication 51, 255 (1984)

[175] Other examples are listed in C. Brosseau, Journal of Applied Physics 91 (2002) 3197

[176] S. Kirkpatrick, Percolation and conduction. Review of Modern Physics 45 (1973) 574–88

[177] I. Balberg, Tunneling and Non universal Conductivity, Physical Review letters 59:12 (1987)

[178] Trionfi, D. H. Wang, J. D. Jacobs, L.-S. Tan, R. A. Vaia, and J.W. P. Hsu, Direct Measurement of the Percolation Probability in Carbon Nanofiber-Polyimide Nanocomposites, Physical Review Letters 102 (2009) 116601

[179] P. H. da Silva Leite Coelho, M. S. Marchesin, A. R. Morales, J. R. Bartoli, 2014 Electrical percolation, morphological and dispersion properties of MWCNT/PMMA nanocomposites Mat. Res. 17:1 (2014)

[180] F. Tanasa, M. Zanoaga, Y. Mamunya, Conductive thermoplastic polymer nanocomposites with ultralow percolation threshold, International Conference of Scientific Paper (2015)

[181] M. Monti, I. Armentano, G. Faiella, V. Antonucci, J. M. Kenny, L. Torre, M. Giordano, Toward the microstructure–properties relationship in MWCNT/epoxy composites: Percolation behaviour and dielectric spectroscopy, Composites Science and Technology 96 (2014) 38–46

[182] Chang J, Liang G, Gu A, Cai S, Yuan L., The production of carbon nanotube/epoxy composites with a very high dielectric constant and low dielectric loss by microwave curing, Carbon 50:2 (2012) 689–98

[183] C. Yuan, G. Chen, J. Yang, Orientation structures in injection-moulded pellets of polystyrene/carbon nanotube nanocomposites, Industrial and Engineering Chemistry Research 51 (2012) 11695−11699

[184] S. Zhou, A. N. Hrymak, M. R. Kamal, Electrical and Morphological Properties of Microinjection Moulded Polystyrene/Multiwalled Carbon Nanotubes Nanocomposites, Polymer Engineering and Science 56:10 (2016) 1182 - 1190

[185] E. Barsoukov, J.R. Macdonald, In: Impedance spectroscopy theory, experiment and applications. John Wiley and Sons (2005)

[186] G. Chakraborty, A.K. Meikap, R. Babu, W.J. Blau, Activation behaviour and dielectric relaxation in polyvinyl alcohol and multiwall carbon nanotube composite films, Solid State Communication 151 (2011) 754–8

[187] H. K. Lee, S. Pejanovic´, I. Mondragon, J. Mijovic´, Dynamics of single-walled carbon nanotube (SWNT)/polyisoprene (PI) nanocomposites in electric and mechanical fields, Polymer 48 (2007) 7345–55

[188] H-S. Bu, S. Z. D. Cheng, B. Wunderlich, Addendum to the thermal properties of polypropylene, Macromolecular Rapid Communications 9 (1988) 75–77

[189] E. Assouline, A. Lustiger, A. H. Barber, C. A. Cooper, E. Klein, E. Wachtel, H. D. Wagner, Nucleation Ability of Multiwall Carbon Nanotubes in Polypropylene Composites, Journal of Polymer Science: Part B: Polymer Physics 41 (2003) 520–527

[190] M.A. Lopez Manchado, L. Valentini, J. Biagiotti, J.M. Kenny, Thermal and mechanical properties of single-walled carbon nanotubes–polypropylene composites prepared by melt processing, Carbon 43 (2005) 1499 – 1505

[191] W. Xu, M. Ge, P-S. He, Nonisothermal Crystallization Kinetics of Polypropylene/Montmorillonite Nanocomposites, Journal of Polymer Science: Part B: Polymer Physics 40 (2002) 408–414

[192] J. F. Vega, J. Martınez-Salazar, M. Trujillo, M. L. Arnal, A. J. Mueller, S. sBredeau, Ph. Dubois, Rheology, Processing, Tensile Properties, and Crystallization of Polyethylene/Carbon Nanotube Nanocomposites, Macromolecules 42 (2009) 4719–4727

[193] K. Chrissafisa, D. Bikiaris, Review Can nanoparticles really enhance thermal stability of polymers? Part I: An overview on thermal decomposition of addition polymers, Thermochimica Acta 523 (2011) 1– 24

[194] G. Gorrasi, V. Romeo, D. Sannino, M. Sarno, P. Ciambelli, V. Vittoria, B. De Vivo and V. Tucci, Carbon nanotube induced structural and physical property transitions of syndiotactic polypropylene, Nanotechnology 18 (2007) 275703

[195] T. Kashiwagi, E. Grulke, J. Hilding, R. Harris, W. Awad, J. Douglas, Thermal Degradation and Flammability Properties of poly(propylene)/Carbon Nanotube Composites, Macromolecular Rapid Communication 23 (2002) 761–765

[196] V. Sivanjineyulu, Y-H. Chang, F-C. Chiu, Characterization of carbon nanotube- and organoclay-filled polypropylene/poly(butylene succinate) blend-based nanocomposites with enhanced rigidity and electrical conductivity, Journal of Polymer Research 24 (2017) 130

[197] L. Wang, J. Qiu, E. Sakai, X. Wei, Effects of multiwalled carbon nanotube mass fraction on microstructures and electrical resistivity of polycarbonate-based conductive composites, Science and Engineering of Composite Materials 24:2 (2015) 163 - 175

[198] S. Abbasi, P. J. Carreau, A. Derdouri, Flow induced orientation of multiwalled carbon nanotubes in polycarbonate nanocomposites: Rheology, conductivity and mechanical properties, Polymer 51 (2010) 922–935

[199] Y. Feilong, D. Hua, Z. Qin, W. Ke, Z. Chaoliang, C. Feng, F. Qiang, Anisotropic multilayer conductive networks in carbon nanotubes filled polyethylene/polypropylene blends obtained through high speed thin wall injection moulding, Polymer 54 (2013) 6425 – 6436

[200] F. Du, R. C. Scogna, W. Zhou, S. Brand, J. E. Fischer, K. I. Winey, Nanotube Networks in Polymer Nanocomposites: Rheology and Electrical Conductivity, Macromolecules 37 (2004) 9048-9055

[201] M-K. Seo, S-J. Park, Electrical resistivity and rheological behaviours of carbon nanotubes-filled polypropylene composites, Chemical Physics Letters 395 (2004) 44–48

[202] M. Monti, A. Terenzi, M. Natali, I. Gaztelumendi, N. Markaide, J. M. Kenny, L. Torre, Development of Unsaturated Polyester Matrix – Carbon Nanofibers Nanocomposites with Improved Electrical Properties, Journal of Applied Polymer Science 117 (2010)1658–1666

[203] A. Chafidz, M. Kaavessina, S. Al-Zahrani, I. Ali, Multiwall Carbon Nanotubes Filled Polypropylene Nanocomposites: Rheological and Electrical Properties, Polymer Engineering and Science 54:5 (2014) 1134 - 1143

[204] N. Gruzzuti, Fondamenti sul comportamento dinamico-meccanico: fluidi polimerici, from ATTI delle giornate didattiche su Caratterizzazione meccanico-dinamica di materiali polimerici (2004)

[205] P. Pötschke, R. A. Bhattacharyya, A. Janke, H. Goering, Melt mixing of polycarbonate /multi-wall carbon nanotube composites, Composite Interfaces 10:4-5 (2003) 389–404

[206] M. T. Müller, B. Krause, B. Kretzschmar, P. Pötschke, Influence of feeding conditions in twin-screw extrusion of PP/MWCNT composites on electrical and mechanical properties, Composites Science and Technology 71 (2011) 1535–1542

[207] G. Y. H. Choong, C. Y. Lew, D. S. A. De Focatiis, Role of processing history on the mechanical and electrical behaviour of melt-compounded polycarbonate-multiwalled carbon nanotube nanocomposites, Journal of Applied Polymer Science 132:28 (2015) 42277

[208] T. Villmow, P. Pötschke, S. Pegel, L. Haüssler, B. Kretzschmar, Influence of twin-screw extrusion conditions on the dispersion of multi-walled carbon nanotubes in a poly(lactic acid) matrix, Polymer 49 (2008) 3500–3509

[209] K. Wang, F. Chen, Z. Li, Q. Fu, Control of the hierarchical structure of polymer articles via "structuring" processing, Progress in Polymer Science 39 (2014) 891–920

[210] S. Stan, C. Fetecau, N. V. Stanciu, R. T. Rosculet, L. I. Sandu, Investigation Of Structure-Property Relationships In Thermoplastic Polyurethane/ Multiwalled Carbon Nanotube Composites, Proceedings of the ASME 2017 12th International Manufacturing Science and Engineering Conference MSEC2017 (2017) MSEC2017-2760

[211] A.E. Eken, E.J. Tozzi, D.J. Klingenberg, W. Bauhofer, A simulation study on the effects of shear flow on the microstructure and electrical properties of carbon nanotube/polymer composites, Polymer 52 (2011) 5178-5185

[212] S. Dönmez, A. Kentli, Influence of injection moulding parameters on electrical resistivity of carbon nanotube reinforced polycarbonate, Science and Engineering of Composite Materials 23:2 (2014)

[213] M. Mahmoodi, M. Arjmand, U. Sundararaj, S. Park, The electrical conductivity and electromagnetic interference shielding of injection moulded multi-walled carbon nanotube/polystyrene composites, Carbon 50 (2012) 1455 –1464

[214] S. O. Carson, J. M. Maia, J. C. Golba, Effects Of Shear And Extensional Flows On The Electrical Properties Of Polycarbonate/Carbon Nanotube Composites During Injection Moulding, SPE ANTEC (2015) 1647

[215] S. Pegel, P. Pötschke, G. Petzold, I. Alig, S.M. Dudkin, D. Lellinger, Dispersion, agglomeration, and network formation of multiwalled carbon nanotubes in polycarbonate melts, Polymer 49 (2008) 974 – 984

[216] P. Poetschke, A. R. Bhattacharyya, A. Janke, Melt mixing of polycarbonate with multiwalled carbon nanotubes: microscopic studies on the state of dispersion European Polymer Journal 40 (2004) 137–148

[217] F. Du, J. E. Fischer, K. I. Winey, Effect of nanotube alignment on percolation conductivity in carbon nanotube/polymer composites, Physical Review B 72 (2005) 121404R

[218] J. Du, L. Zhao, Y. Zeng, L. Zhang, F. Li, P. Liu, C. Liu, Comparison of electrical properties between multi-walled carbon nanotube and graphene nanosheet/high density polyethylene composites with a segregated network structure, Carbon 49 (2011) 1094 –1100

[219] P. F. Rios, A. Ophir, S. Kenig, R. Efrati, L. Zonder, R. Popovitz-Biro, Impact of Injection-Moulding Processing Parameters on the Electrical, Mechanical, and Thermal Properties of Thermoplastic/Carbon Nanotube Nanocomposites, Journal of Applied Polymer Science, 120 (2011) 70–78

[220] B. Kiss-Pataki, J. Tiusanen, G. Dobrik, Z. Vértesy, Z. E. Horváth, Visualization of the conductive paths in injection moulded MWNT/polycarbonate nanocomposites by conductive AFM, Composites Science and Technology 90 (2014) 102–109

[221] C.Y. Lew, C. Dewaghe, M. Claes, Injection moulding of polymer–carbon nanotube composites, Chapter 6 in book: Polymer–Carbon Nanotube Composites (2011) 155-192